UNIVERSITY OF OKLAHOMA

GRADUATE COLLEGE

AN INVESTIGATION OF ICE PRODUCTION MECHANISMS USING A 3-D CLOUD MODEL WITH EXPLICIT MICROPHYSICS

A Dissertation

SUBMITTED TO THE GRADUATE FACULTY

in partial fulfillment of the requirements for the

degree of

Doctor of Philosophy

By

MIKHAIL OVTCHINNIKOV
Norman, Oklahoma
1997

UMI Number: 9812254

AN INVESTIGATION OF ICE PRODUCTION MECHANISMS
USING A 3-D CLOUD MODEL WITH EXPLICIT MICROPHYSICS

A Dissertation APPROVED FOR
THE SCHOOL OF METEOROLOGY

BY

Peter Lamb

Leonid Dickey

Brian Fiedler

J M Straka

J Hoggs

ACKNOWLEDGMENTS

Following the chronological order, I must first thank Anton Rudich, who incidentally pushed me into the intriguing world of atmospheric science, and Prof. Khvorostyanov, who enthusiastically made me part of it.

I am grateful to my research advisor, Yefim L. Kogan, my academic advisors, Peter Lamb and Douglas K. Lilly, and the members of my doctoral committee Brian Fiedler, Jerry M. Straka, and Leonid A. Dickey, for their assistance. In particular, Prof. Kogan carefully guided me through the whole program. He and Prof. Lamb have always provided their generous support including research assistantships under the grants by the Environmental Sciences Division of the U.S. Department of Energy (through Battelle PNL Contract 144880-A-Q1 to the CIMMS) as part of the Atmospheric Radiation Measurement Program, by NOAA's Climate and Global Change Program under the Grant NA37RJ0203, and by the NASA Earth Science and Applications Division, Radiation Dynamics and Hydrology Branch, through Task 460-23-54-20.

Prof. Fielder, being a graduate liaison for most of my five years in the program, always gave his attention and fought bureaucracy over my "special circumstances". It is certainly not his fault that we lost most of these fights because that is what bureaucracy is all about. Consequently, I extend my gratitude to this almighty and yet elusive entity called the Graduate College that, by not admitting my Master degree from the Moscow Institute of Physics and Technology, forced me to take additional courses from which I have learned a great deal.

Alan Blyth, Mike Poellot, and Pete Daum kindly supplied aircraft measurements for the two studied cases. Our discussions also have added to my understanding of observational aspects of the work and hopefully improved the quality of the presented analysis.

All members of my family endured stoically the burden of my selfish departure at a very difficult time. They have provided all around support when I needed it most and managed to remain close, despite years and 6,000 miles of separation.

I cannot overestimate the importance of Zara's friendship. It took her tremendous efforts to keep me socialized and to prevent my otherwise inevitable transformation into a zombie.

Finally, I thank my dear friend Anna. Her role in who I am, where I am, and what I do has been much greater than she could ever imagine.

TABLE OF CONTENT

LIST OF TABLES

LIST OF FIGURES

ABSTRACT

Ice formation in midlevel clouds is studied using a newly developed cloud-scale model that combines three-dimensional dynamics with an explicit ice and liquid-phase microphysics and a detailed treatment of ice origination processes. One of the most important novel features of the model is that the effect of the Hallett-Mossop ice multiplication process is explicitly calculated in a dynamically evolving framework.

Two case studies have been conducted: (1) the cloud formed over the Magdalena Mountains, New Mexico, on 9 August 1987; and (2) the midlevel stratiform cloud layer over the northern Oklahoma on 7 April 1997. The model reproduces well the observed clouds in terms of cloud geometry, liquid water content, and concentrations of cloud drops and ice particles. Ice formation mechanisms are found to operate differently in the two environments. The difference is attributed to the changes in the liquid-phase microstructure.

In the case of the New Mexico cumulus cloud, when raindrops are produced through the warm-rain process, the Hallett-Mossop mechanism then generates ice particles in concentrations of order 100 L^{-1} in about 10 minutes. The secondary ice crystal production is confirmed to be a likely explanation for the large ice particle concentrations found in New Mexican summertime cumulus.

Sensitivity tests show that when the conditions for the Hallett-Mossop process are met, high concentrations of ice splinters can be produced even when the concentration of primary ice crystals is very low. The efficacy of the rime-splintering mechanism depends strongly on the liquid-phase microphysics, and the presence of

drizzle-size drops and their freezing by capture of ice splinters are essential to accelerate the Hallett-Mossop process.

In the case of the stratiform cloud deck, liquid water content is lower, and the production of large drops is inhibited. Consequently, the Hallett-Mossop process is relatively inefficient in this case. Thus, when there are few or no raindrops, as in the case of the simulated stratiform layer, the primary nucleation dominates ice production in the cloud.

Chapter I

INTRODUCTION

"Dr. Hoenikker used to say that any scientist who couldn't explain to an eight-year-old what he was doing was a charlatan."

Kurt Vonnegut, **"Cat's Cradle"**

1.1 Preamble

The importance of ice phase in clouds was probably first recognized in the early 1930's when Bergeron (1933) hypothesized that ice is required for most heavy rainfall from supercooled clouds. Since that time, much work has been done to further our understanding of precipitation formation although the role of the solid phase in development of precipitation is still plagued with many uncertainties. The effect of cloud ice is not limited to precipitation formation, however. The latent heat released in a glaciating cloud may significantly affect a cloud's dynamics, intensify the cloud, and prolong its life cycle. Interactions between ice and liquid cloud particles are believed to play an important role in charge separation and ultimately in formation of an electric structure of the cloud. The appearance of even a small number of ice crystals may alter the cloud albedo and other radiative characteristics. The modulation of the net radiation balance by the ice crystals in the Arctic troposphere is so significant that it is believed to have a global climatological effect. Most of the above effects depend drastically on concentration, size, and shape of ice particles. The evident importance of ice leads naturally to the question of how it originates in clouds.

The work of Fletcher (1962) can be undoubtedly considered a milestone in the history of ice formation research. It is, however, surprising and somewhat disappointing that after more than three decades of continuing research many investigators are still using Fletcher's parameterization for ice nuclei as a predictor of ice particle concentration in all types of clouds. Many more recent studies summarized nicely in Meyers et al. (1992) have shown that this parameterization should not be blindly extrapolated outside the temperature range for which it was designed, which is approximately -15° to -25°C. Despite the fact that our knowledge of many aspects of ice nucleation expanded significantly during the last several decades, the comprehensive picture of ice initiation is lacking. Consequently, the development of ice in clouds remains today, as it was 30 years ago, one of the outstanding questions in cloud physics.

There are several problems that hinder the progress in this area. The determination of a precise ice initiation mechanism represents a great challenge. The earliest stages of ice formation are not observed with radar. *In-situ* measurements provide more detailed information, but present measuring techniques experience difficulties in resolving small ice crystals. In addition, these data are usually incomplete, both spatially and temporally. Much of what we know about ice nucleation and development comes from laboratory experiments. Caution, however, must be taken in applying some of these empirical findings to natural cloud processes because in many cases conditions under which these experiments were conducted are not representative of the real cloudy atmosphere.

According to our current knowledge, ice originates, at least at temperature above approximately -40°C, through the process of heterogeneous nucleation that requires a presence of ice nuclei (IN). Despite constantly increasing number of experimental and theoretical studies, there is still a great deal of uncertainty in IN concentrations as well as in nucleation mechanisms. Because of limitations in instrumentation, it is extremely difficult to conduct reliable *in-situ* measurements of IN. It is even more difficult to clearly distinguish between various modes of IN activated through different mechanisms such as immersion-freezing, deposition, condensation-freezing, and contact-freezing nucleation. One of the puzzling aspects of ice formation is that the observed ice particle (IP) concentrations, particularly in relatively warm clouds (i.e., clouds with cloud-top temperature warmer than -15°C), often exceed even the highest estimate of background IN concentrations. This phenomenon is commonly referred to as "ice enhancement". Although the problem of ice formation has stirred much interest and debate in cloud physics and several possible explanation for the phenomenon has been proposed (for the recent review the reader is referred to Beard, 1992), it is still unclear what mechanisms produce the observed high IP concentrations. One of the widely discussed possibilities is ice splinter production during riming of ice particles. Among other possible explanations under consideration are the enhanced ice nucleation in regions of high supersaturation and intense production of ice nuclei by evaporating drops. Despite all uncertainties, observations clearly show that at temperatures warmer than -15°C the amount of ice in clouds strongly depends on liquid-phase microphysics, probably more so than on temperature.

Modeling studies represent a powerful supplement to observations. Numerical models with various degrees of complexity have been extensively applied to investigate various ice nucleation mechanisms, their production rates and dependence on cloud microphysical structure (Young 1974a,b; Cotton et al. 1986; Meyers et al. 1992). During the past two decades one-, two-, and three-dimensional cloud models that include description of warm rain, and in a number of cases, some ice phase processes have been developed (Clark 1973; Scott and Hobbs 1974; Takahashi 1976; Hall 1980; Farley and Orville 1986; Murakami 1990; Kogan 1991, Reisin et al. 1996). Modeling studies encounter their own difficulties, however. Multidimensional models often use bulk formulation of microphysics and highly simplified, if any, ice nucleation parameterizations, while Lagrangian or parcel models with a refined treatment of microphysical processes are unable to reproduce the interactions among cloud elements. These latter models enhance our understanding of individual processes but they are unable to create a comprehensive picture of ice initiation in a dynamically evolving cloud.

In this study, we attempt to advance our understanding of ice formation mechanisms by removing some of the limitations of previous modeling efforts.

1.2. Research Objectives and Methodology

The goal of this work is to investigate the ice production mechanisms using numerical modeling. The plausibility of various proposed explanations for enhanced ice formation in clouds is to be studied. The three hypotheses to be specifically addressed are:

- The enhanced contact nucleation in dissipating parts of the cloud;
- The increased rate of ice nucleation in regions of high supersaturation;
- The production of ice splinters during riming growth of graupel.

The research is subdivided into four main parts. The first one is to develop a modeling tool, which is adequate to address the research goals. A fairly extensive review of previous observational and modeling work presented in Chapter II, shows that although our understanding of physical processes involved in cloud ice production is by no means complete, the existing knowledge base is broad enough to build a model that combines three-dimensional dynamics, explicit ice and liquid-phase microphysics, and a thorough treatment of ice origination processes. To the author's knowledge no such model exists at present time. The model allows us to investigate the ice nucleation and multiplication processes at a much higher level of sophistication than has been done before. As our main goal is to gain insight into the ice formation, both three-dimensionality and detailed microphysics are crucial for the study.

Once the model is developed, it has to be thoroughly tested. This comprises the second theme of the study. One way to do so is to conduct a case study, or, in other words, to simulate a well-documented event to see if the model can reproduce the basic dynamical and microphysical features of an observed cloud. Two cases are simulated. The first one is a convective cloud that formed over the Magdalena Mountains, New Mexico, on 9 August 1987. The second is the case of a stratiform cloud deck that was observed over the Southern Great Plains (SGP) Atmospheric Radiation Measurement (ARM) site on 7 April 1997. In both instances, clouds were sampled by multiple penetrations of aircrafts equipped with cloud physics and standard meteorological equipment. These observations provide microphysical data allowing for a comparison between simulated and observed clouds.

The third part of the research deals with physical mechanisms and conditions behind the ice enhancement. In particular, we focus on the details of the Hallett-Mossop process, including investigation of the range of cloud drop and ice particle parameters, as well as ambient conditions that favor or inhibit ice multiplication.

In assessing the results of the simulation, it is essential to evaluate the model's sensitivity to various parameters and parameterizations used. This is the fourth main element of the present work. The role of sensitivity tests is at least twofold. Such tests provide a range of possible model results due to uncertainties in the employed parameterizations. Equally important, however, is that through the comparison of model runs with some parameterizations turned on and off we can estimate the relative significance of various physical processes, as well as to get insight into process interaction; something that is extremely difficult if not impossible to do in physical experiments.

These aspects of the sensitivity study are closely related to the interpretation of the results, which is a very important step in both, experimental and theoretical, work. Based on the simulations, a conceptual model of ice initiation is developed and compared to those derived from observations. Finally, the possible reasons for the discrepancy between model results and observation are discussed.

The rest of the dissertation is organized according to the above outline. Chapter II presents a review of earlier ice initiation research and cloud modeling. The model, including the detail on ice parameterization and initialization procedure, is described in Chapter III. Chapter IV outlines the results of a case study of New Mexican cumulus clouds. Ice formation mechanisms operating in such clouds are analyzed in Chapter V, while in Chapter VI, we report model sensitivity to variations in some of the employed parameterizations. In Chapter VII, the role of various ice formation mechanisms is addressed in the case of a stratiform cloud layer. Finally, Chapter VIII provides a brief summary of the whole study and conclusions.

Chapter II

REVIEW

"*Re*-search means *look again*, don't it? Means they're looking for something they found once and it got away somehow, and now they got to *re*-search for it? ... What is it they're trying to find again? Who lost what?"

Kurt Vonnegut, "Cat's Cradle"

2.1. Previous Research on Ice Initiation

An analysis of satellite observations shows that about half of the earth's clouds extend above the freezing level and, therefore, are capable of ice production. The clouds, however, do not glaciate instantly as they are exposed to negative temperatures. Mixed-phase clouds are commonly observed at temperatures down to -20°C and below. Nucleation of ice crystals in clouds may occur either by homogeneous freezing of drops or by heterogeneous nucleation on ice nuclei. The former process is believed to be important at temperatures below about -40°C. This process is essential for cirrus formation but its effect may be neglected for most low and middle tropospheric clouds in mid-latitudes. In this study, we will focus on heterogeneous nucleation, i.e., on ice formation on ice nuclei.

Ice nuclei comprise a special subset of the total atmospheric aerosol, similar to cloud condensation nuclei (CCN). The process of ice nucleation however, is substantially more complicated than the formation of droplets on CCN. There are at least four distinct nucleation modes (or mechanisms) through which IN may operate, compared to the one process of activation of CCN. These modes are (1) immersion-freezing nucleation, (2) deposition nucleation, (3) condensation-freezing nucleation, and (4) contact nucleation. In addition, the activity of IN depends on temperature and supersaturation, while CCN is sensitive primarily only to supersaturation. The improvement of our understanding of ice nucleation mechanisms is important although they are only a part of the puzzle of ice formation in clouds.

As was mentioned in the Introduction, many clouds, particularly at relatively high temperatures (higher than about -15°C), contain IPs in concentrations well in excess of estimated background IN concentration. These clouds are said to exhibit "ice multiplication" or "ice enhancement". Hobbs and Rangno (1985) define the ice enhancement ratio (ER) as the ratio of the maximum concentration of ice particles to the concentration of ice nuclei at cloud-top temperature. It has been found that the ER varies widely from cloud to cloud and often lies between 10 and 10^4, sometimes taking even higher values. If the measurements do not overestimate the IP concentrations, which is almost certainly true, then there are only two possible explanations for this phenomenon.

First, one may assume that most of the ice is generated via primary nucleation and the ER, therefore, should be on the order of unity. This would imply that our present knowledge of IN concentration may be inadequate and that there are, in fact, many more ice nuclei, or nucleation mechanisms are more efficient than is generally believed. Anomalous ice nucleus activity under high supersaturation conditions or in presence of electrostatic charges, as well as production of ice nuclei through the evaporation of cloud drops are among the hypothesis under investigation.

Alternatively, if the estimates of IN concentrations are basically correct then it must be some secondary ice production mechanism that is responsible for ice multiplication. The term "secondary" refers to the process when the production of new ice crystals involves already existing ice particles. This is in contrast to "primary" ice formation, when ice nucleation is governed by liquid and vapor water phases only. Examples of secondary ice production mechanisms include ice splinter production during riming and ice crystal fragmentation.

Let us look in more detail, first, at the various modes of primary ice nucleation and then at the secondary ice production mechanisms.

2.1.1. Primary ice nucleation

The first quantitative description of average spectrum of ice-forming nuclei in the atmosphere probably should be attributed to Fletcher (1962). He combined data from a dozen sets of measurements by various instruments to arrive to now famous exponential expression:

$$N = N_0 \exp(-\beta \cdot T_c), \qquad (2.1)$$

where N is the number of nuclei active at temperature warmer than T_c, T_c is the Celsius temperature, and the values of $N_0 = 10^{-2}$ m^{-3} and $\beta = 0.6$ were suggested. Note that Fletcher did not distinguish between different nucleation modes and used measurements only in -15° to -30°C temperature range. He also noticed large variations in the parameters N_0 and β. In particular, it was common for β to take values between 0.4 and 0.8. N_0 varied even more, sometimes as much as several orders of magnitude.

2.1.1.1. IMMERSION-FREEZING NUCLEATION

Immersion nuclei are immersed in droplets and activate their freezing at specific temperatures. An important distinction of this form of nucleation from the others is that immersion freezing consists of two events separated in time: a nucleus getting into the droplet and freezing of the droplet. For example, an ice nucleus may serve as a cloud condensation nucleus near warm cloud base. The droplets then gets transported by an updraft to the supercooled part of the cloud where it freezes, say, five minutes later. Since it is impossible to keep track of history and composition of all individual droplets, parameterizations of immersion freezing do not consider how ice nucleus gets into droplets. Instead, it is assumed that immersion nuclei are distributed homogeneously throughout liquid cloud water. Thus, larger drops have larger probability of containing an immersion nucleus. It is also assumed that the activity of immersion nuclei increases with decreasing temperature (or increasing supercooling). Constructed in such a way parameterization reproduces two experimentally determined tendencies that more drops of a given size freeze at colder temperature, and that larger drops freeze more rapidly at a given temperature.

The temperature spectrum of immersion nuclei is given by (Vali, 1975):

$$N_{in} = N_{in0}(0.1 \cdot T_c)^{\gamma}, \qquad (2.2)$$

where N_{in} is a number of active immersion nuclei per unit volume of liquid water; $N_{in0} = 10^7$ m^{-3}, $\gamma = 4.4$ for cumuliform clouds, and $N_{in0} = 3 \cdot 10^5$ m^{-3}, $\gamma = 11.4$ for stratiform clouds (Vali 1975). At relatively high temperatures (warmer than -10°C), the concentration of active immersion nuclei is usually much lower than the concentrations of nuclei in other modes.

2.1.1.2. DEPOSITION AND CONDENSATION-FREEZING NUCLEATION

Deposition nucleation is a process when water vapor is absorbed directly onto the surface of nucleus where it is transformed into ice. The environmental vapor pressure must exceed its ice saturation value, but supersaturation with respect to water is not required. Condensation-freezing is a sequence of events when, first, a film of liquid is formed on the surface of the nucleus, and then the condensate freezes. In contrast to immersion freezing, here condensation and freezing occur practically simultaneously. An important distinction from deposition nucleation is that supersaturation with respect to liquid water is necessary for condensation freezing mode to operate. Under these conditions, however, the deposition nucleation may also take place. Therefore, under water supersaturation condition, which is usually satisfied in clouds, it is practically impossible to distinguish between the two mechanisms. In cloud modeling, it is common to use a single parameterization to predict the combined effect of the two mechanisms.

Cotton et al. (1986) combined the temperature dependence of Fletcher (1962) with supersaturation dependence of Huffman and Vali (1973) to get the number concentration of nuclei (N_{dn}) active at the temperature warmer than T:

$$N_{dn} = N_{dn0}\left(\frac{S_i}{S_{i0}}\right)^{4.5} \exp(-0.6 \cdot T_c), \tag{2.3}$$

where $N_{dn0} = 10^{-2}$ m^{-3}; S_i is the fractional supersaturation over ice; and S_{i0} is the value of S_i under the condition of water saturation.

Another parameterization of deposition/condensation-freezing nucleus concentration was proposed by Meyers et al. (1992):

$$N'_{dn} = N'_{dn0} \exp(a + bS_i), \tag{2.4}$$

where $N'_{dn0} = 10^3$ m^{-3}, a=-0.639, b = 12.96. This formulation predicts about $4 \cdot 10^3$ m^{-3} pristine ice crystals due to deposition and condensation freezing at -15°C under water saturation condition. Nucleation is prevented for temperatures warmer than -5°C.

Under conditions of near saturation with respect to water, parameterization (2.3) predicts higher IP concentrations at temperatures below -20°C, while parameterization (2.4) produces more ice crystals at warmer temperatures (above -10°C), with comparable results in-between.

2.1.1.3. CONTACT-FREEZING NUCLEATION

A contact nucleus causes freezing when colliding with a supercooled drop. The role of contact nucleation in cloud glaciation has been the most controversial and needs a more detailed discussion.

Gokhale and Goold (1968) found that silver iodide particles and particles of naturally occurring silicates were much more effective in freezing supercooled millimeter-size water drop by surface contact then when particles were embedded in the drops. Freezing of drops occurred at temperatures five to ten degrees warmer for contact mode than for immersion mode. Micron-size particles appeared to be more effective contact nuclei than submicron particles. Gokhale and Goold also hypothesized that surface nucleation might be fairly intense in mixing regions of cumulus clouds.

In order to describe the rate of drop freezing due to contact nucleation one needs to know not only the concentration of contact nuclei but also the rate at which these nuclei are collected by cloud drops. The determination of this rate is a classical problem of in-cloud scavenging. The mechanisms by which contact nuclei may be captured by cloud droplets or raindrops include aerodynamic (inertial) impaction, Brownian motion, diffusio- and thermophoresis, and electrical interaction. The relative effectiveness of these mechanisms depends on the properties of interacting particles (sizes, electric charges, thermal conductivity, etc.) as well as ambient conditions (temperature, pressure, temperature and vapor gradients between the collecting drop and environment, presence of external electric field, etc.).

One of the earliest theoretical studies on atmospheric scavenging was conducted by Greenfield (1957). He considered capture of aerosol particles by cloud drops through the processes of Brownian and turbulent diffusion and inertial impaction. Diffusion was shown to dominate the capture of particles of radii $r < 0.1$ μm while inertial impaction dominated the capture of larger particles $r > 1$ μm. The two scavenging processes combined were least efficient for particles of radii $0.1 < r < 1$ μm. This window of particle sizes sometimes is called the "Greenfield gap". Neither phoretic nor electrostatic forces were accounted for in Greenfield's calculations. Later studies have shown that in the aerosol size range 0.01 to 1 μm phoretic effects become dominant and cannot be neglected.

Thermophoresis and diffusiophoresis are phenomena in which aerosol motion is induced by gradients in temperature, and concentration of the gas constituents (e.g., water vapor), respectively. The thermophoretic force pushes the particle toward the colder temperature while the diffusiophoretic force is directed toward the lower water vapor pressure. Around an evaporating droplet, diffusiophoresis and thermophoresis work against each other with thermophoresis dominating for aerosol particles smaller than 1 μm. Because nuclei larger than 1 μm are rare in the atmosphere, evaporating cloud drops are more likely to freeze via contact nucleation than the drops growing by diffusion.

The effect of phoretic forces on aerosol particles scavenging by cloud drops was studied by Slinn and Hales (1971). They showed that thermophoresis was a predominant mechanism for below-cloud washout of particles in the size range of 0.01 - 1 μm, where scavenging by inertial and diffusive mechanisms is ineffective. They also pointed to the possibility of enhanced contact ice nucleation resulting from capture of aerosol particles by evaporating droplets.

The idea was further elaborated by Young (1974a). Using Blanchard's (1957) drop freezing data and assuming contact nuclei of 0.3-0.5 μm, he deduced concentration of 10^5 to 10^6 m^{-3} for nuclei active at -4°C. These values are at least two orders of magnitude higher than any other estimates deduced from measurements (e.g., that of Vali 1974, 1976; Cooper 1980; Deshler 1982; Deshler and Vali 1992). It should be noted that in addition to all difficulties of measuring concentration of natural ice nuclei in general, evaluation of concentration of contact nuclei represents even a greater challenge. The reason for additional uncertainty is that nucleation rate of contact mode crucially depends upon nucleus size which is not known and is difficult to measure. Assuming different sizes and therefore different efficiencies of various capturing mechanisms one would deduce values of ice nucleus concentrations that vary by orders of magnitude and, yet, are based on the same data set. For example, Deshler and Vali (1992) reevaluated the Blanchard's experiment assuming nucleus radii of 0.05 μm and found that the required concentration reduces to $2 \cdot 10^4$ m^{-3} for temperature of -4°C. Beard (1992) came to similar estimate for nucleus radii of 0.01 μm. He also showed that if the assumed size is changed to 2-5 μm, only in order of 10^2 m^{-3} of such giant nuclei are needed to explain observed freezing rate. This led Beard to the conclusion that freezing in Blanchard's experiment *"was probably caused by giant rather than small contact ice nuclei, that is, by impaction rather than thermophoresis."*

Carstens and Martin (1982) refined the analysis of relative importance of phoretic processes presented by Young (1974a). They studied the in-cloud scavenging of sub-micron ($0.05 < r < 1$ μm) particles by thermophoresis, diffusiophoresis, and Brownian diffusion. Their result was that even though the diffusive and phoretic effects are not additive, for particles in the studied size range and for typical atmospheric conditions, the phoretically-induced scavenging mechanism almost always dominates that due to diffusion, often by an order of magnitude. They determined that the purely phoretic solution secures a better approximation that superposition of phoretic and diffusive solutions when Péclet number $N_{Pe}>5/4$. (Péclet number shows the relative strength of the particle diffusion and convective transport processes.) Another important conclusion was that only a very small fraction (less than 1%) of scavengable particles is removed during one evaporation cycle of a given amount of liquid cloud water. For example, only 0.16% depletion of aerosol would occur due to the total evaporation of a cloud of liquid water content (LWC) of 1 g m^{-3}, regardless of the undersaturation experienced by the cloud during evaporation. Even though the net thermophoretic velocity of a particle toward the drop is proportional to the temperature gradient, and thus, in a quasi-steady state, to the undersaturation, the total number of scavenged particles is proportional to the total amount of evaporated water and not to the rate of evaporation.

Similar results were obtained by Baker (1991a) who found that if X m^{-3} contact nuclei were present, $5\cdot10^{-4}$ to $5\cdot10^{-3}$ X m^{-3} of ice particles would be formed due to phoretic scavenging during evaporation of 0.2 to 2 g m^{-3} of liquid water. In terms of Carstens and Martin, this corresponds to 0.05 to 0.5 % depletion in aerosol (contact nucleus) concentration.

Beard (1992) also confirmed the two estimates sited above. Furthermore, he evaluates possible mechanisms for enhanced ice nucleation. Among those relevant to contact nucleation are the enhanced capture efficiencies due to electrostatic charge on droplets and enhancement of ice nucleus concentrations through the formation of evaporation nuclei.

Due to the difficulty in distinguishing between different nucleation modes very few measurements of natural contact nucleus concentrations are presently available (Vali, 1974, 1976; Cooper, 1980; Deshler, 1982; Deshler and Vali, 1992). No data exist for temperatures warmer than -10°C. Hence, any extrapolation of found dependencies into this temperature region is of speculative nature.

Young (1974b) parameterized contact nucleus concentration in the form:

$$N_{cn} = N_{cn0}(270.15-T)^{1.3}, \tag{2.5}$$

where T is absolute temperature and N_{cn0}=$2\cdot10^5$ m^{-3} at sea level. Young also assumed that N_{cn0} decreases linearly with height to 10^4 m^{-3} at 5 km. Cotton et al. (1986) assumed aerosol radius of 0.3 μm and N_{cn0}=2·10^5 m^{-3} at all levels. It is now generally agreed that these two parameterizations grossly overestimated the concentration of contact nuclei.

Deshler and Vali (1992) determined average concentrations of contact-freezing nuclei of 1.7·10^3 m^{-3} at -15°C and 3.1·10^5 m^{-3} at -18°C for an assumed nucleus radius of 0.01 μm.

Recently Meyers et al. (1992) analyzed more data that became available after 1974 and offered another parameterization by fitting a function to the measurements of Vali (1974, 1976), Cooper (1980), and Deshler (1982):

$$N'_{cn} = N'_{cn0}\exp(\alpha - \beta T_c), \tag{2.6}$$

where α=-2.80, β = 0.26296 °C^{-1}, and N'_{cn0} =10^3 m^{-3}. A contact-freezing nucleus size of 0.1 μm radius was assumed.

As was mentioned above, evaporating cloud droplets may provide an additional source of IN although this is merely a hypothesis. There is only circumstantial evidence that evaporation ice nuclei exist at all. It is even less clear if these nuclei are active in contact mode. However, evaporation nuclei may provide an attractive explanation for observed ice enhancement. First, this mechanism appears to be fairly general since droplets evaporate in any cloud in great numbers. Secondly, the common locations for ice initiation, e.g., downdrafts, mature and eroding turrets, are also the locations favorable for the formation of evaporation nuclei. Finally, the activity of these nuclei may be enhanced because of the electrical charge accumulated on their surface during evaporation.

The results summarized above make it clear that in order to account properly for contact nucleation a scavenging model is necessary. Models in which all contact nuclei result in formation of ice crystal (e.g., Reisin et al. 1996) largely overestimate the production rate of contact nucleation. In addition, without a scavenging model the size distribution of newly created ice crystals cannot be calculated and has to be specified *a priory*.

2.1.2. Secondary ice production

The hypothesis that nucleation is not the only mechanism of ice production in cloud is almost as old as first measurements of ice nucleus concentrations. Since the early '60s many attempts have been made to gain insight into "ice multiplication". Some key results are summarized here.

2.1.2.1. FIELD EVIDENCE ON ICE MULTIPLICATION

Koenig (1963) studied glaciating of summer clouds in southern Missouri. These clouds contained ice particles in concentrations that are several orders of magnitude greater than could be expected from ice nucleus measurements. Koenig concluded that there was "*apparently a direct relationship between the presence of large liquid drops and high ice particle concentrations in clouds that ultimately glaciate*". It was found that large concentrations of ice particles follow the appearance of precipitation-size drops (about 1 mm in diameter in concentrations of 50 m^{-3}). Another characteristic feature of rapidly glaciating clouds was their pulsating growth.

Mossop (1985) also detected nearly simultaneous appearance of large drops (>300 μm in diameter) and graupel in a small cumulus near Tasmania. The following exponential growth in IP concentration was attributed to the Hallett-Mossop process described below.

Hobbs and Rangno (1985) presented observations of ice particle concentration in 90 cumuliform clouds, both maritime and continental. Ice enhancement was stronger in maritime than in continental clouds. It was most pronounced when cloud top temperature was between -7° and -15°C and almost never was observed in cases when cloud top temperature was < -20°C. The maximum concentrations of ice particles were independent on cloud top temperature, but correlated well with the broadness of the droplet spectrum measured by the threshold diameter (D_T) and with the concentration of droplets > 20 μm diameter. Ice enhancement occurred when the threshold diameter exceeded 20 μm. Telford et al. (1987), using the same data set, showed that the cloud base temperature is as good predictor of ice enhancement as D_T. Cumuliform clouds with top temperatures between -6° and -20°C generally exhibit ice enhancement if the cloud base temperature is warmer than -3°C. Hobbs and Rangno (1985) hypothesize that the mixing near the cloud top first leads to partial evaporation and freezing of a small fraction of drops (approximately 0.1%), possibly by contact nucleation. Large concentration of ice particles is developed then by crystal fragmentation and rime-splintering mechanisms.

A two-stage ice-forming process was again suggested in later studies (Hobbs and Rangno 1990, Rangno and Hobbs 1991, 1994). First, large ice particles (graupel) appear in low concentrations (10^3 m^{-3} or less). Then, high concentrations (10^4 to 10^5 m^{-3} or more) of pristine ice crystals may appear very rapidly near cloud top depending on presence of large droplets in sufficient concentrations.

Hobbs and Rangno (1990) gave an example of small polar maritime cumuliform clouds that rapidly produce extremely high ice particle concentrations (10^5 to 10^6 m^{-3} within about 10 min.). They argued that the riming-splintering mechanism in its present formulation is incapable of such a production rate under conditions observed. Hobbs and Rangno (1990) suggested that high ice particle concentrations might form in localized pockets (presumably not larger that tens of meters wide), where the supersaturation with respect to water is unusually high (~ 5-10 %). There is evidence that the number of active ice nuclei increases greatly with increasing supersaturation. Supersaturation in clouds is not measured. Whether or not a supersaturation higher than 5% may exist in real clouds, even locally, is still an open question. Although some models (e.g., Ochs 1978) predict high supersaturation under specific conditions, these are usually Lagrangian type models that neglect mixing and other dynamical processes that may be important. In more sophisticated and supposedly more realistic two- and three-dimensional cloud models the maximum values of supersaturation with respect to water do not exceed 2-3% even in the regions of large updrafts and intense coalescence (Kogan 1991).

Blyth and Latham (1993) analyzed the development of ice using airborne microphysical measurements from New Mexican summertime cumulus clouds. Multiple penetrations were made through about twenty clouds. It was found that the first measurable ice usually appears when the cloud attains a temperature of -10° to -12°C.

No preferential region of the first ice nucleation in cloud was determined. Blyth and Latham concluded that the Hallett-Mossop process is a plausible explanation for the observed enhanced concentrations of ice. Ice nucleus concentrations were not measured during this study.

Although the above results vary in details, the following common features were observed in all or many cases:

- ice crystal concentration often exceeds IN concentration estimated at cloud-top temperature by up to four orders of magnitude;
- ice crystal concentration shows no clear dependence on temperature;
- first ice is often detected in downdrafts and near cloud top;
- clouds with broader cloud droplet spectra develop ice more rapidly;
- large, drizzle size drops are observed just before intense ice formation;
- graupel particles in relatively low concentration precede the appearance of a large number of pristine crystals;
- high concentrations of ice particles are developed in a short time (sometimes in less than 10 min);
- high concentrations of ice particles occur in small segments of a cloud;
- multi-thermal structure of a cloud contributes to its rapid glaciating.

2.1.2.1. LABORATORY STUDIES ON SPLINTER FORMATION

Hallett and Mossop (1974) reported on laboratory experiments which indicated the production of ice "splinters" when a moving target gathers rime in a supercooled artificial cloud. This was the first convincing demonstration that secondary ice crystals are associated with riming graupel, as had long been suspected. Hallett and Mossop (1974) also found that this phenomenon occurs under a narrow range of conditions. Ice splinters formed only when temperature was in the range - 3° to - 8°C. For target velocity of 2.7 m s^{-1} and temperature of - 5°C, a maximum of about 350 splinters was produced per milligram of rime deposited. As the impact velocity decreased, the splinter production rate reached maximum at around 1.4 m s^{-1} and then fell to zero at 0.7 m s^{-1}. Subsequent experiments (Mossop and Hallett 1974) revealed that the rate of production of secondary ice crystals is not, in general, a function of the rime rate but is proportional to the number rate at which drops with drops diameter larger than 23 μm are accreted. One ice crystal is shed for approximately 160 accreted drops larger than 23 μm.

Later, Mossop (1976) found that the temperature limits (-3° to -8°C) are independent of target velocity over the range 1.4 to 3 m s^{-1}. No splinters were found at temperatures from -8° to -17°C. Mossop (1976) also applied more accurate estimates of collision efficiency to determine that 250 (instead of 160) drops larger than 24 μm must be accreted at a temperature of -5±0.5°C in order to produce one secondary ice crystal.

The precise mechanism of splinter formation, which is often referred to as the Hallett-Mossop (hereafter H-M) process, is not yet known, although several hypotheses have been put forward (e.g., Mossop 1976, Griggs and Choularton 1983, Dong and Hallett 1989, and Mason). Nevertheless, the H-M mechanism is the only ice multiplication process that has a quantitative description thus allowing its incorporation into a numerical model.

2.2. Previous Convective Cloud Modeling

Over the years, many numerical models of convective clouds have been developed. The models cover a wide range of phenomena from non-precipitating boundary layer convection to supercell thunderstorms. They also differ greatly in sophistication of treatment of cloud physics and dynamical processes. According to dynamical framework used, models are usually classified as Lagrangian (parcel) models, one-dimensional models, two-dimensional slab and axisymmetric models, and three-dimensional models. Microphysical treatment in cloud models can be either bulk or detailed (the latter is also often referred to as explicit, spectral detailed, bin or size-resolving). In the bulk approach, the shape of cloud particle spectra is prescribed by a simple analytical function (e.g., monodisperse spectrum, gamma distribution, Marshall-Palmer distribution, etc.) and only one or two parameters or moments of the spectrum are predicted (e.g., mixing ratio and total number concentration). The detailed model, on the other hand, explicitly calculates size distributions of cloud particles of different types. Compared to bulk microphysics, the explicit microphysical treatment requires considerably more computational resources to handle numerous size categories. A compromise has to be reached between microphysical and dynamical approaches. The choice of the appropriate model for each particular study is rather subjective and depends on the goal of the study and available resources as illustrated by the following examples.

Earlier two- and three-dimensional models of cumulus clouds (Steiner 1973, Hill 1974, Lipps and Hemler 1982, Randall and Huffman 1982) used bulk parameterizations of microphysical processes. Ice phase was not considered in all these models (clouds in these simulations barely, if ever, reached the freezing level); neither was it included in three-dimensional simulations of cumulonimbus clouds (Schlesinger 1975, Klemp and Wilhelmson 1978, Clark 1979), or even a supercell thunderstorm (Klemp et al. 1981). The above simulations addressed mostly dynamical aspects of cloud development and produced reasonable results although ignoring the ice-phase processes was hardly justified in the latter studies.

Dynamical behavior of non-precipitating cloud with little or no ice is determined mostly by environmental thermodynamic conditions and supply of water vapor. Using a bulk microphysics for this type of problems may be justified because it allows one to increase spatial resolution, to employ better parameterization of subgrid processes, and to run models for longer periods of time. An example of such an approach is the work of Carpenter et al. (1997) who used a three-dimensional nested-grid model with 50 m maximum resolution to study entrainment in small cumulus clouds. A new and quite elaborate initialization procedure was applied in order to generate a realistic cloud. The cloud was sustained by the prescribed surface heat and moisture fluxes. A simple Kessler-type bulk parameterization of the condensation process did not allow precipitation or ice formation. Consequently, these aspects were not addressed in the study. The work, however, is of particular interest to us since clouds simulated in Carpenter et al. (1997) preceded the formation of a cloud we are studying here (the case of 9 August 1987).

Although some dynamical aspects can be addressed using models with only warm microphysics, the incorporation of ice-phase processes is required to study the precipitation formation in supercooled clouds. Cotton (1972) developed a Lagrangian model with bulk microphysical parameterization that incorporated ice phase. In the '80s and '90s a number of multi-dimensional models included bulk parameterization of ice-phase processes (e.g., Bennetts and Rawlins 1981, Farley and Orville 1986, Cotton et al. 1986, Straka 1989, Wang and Chang 1993, Murakami et al. 1994, Ferrier 1994). The models predicted mixing ratios and, in some cases, number concentrations of the cloud and ice particles. A comparison between various bulk ice schemes by McCumber et al. (1991) indicated that reasonable agreement between simulated and observed hydrometeor structures (as, e.g., manifested by radar reflectivity) is often obtained only after adjustment of numerous coefficients in the parameterizations. Furthermore, it is shown that better results are obtained if different parameterizations are used for different types of convection (e.g., tropical maritime vs. midlatitude continental storms).

Many of the deficiencies of bulk parameterizations come from assuming an analytical size distribution for cloud and precipitation particles. Detailed microphysics removes this restriction but requires prediction of many additional variables. Therefore, early simulations of detailed microphysics of mixed-phase clouds were limited to Lagrangian and one-dimensional models (Young 1974, Scott and Hobbs 1977). Takahashi (1976) and Hall (1980) were among the first to incorporate explicit liquid and ice-phase microphysics into a two-dimensional dynamical framework.

Hall (1980) divided the size range of ice particle spectra into three regions: ice crystals, graupel, and transitional particles. Each region contained several size categories and had prescribed particle growth characteristics. Two-dimensional slab symmetric simulations of a continental cloud included the ice-phase processes of diffusional and non-stochastic accretional growth. The formation of graupel was analyzed and the following scenario was proposed. Ice crystals nucleated in the upper portion of the cloud first experience diffusional growth and, in about 400 s, reach diameters larger than 300 μm when they start grow by riming. As ice crystals are carried downward by vertical motions, some of them are incorporated into the adjacent updraft region with larger liquid water content where the preferential riming takes place. Consequently, the maximum concentrations of the largest ice particles are found within and near the edges of the updraft regions. At later times, the maxima of graupel concentration correspond to the maxima in the LWC. The overall ice formation was very weak even though the cloud top temperature was below -30°C. Nucleation of ice crystals was parameterized by a simple prescribed temperature dependency. Ice multiplication processes were not considered in the model. Due to the insufficient ice production, warm rain processes dominated precipitation formation, which was thought to be unrealistic for this type of continental clouds. Unfortunately, this very interesting model did not receive further development.

An explicit microphysical approach was used by Khain and Sednev (1996). Their one-dimensional time-dependent model employs seven size distribution functions to describe water drops, ice crystals of columnar, plate-like, and dendrite shapes, snowflakes, graupel, and frozen drops. Comparison between model runs for liquid only and mixed-phase clouds indicate that ice-phase processes increase the duration of rainfall.

One of the latest developments in simulation of mixed-phase convective clouds is the model of Reisin et al. (1996). The model includes a thorough treatment of all major microphysical processes by considering time and space evolution of size distribution functions for water drops, ice crystals, graupel and snow particles. The size distribution function for each type of particles is divided into 34 spectral bins, and two moments (number and mass concentration) are independently calculated in each spectral category. While removing the constraint of constant average mass within each size category, the two-moment approach doubles the number of microphysical variables compared with the one-moment method. Thus, the advantages of multi-moment approach come at the expense of a simplified dynamics. In Reisin et al. (1996), for example, the dynamics is limited to the axisymmetric framework that carries with it all the problems of two-dimensional treatment of fundamentally three-dimensional turbulence and also precludes any simulations in a sheared environment.

Neither Khain and Sednev (1996), nor Reisin et al. (1996) included the H-M multiplication process. In addition, both models assume that all contact nuclei produce ice crystals of the smallest resolvable size when in fact, first, only few percent of these nuclei result in freezing drops, and, second, frozen drops of various sizes may be produced.

Chapter III

MODEL DESCRIPTION

"When we mean to build,
We first survey the plot, then draw the model;
And when we see the figure of the house,
Then must we rate the cost of the erection."

William Shakespeare, "King Henry IV"

The dynamical framework of the model and the liquid-phase microphysics are fully described in Kogan (1991), where the reader can find details of theoretical formulation and employed numerical techniques. Below is a brief description of the basic features of the dynamical framework and formulation of the liquid-phase processes. Newly developed ice-phase microphysics and initialization procedure are described in more detail.

3.1. Dynamical Framework

The nonhydrostatic momentum equations are used in an anelastic form of Ogura and Phillips (1962). The numerical algorithm is designed as following. First, the advective and turbulent transport of thermodynamic variables, such as temperature, moisture, and momenta are calculated using the alternating direction implicit method. The predictor-corrector scheme used in time integration increases stability of calculations and insures second-order accuracy in time (Kogan 1991). The multidimensional positive definite advection transport algorithm (Smolarkiewicz 1984) is employed in calculation of advection of microphysical variables. Once the dynamical tendencies of all variables are determined, they are used and adjusted in quasi-Lagrangian calculations of the microphysical processes. Using new values of thermodynamic variables, the elliptic Poisson equation for a pressure perturbation is solved by the two-step implicit successive overrelaxation method (Kogan 1991). Finally, the resultant wind field is obtained by adding pressure gradient terms to each of the three wind components.

A uniform grid spacing of 100 m is used throughout the domain 7.5×7.5×7.5 km. Time steps of 5 s and 0.2 s are used in dynamical and microphysical calculations, respectively. Up to one hour of cloud evolution is simulated during each of the model runs.

3.2. Liquid-Phase Microphysics

Liquid-phase cloud physics processes are treated explicitly based on the prediction equations for cloud condensation nuclei (CCN) and cloud drop spectra. A mass distribution function containing 28 categories in the size range from 8 to 4096 μm is used to describe cloud droplet and raindrop spectra in each grid point. A separate distribution function for CCN that are represented by 12 categories in the 0.015 to 2.6 μm size range is a distinctive feature of this model. It eliminates the need for parameterization of the spectrum of newly activated droplets. The latter is determined based on the critical supersaturation and the equilibrium radius of "wet" nuclei as described in Kogan (1991). In addition, a parameterization of the CCN regeneration process has been utilized, by which drops smaller than the minimal resolvable size in an unsaturated environment are replaced by nuclei according to an algorithm which insures the conservation of the total number of CCN and cloud droplets during the condensation/evaporation process.

Processes of nucleation, diffusional growth/evaporation, and coalescence are formulated as described in Kogan (1991). The stochastic coagulation equation is solved numerically using a procedure similar to that of Berry and Reinhardt (1974) with collision efficiencies tabulated in Hall (1980).

3.3. Ice-Phase Microphysics

The formulation of ice-phase microphysics is much more complex than that of the warm rain processes. With accuracy sufficient for most cloud modeling applications, all properties of a cloud drop (growth/evaporation rate, fall velocity, Reynolds number, etc.) can be derived from a single parameter such as drop mass. In the case of solid hydrometeors, however, a variable bulk density and a great variety of shapes provide many possible combinations for IP properties.

3.3.1. Particle properties

In the current version of the model, the mass range of IPs is discretized in the same manner as that of liquid drops using 28 categories with mass doubling every other category. Due to computer limitations, we consider only one type of IPs for each size category. The smallest 15 categories of IPs are considered as ice crystals while the largest 13 categories are considered as graupel. For the case study of New Mexican cumuli, this approach is justified by observations of Blyth and Latham (1993), Raymond and Blyth (1989), and Dye (1983). They found that most common precipitation particles in this type of clouds are graupel. Also, since the most important initial diffusional growth of ice crystals occurs in the temperature range -8° to -15°C, it is reasonable to assume that small ice crystals have the plate-like shape. The plate density ρ_C equals to 0.9 g cm^{-3} (Heymsfield 1972) while the dimensional relationship is taken from Pruppacher and Klett (1997). This relationship leads to the expressions for the plate diameter (d) and the thickness to diameter ratio ($e = h/d$) in terms of crystal mass (m):

$$d = 7.476\, m^{0.408}, \qquad e = 0.0041\, m^{-0.0225}, \tag{3.1}$$

where d is in centimeters and m is in grams.

The plate diameter ranges from 9.2 to 486 μm. The terminal velocities of the crystals are determined by the procedure described in Pruppacher and Klett (1997). Graupel particles are assumed to be spherical (e=1) and have the density of 0.4 g cm^{-3}. Their sizes vary from 0.34 to 5.56 mm.

3.3.2. Water vapor deposition and sublimation

The sublimation/evaporation rate for an individual IP of mass m is given by

$$\left(\frac{dm}{dt}\right)_c = \frac{4\pi C D_v F_v}{\left(\frac{R_v T}{e_{si}} + \frac{L_s^2 D_v F_v}{R_v T^2 k_a F_h}\right)} \cdot \left(S_i - \frac{L_s Q_h}{4\pi C k_a F_h R_v T^2}\right), \tag{3.2}$$

where S_i and e_{si} are the supersaturation and saturation vapor pressure over ice; T is the temperature; L_s is the latent heat of sublimation; Q_h the additional heat source (e.g., due to water freezing during riming); C is the capacitance of the crystal; D_v and R_v are the diffusivity and specific gas constant of water vapor; k_a is the thermal conductivity of air;

F_v and F_h are ventilation coefficients for vapor and heat diffusion, respectively. For crystals of a plate-like form the capacitance is

$$C = \frac{d}{2}\frac{\varepsilon}{\sin^{-1}\varepsilon}, \qquad \varepsilon = 1-\left(\frac{h}{d}\right)^2, \tag{3.3}$$

where h is the crystal thickness and ε is the eccentricity. For a spherical particle, C reduces to the particle radius.

Similarly to the quasi-Lagrangian representation of the condensation process for cloud drops (Kogan 1991), remapping of the mass distribution function to the Eulerian size space is done only at the end of the dynamical time step while mass change in each size category is calculated using (3.2) for each microphysical time step. In each of these sub-steps, the right hand side of (3.2) is adjusted using dynamical and microphysical tendencies. This approach requires calculation of new values of C as a function of m for each size category at each microphysical step. Instead of using (3.1) and (3.3), which would require expensive calculations of transcendental functions, a best fit in the form

$$C = 1.908\, m^{0.384} \tag{3.4}$$

is used in the model. Here C is in centimeters and m is in grams. For the considered range of ice crystal sizes, (3.4) is accurate to within 5% (Fig. 3-1). Considering that the dimensional relationships in (3.1) are only approximations themselves, we believe that parameterization (3.4) is sufficiently accurate to be used in the model.

The ventilation coefficient for vapor diffusion, F_v, is expressed in the form (Pruppacher and Klett 1997):

$$F_v = \begin{Bmatrix} 1+0.14X^2, & X \geq 1.0 \\ 0.86+0.28X, & X \geq 1.0 \end{Bmatrix} \tag{3.5}$$

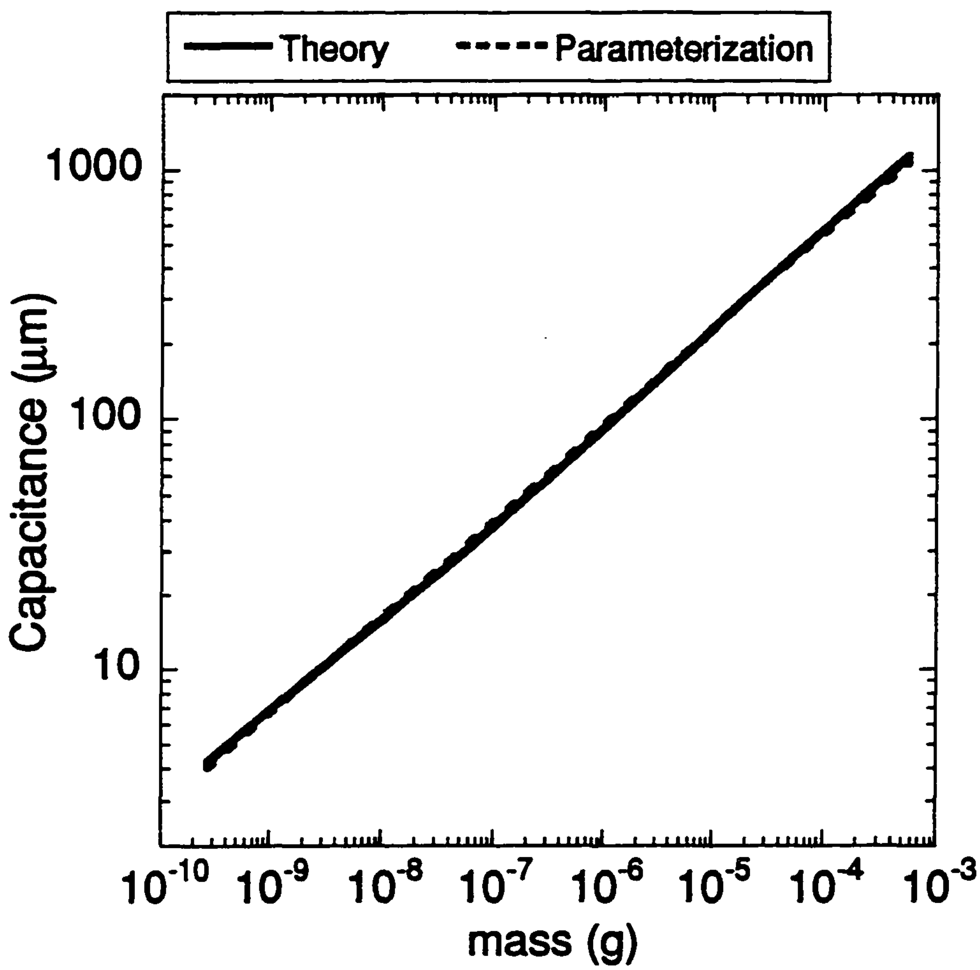

Figure 3-1. Comparison of parameterized, as described by (3.4), and full theoretical, as described by combination of (3.1) and (3.3), expressions for capacitance of plate-like crystals.

where $X = Sc^{1/3}Re^{1/2}$, $Sc = \nu_a / D_v$ is the Schmidt number, and $Re = L^* V_c / \nu_a$ is the Reynolds number; ν_a is the kinematic viscosity of air; V_c is the particle's fall velocity; and $L^* = \Omega_c / P_c$ is the length scale for a particle with the surface area Ω_c and perimeter P_c. The ventilation coefficient for heat diffusion, F_h, may be obtained from the expression for F_v by substituting Prandtl number $Pr = \nu_a \rho_a c_p / k_a$ for the Schmidt number; ρ_a and c_p are the density and specific heat of air, respectively.

3.3.3. Ice-liquid and ice-ice interactions

The interaction among IPs and cloud drops through collision-coalescence processes is very important in convective clouds. Starting from a certain size, graupel particles grow primarily by riming. Large drops collecting small ice crystals may freeze and become new riming centers resulting in an explosive secondary ice production. It is therefore imperative to account for ice-drop interactions in the model. Unfortunately, the information on interaction between liquid and ice cloud particles is rather scarce. Both experimental and theoretical studies on the collection efficiencies cover a limited range of particle sizes and shapes.

There are two situations where the ice-drop interaction appears to be of primary importance in small cumuli studied here. In the first one, a graupel particle is collecting cloud droplets up to 40 μm in diameter. Pflaum and Pruppacher (1979) used the UCLA Cloud Tunnel to determine the collection kernels of graupel collecting cloud droplets and compared those with theoretical collection kernels for large drops collecting small droplets derived by Beard and Grover (1974). It was found that regardless of whether the collector was a graupel particle or a water drop, the collection kernel is dependent on the collector's momentum and the cloud droplet size. For particles of equivalent masses, the momentum of a raindrop is greater than the momentum of a graupel because the former falls faster. Sedimentation velocities for graupel vary greatly depending on shape and density of the particles but are usually 20 to 50% smaller than the terminal velocities of drops of equivalent mass. This means that the collection kernel for graupel is 50 to 80% of that for raindrops.

A second case of interest is when a large drop collides with a small ice crystal (splinter) to become a new graupel particle. A relevant study here is that of Lew and Pruppacher (1983) who investigated the collision efficiency of small columnar ice crystals captured by large drops. Using a theoretical model, they found that except for small needles (columns with length to diameter ratio greater than 10 and mass smaller than 10^{-8} g) the collision efficiencies were generally about 10-20% smaller than the collision efficiencies for spherical particles of equivalent masses.

Taking into account the above findings, as a first approximation we prescribe the collection kernel for ice-drop interaction to be proportional to the collection kernel for drop-drop interaction. The coefficient of proportionality is initially set to 0.8. The sensitivity of the model to this coefficient has been studied and will be discussed later. All drops collected by a riming IP are assumed to freeze instantly; wet growth is not considered in the model.

The collection efficiency for ice-ice type interaction is specified equal to that for drops of corresponding masses. The contribution of these interactions to IP spectra evolution is minimal due to relatively low concentrations of IP compared to the drop concentrations. For simulation of clouds where snowflake (aggregates of ice crystals) and hail formation is important the parameterization of ice-ice interaction needs to be revised.

Melting is treated in a simplified way by instantaneous conversion of all IPs into drops of corresponding mass at the first grid level below 0°C isotherm. While not adequate for all applications, we consider this parameterization to be appropriate for the purpose of present study. This is because the observed ice particles in clouds we are simulating are of such types and sizes that they are likely to melt within the distance smaller or comparable to the model's vertical resolution after falling through the 0°C isotherm. A more sophisticated procedure is required if the model is to be used in simulations of more vigorous, heavily raining, or hail bearing clouds.

3.3.4. Primary ice nucleation

All basic mechanisms of ice nucleation are considered in the model including activation of immersion-freezing, deposition, condensation-freezing, and contact-freezing ice nuclei.

3.3.4.1. IMMERSION-FREEZING NUCLEATION

It is assumed that immersion nuclei are distributed homogeneously throughout liquid cloud water and increase their activity as temperature decreases. The first assumption means that the freezing probability is proportional to the drop's mass or volume. As mentioned in previous chapter, constructed in such a way the parameterization reproduces two experimentally determined tendencies that more drops of a given size freeze at colder temperature, and that larger drops freeze more rapidly at a given temperature.

The temperature spectrum of immersion nuclei is given by (Vali 1975):

$$N_{in} = N_{in0}(0.1 \cdot T_c)^{\gamma}, \tag{3.6}$$

where N_{in} is a number of active immersion nuclei per unit volume of liquid water; T_c is the Celsius temperature (°C); and $N_{in0} = 10^7$ m^{-3}, $\gamma = 4.4$ (Vali 1975). Concentration of drops frozen via this process is usually small compared to the concentration of IP generated by the other two nucleation modes. This is especially true for temperatures warmer than -10°C.

3.3.4.2. Deposition and condensation-freezing nucleation

Following Meyers et al. (1992) the combined concentration of deposition and condensation-freezing nuclei in the model is given by

$$N_{dn} = N_{dn0}\exp(a + bS_i), \tag{3.7}$$

where $N_{dn0} = 10^3$ m^{-3}, a=-0.639, b = 12.96. This formulation predicts about four pristine ice crystals per liter due to deposition and condensation freezing at -15°C under condition of water saturation. Nucleation is arbitrarily prevented at temperatures warmer than -5°C. Ice crystals formed by this mechanism are assumed to be of the smallest size resolvable by the model.

IN concentration is not a predicted variable in the model. It means that ice nuclei are not subject to advection and N_{dn0} is constant in time and space. The number of the newly activated ice crystals at each time step in a particular grid point, ΔN_{dn}, is determined from

$$\Delta N_{dn} = \left(\frac{\partial N_{dn}}{\partial S_i} \right) \cdot \Delta S_i \quad , \tag{3.8}$$

where ΔS_i is a change of supersaturation over ice during a time step at this point. New ice crystals are formed only when S_i increases over a time step. In addition, for the nucleation to occur, either the point must be saturated with respect to liquid water, or hydrometeors of any type, liquid or frozen, must be present.

3.3.4.3. CONTACT NUCLEATION

Due to the difficulty in distinguishing between different nucleation modes very few measurements of natural contact nucleus concentrations have been conducted. Recently Meyers et al. (1992) analyzed nearly all available data and offered a parameterization by fitting a function to the measurements of Vali (1974, 1976), Cooper (1980), and Deshler (1982):

$$N_{cn} = N_{cn0} \exp(\alpha - \beta T_c), \tag{3.9}$$

where N_{cn} is a number concentration of contact nuclei active at temperature T_c (in degrees Celsius), α=-2.80, $\beta = 0.26296$ °C^{-1}, and N_{cn0} =10^3 m^{-3}.

It should be noted that although there is evidence that this nucleation mode may operate at temperature close to zero, no data exist for contact nucleus concentration at temperatures warmer than -10°C. Hence, any extrapolation of the found dependency into this temperature region is speculative. In the model, the contact nucleation is prohibited at temperatures warmer than -3°C. A contact-freezing nucleus radius of 0.3 μm is assumed in present simulation.

Unlike deposition or condensation-freezing nuclei, the presence of active contact nuclei does not automatically lead to formation of IPs. For a supercooled water drop to freeze, it must first collide with a contact ice nucleus. These collisions are prompted by Brownian diffusion, thermophoresis, diffusiophoresis, and inertial impact. In order to properly account for the contact nucleation rate, scavenging of aerosol has to be modeled. Because of the chosen size of contact nuclei of 0.3 μm, the effect of the inertial impaction is negligible.

Following Young (1974a), we define the relative collection rate as the number of collection events per unit drop number concentration per unit time.

The relative collection rate for Brownian diffusion, F^{BR}, is

$$F^{BR}=4\pi r_d D_c \left(1+0.3\,\mathrm{Re}^{0.5}\,\mathrm{Sc}^{0.33}\right) N_{cn}\,, \tag{3.10}$$

where r_d is the radius of a collecting drop, Re and Sc are the Reynolds and Schmidt numbers respectively; N_{cn} is the concentration of contact nuclei; and D_c is the diffusivity of the nuclei in the air given by

$$D_c=\frac{\kappa T\left(1-\mathrm{Kn}\right)}{6\pi r_{cn}\eta_a}\,, \tag{3.11}$$

where κ is the Boltzman's constant; η_a is the dynamic viscosity of air; the Knudsen number, Kn, is defined as the ratio of the mean free path of air molecules, λ, to the particle radius, r_{cn}, $\mathrm{Kn}=\lambda/r_{cn}$.

For thermophoresis

$$F^{TH} = \frac{F_i L_e}{p}\frac{dm}{dt}\left(1+0.3\mathrm{Re}^{0.5}\,\mathrm{Pr}^{0.33}\right)N_{cn}, \tag{3.12}$$

where p is the atmospheric pressure; L_e is the latent heat of vaporization; (dm/dt) is the condensation/evaporation rate; and Pr is the Prandtl number. The factor F_i is defined as

$$F_i = \frac{0.4\left[1+1.45\mathrm{Kn}+0.4\mathrm{Kn}\exp(-1/\mathrm{Kn})\right]\left(k_a+2.5\mathrm{Kn}\,k_{cn}\right)}{\left(1+3\mathrm{Kn}\right)\left(2k_a+5\mathrm{Kn}\,k_{cn}+k_{cn}\right)}, \tag{3.13}$$

where k_a and k_{cn} are the thermal conductivity of air and ice nucleus, respectively.

For diffusiophoresis

$$F^{DF} = 4\pi r_d D_v\left(1+0.3\mathrm{Re}^{0.5}\,\mathrm{Sc}^{0.33}\right)\left(\frac{M_a}{M_w}\right)^{0.5}\left[q_v - q_{vs}\exp\left(\frac{L_e^2\rho_w}{R_v k_a T^2}r_d\frac{dr_d}{dt}\right)\right]N_{cn}, \tag{3.14}$$

where q_v is specific humidity; q_{vs} is water saturation specific humidity; ρ_w is the liquid water density; M_a and M_w are the molecular masses for air and water, respectively; R_v is the specific gas constant for water vapor; T is the temperature.

The total collection rate, F^{tot}, is defined as the sum $F^{tot}=F^{BR}+F^{TH}+F^{DF}$. When F^{tot} becomes negative it is set to zero which means that none of the contact nuclei is collected and no freezing occurs.

3.3.5. Secondary ice production

Hallett and Mossop (1974) reported on laboratory experiments which indicated the production of ice "splinters" when a moving target gathers rime in a supercooled artificial cloud. This was the first convincing demonstration that secondary ice crystals are associated with riming graupel, as had long been suspected. It was also found that this phenomenon occurs under a narrow range of conditions. Following Hallett and Mossop (1974) and Mossop and Hallett (1975), the conditions for secondary IP production are set as follows. At temperature -5°C, one splinter (ice crystal of the smallest resolvable size) is created for every 200 drops with diameter greater than 24 μm collected by riming graupel. This maximum splinter production rate decreases linearly toward both ends of the -3° to -8°C temperature interval as in Cotton et al. (1986). No splinters are produced outside this temperature range. The effect of the impact velocities is neglected in this study.

The distinct feature of the presented model is that the rime rate is directly calculated by solving the stochastic collection equation for drops and ice particles with size distributions that are explicitly predicted in the model. No assumptions on the shape of particle spectra are made.

Even though the precise mechanism of splinter formation, is not yet known the H-M process remains the only ice multiplication process that has a quantitative description allowing its incorporation into a numerical model. Other ice multiplication mechanisms may be incorporated when theoretical and experimental studies provide firmer background for their parameterization.

3.4. Initial and Boundary Conditions

Special attention is given to initialization procedure to ensure that the model generates a cloud with realistic geometry and dynamical parameters. A common procedure to initiate convection in cloud models is to specify perturbations in the initial temperature and/or moisture fields in a form of a positively buoyant bubble. This approach is appealing, particularly for studies focusing on microphysics, because it produces a cloud rapidly and at the prescribed location. The drawback, on the other hand, is that the size and magnitude of the perturbation specified without taking into account the environmental characteristics may lead to unrealistic model response.

We specify the scale and intensity of the initial thermal perturbation based on the boundary layer similarity theory. The procedure is similar to that of McNider and Kopp (1990) with the exception that we introduce a random part to the specified perturbation. The initial thermal perturbation, is therefore given by

$$\theta'(x,y,z)=A\sigma_\theta(z)\exp\left(-\frac{(x-x_0)^2+(y-y_0)^2}{0.5\lambda}\right), \tag{3.15}$$

where λ is a horizontal length scale of the perturbation, σ_θ is the standard deviation of thermal fluctuations in the boundary layer, x_0 and y_0 are the coordinates of the center of the perturbation. The horizontal length scale, λ, is assumed to be the wavelength of the maximum density spectra for temperature fluctuations and is approximated by $\lambda= 1.5\ z_i$, where z_i is the boundary layer height. The parameter A indicates the magnitude of the perturbation relatively to the mean of the temperature fluctuation distribution. Although specified in a somewhat ad-hoc manner, this parameter allows for a clear physical interpretation. For instance, A=2 means that the selected perturbation is two standard deviations above the mean value and, therefore, is in the top 2% of all fluctuations. To introduce inhomogeneities at scales smaller than λ, we re-write A as $A= A_0 + A_1\alpha(x,y)$, where A_0 and A_1 determine the magnitudes of larger and smaller scale components of the perturbation, respectively, and $\alpha(x,y)$ is the random number in the range -1 to 1. In a simulation presented here A_0 =3 and A_1 =1. The standard deviation, σ_θ, is related to the surface heat flux, H, as (McNider and Kopp 1990):

$$\sigma_\theta(z) = 1.34 z^{-\frac{1}{3}} \left(\frac{H}{\rho c_p} \right)^{\frac{2}{3}} \left(\frac{\theta}{g} \right)^{\frac{1}{3}}, \tag{3.16}$$

where z is the height, ρ is the air density, c_p is the specific heat capacity, θ is the potential temperature, and g is gravity acceleration. The surface heating is an external parameter in our model. Perturbation to the initial moisture field is such that the relative humidity is horizontally uniform throughout the domain at the beginning of the integration.

An alternative approach to the bubble initialization procedure is to provide a surface heat and moisture fluxes that can be either specified or calculated using surface layer parameterization and surface energy balance. Recently, Carpenter et al. (1997) showed that placing several regions of surface heating within the domain for the first hour and a Gaussian shape heat source in the middle of the domain thereafter could generate realistic convective clouds. The former served to introduce turbulent motions and to generate a well-mixed boundary layer while the latter promoted the cloud to be studied. Results of the first two hours of the simulations, however, had to be discarded making this technique computationally too expensive to be applied in the present study.

The model allows for either periodic or open lateral boundaries with the former used in simulations of stratiform clouds and the latter applied in convective cases. The horizontal velocity components are subject to the free slip boundary condition at the lower boundary.

Chapter IV

SIMULATION OF A CUMULUS CLOUD: CASE OF 9 AUGUST 1987

HAMLET:	Do you see yonder cloud that's almost in shape of a camel?
POLONIUS:	By th' mass, and 'tis like a camel, indeed.
HAMLET:	Methinks it is like a weasel.
POLONIUS:	It is backed like a weasel.
HAMLET:	Or like a whale?
POLONIUS:	Very like a whale.
HAMLET:	... They fool me to the top of my bent.

William Shakespeare,
"The Tragedy of Hamlet, Prince of Denmark"

In this Chapter, we present a numerical simulation of summertime New Mexican mixed-phase cumulus clouds. During August of 1987, an extensive field experiment involving the NCAR King Air airplane was conducted to investigate the development of morning storms over the Magdalena Mountains. Our numerical study of ice development is based on observations from this program. Several aspects contributed to this choice. First, the cloud studied in the program often exhibited ice enhancement. Secondly, these clouds were of moderate vertical extension with limited precipitation and little electrification present, making them suitable for aircraft sampling. The NCAR King Air airplane was fully equipped with cloud physics and standard meteorological equipment, thus providing measurements that allow for a comprehensive comparison between simulated and observed clouds. Microphysical instrumentation onboard the aircraft included a Forward Scattering Spectrometer Probe (FSSP), a 200X 1D probe, a 2DC (cloud) probe, and 2DP (precipitation) probe. Finally, the focus of the observations was on ice and precipitation development; very well inline with the goals of this study.

This allows us to use not only raw, but also processed data and to check if model results agree with generalizations made on the basis of the measurements. The detailed information about the field project, in general, and instrumentation, in particular, was reported by Blyth and Latham (1993) and Blyth et al. (1997). In addition, a numerical study of ice-free clouds for two of the days was performed by Carpenter et al. (1997). We confine our study to simulation of the cloud developed over the Magdalena Mountains in the afternoon of 9 August 1987.

4.1. Model Initialization

The model was initialized as described in Chapter III. The initial environmental conditions are set by the sounding constructed primarily from aircraft observations in the vicinity of the cloud observed over the Magdalena Mountains on August 9, 1987 (Fig. 4-1). A well-mixed boundary layer of the depth z_i =1.6 km is specified in the lower part of the troposphere to account for convective activity that occurred earlier that day (Carpenter et al. 1997). The corresponding horizontal scale for the initial temperature perturbation, $\lambda = 1.5\, z_i$, is equal to 2.4 km. The surface heating, H, in (3.16) is set to H = 450 W m^{-2}. This large flux, which is somewhat greater than the average value for the region, is necessary to generate a vigorous first turret in a stagnant and cloud free initial model environment.

CCN measurements are not available for this particular day. The assumed activation spectrum for CCN is shown in Figure 4-2. It is close to the typical spectrum for a moderate continental cloud (Twomey and Wojciechowski 1969). Number

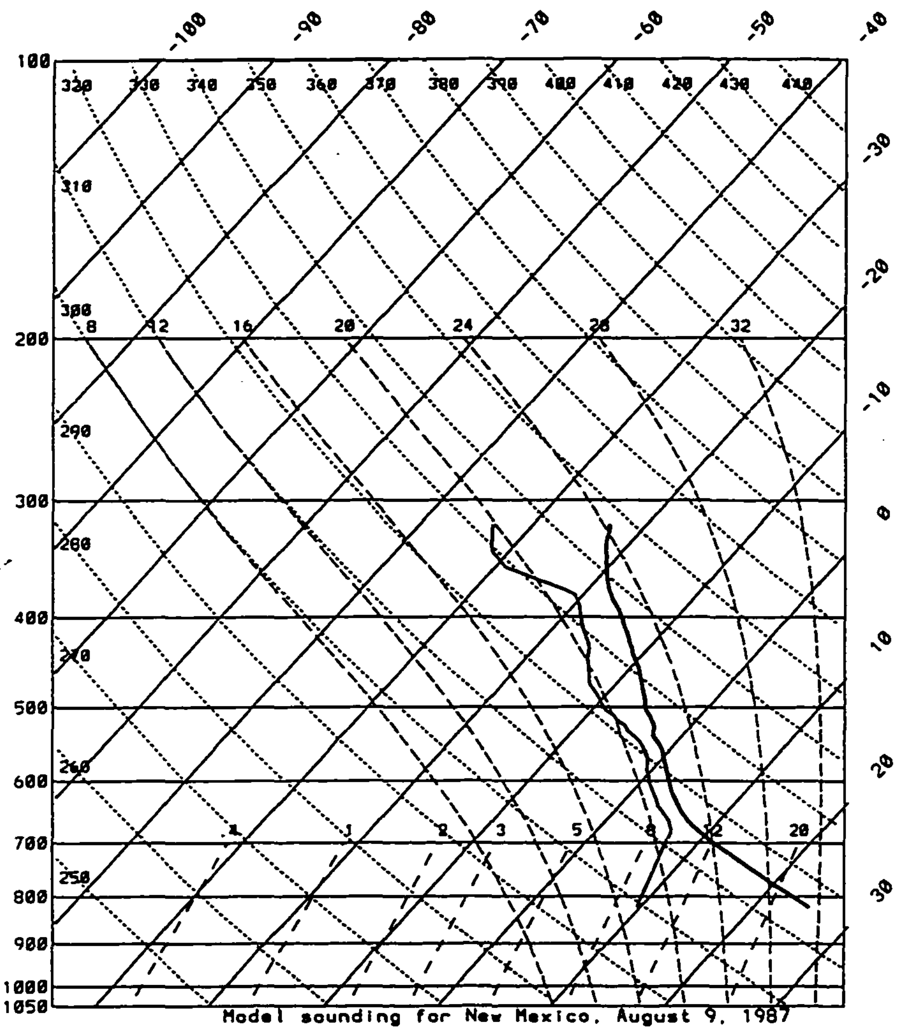

Figure 4-1.Skew-*T* log-*P* diagram of environmental conditions for the 9 August case study. Temperature and dew point temperature profiles are represented by thick and thin lines, respectively. The skewed abscissa is temperature (°C) and the ordinate is pressure (mb). Short-dashed lines labeled in Kelvins represent dry adiabats, while curved long-dashed lines labeled in °C are pseudoadiabats. Straight dashed lines are the lines of constant saturation water vapor mixing ratio, with values labeled in g kg^{-1}.

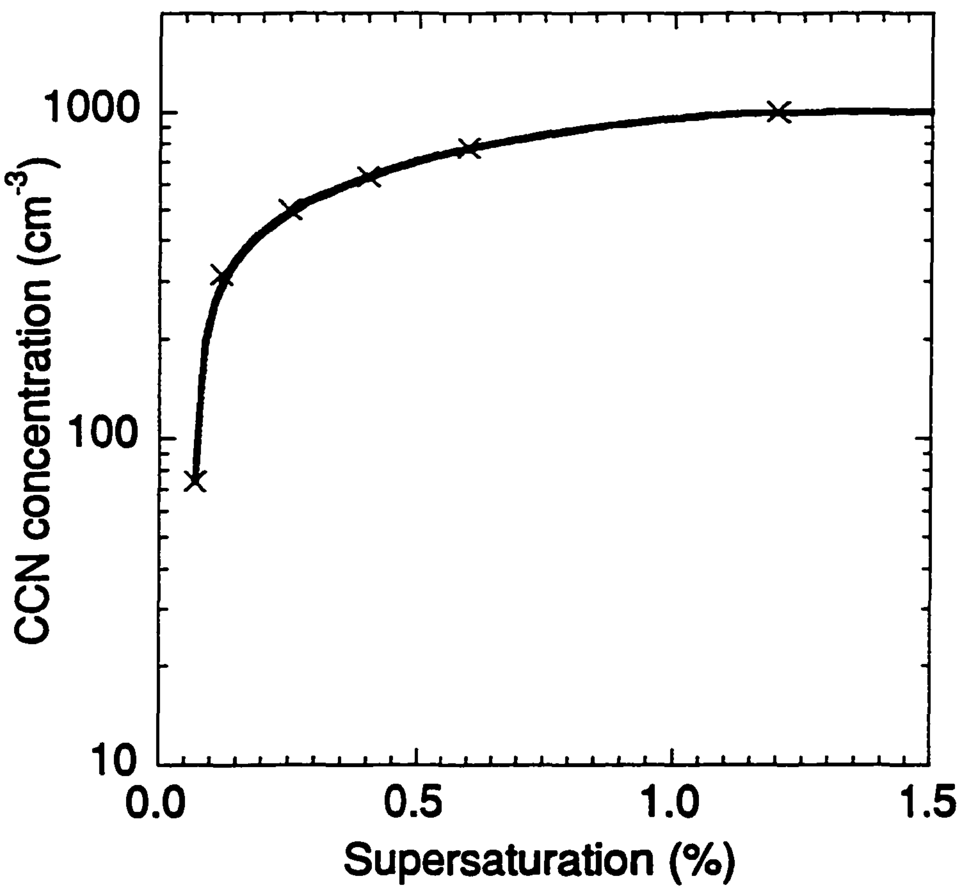

Figure 4-2. Cloud condensation nucleus concentration as a function of supersaturation required for activation. Crosses show the representation of the spectrum in the model using 12 size categories of CCN. The largest six categories are activated at supersaturations less than 0.05% and are not shown.

concentration of CCN often decreases with height. The microstructure of a relatively short living cumulus originating from a rising thermal, however, is determined mostly by CCN characteristics at cloud base, which in this case is just above the well-mixed boundary layer. Thus, at the beginning of the integration, CCN distribution is spatially uniform throughout the computational domain.

4.2. Comparison with Observations

Models utilizing the bubble initialization procedure are known to suffer from producing tall undiluted turrets due to lack of entrainment (Carpenter et al. 1997). By introducing a random component to the initial perturbation, as described in Section 3.4, we largely alleviate this problem by promoting more efficient mixing at earlier stages of cloud development.

The general view of the simulated cloud at five-minute intervals is shown in Figure 4-3. The cloud is characterized by a three-dimensional structure and deviates substantially from a "bubble-like" or mushroom shape typical to axisymmetrical models or models using axisymmetrical initial perturbations (Ovtchinnikov et al. 1995, Reisin et al. 1996). The effect of new initialization procedure, however, is not limited to the improved appearance of the simulated cloud. As we will see, the physics has also been strongly affected. In particular, the entrainment has been enhanced.

A common technique to describe the effect of mixing is to look at the departure of the liquid water content, L, from the adiabatic values, L_a (Warner 1970, Cotton 1975, Blyth and Latham 1990). Figure 4-4 shows observed and simulated profiles of the ratio L / L_a. Only cloudy points where $L > 0.1$ g m^{-3} were used in averaging procedure for

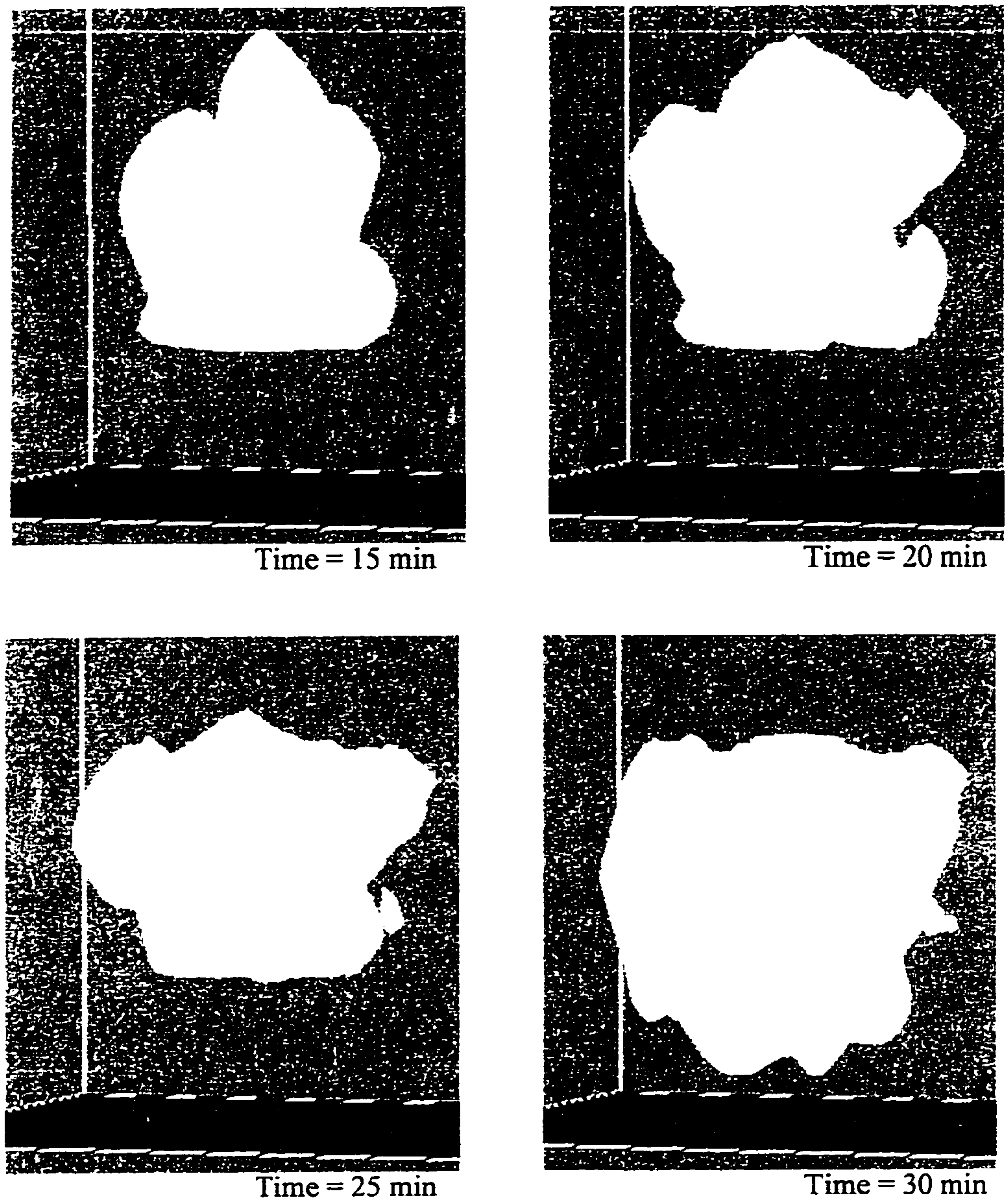

Figure 4-3. General view of the simulated cloud at various stages of its development. Cloud boundary is defined as 0.001 g m^{-3} isosurface of liquid water content. Axes are shown in white and the bottom of the domain is darkened. Only part of the model domain is shown to enhance the cloud structure. Time elapsed from the beginning of the integration is indicated below each image.

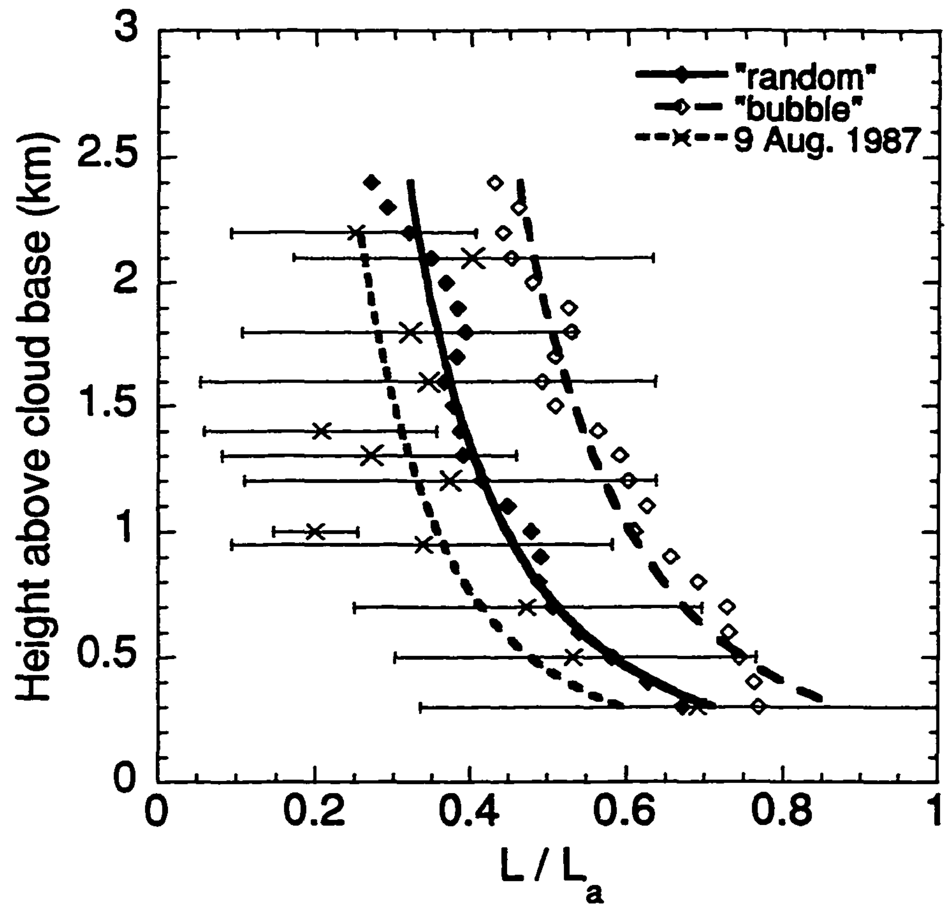

Figure 4-4. Ratio of the mean liquid water content at a given height above cloud base to the adiabatic value. Crosses mark data from aircraft penetrations, diamonds are from the two model runs. For each set of data, best-fitted power curves are also shown. See text for details.

both simulated and observed clouds. Aircraft measurements from all penetrations on August 9, 1987 are averaged over 10 mb thick slabs (about 200 m). Each cross in Figure 4-4 represents an average of 10 to 225 points, with larger symbols corresponding to the levels with larger pools of measurements. Since the cloud-base height changed little during that day (Blyth and Latham 1993, Carpenter et al. 1997), it is assumed the same for all penetrations. Two simulated profiles correspond to model runs with axisymmetrical initial perturbation ("bubble") and with randomly modified initial perturbation ("random"). The predicted profiles represent averages over the three simulated clouds that are 20, 25, and 30 minute old. Such averaging, makes the comparison with the experiment more justified, since the age of sampled clouds is not known precisely. Standard deviations for model data from both runs are not shown but they are of the same magnitude as for penetration averages. Despite the large scatter in the measured L to L_a ratio, Figure 4-4 illustrates that introduction of a random component to the initial thermal perturbation results in a simulated cloud in which liquid water content is less adiabatic and much closer to the observed values.

Unlike L, vertical velocity averaged over the cloud width, W, shows no consistent variation with height (Warner 1970). In addition, W varies with time for any given altitude within the cloud. It is therefore difficult to make unambiguous and meaningful comparison aside from notion that both simulated and observed clouds had one major updraft region surrounded by downdrafts. This general observation is illustrated by two successive penetrations for which one-second averages of liquid water content and vertical wind are plotted in Figure 4-5. In the middle of a growing cloud, the core with high values of liquid water content and high updraft velocity is well

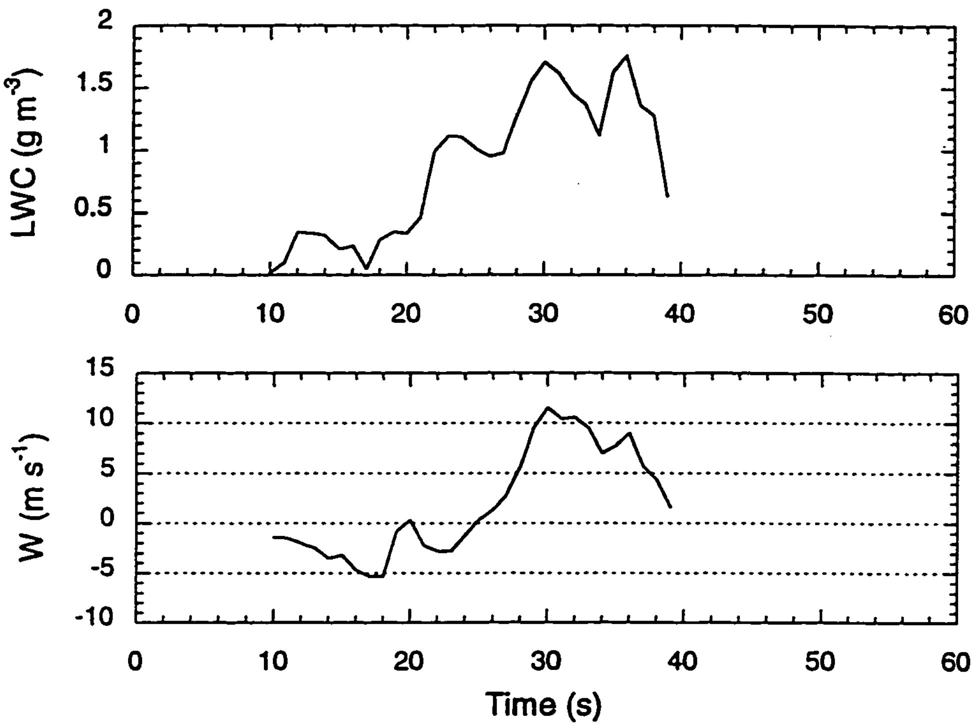

(a)

Figure 4-5. Liquid water content (LWC) and vertical wind (W) measured in two aircraft penetrations at 1851 (a) and 1857 GMT (b). Note that 10 seconds represents approximately 1 km of flight. LWC is derived from the FSSP. Penetrations were made at levels where temperatures were -1.5°C (a) and -7°C (b).

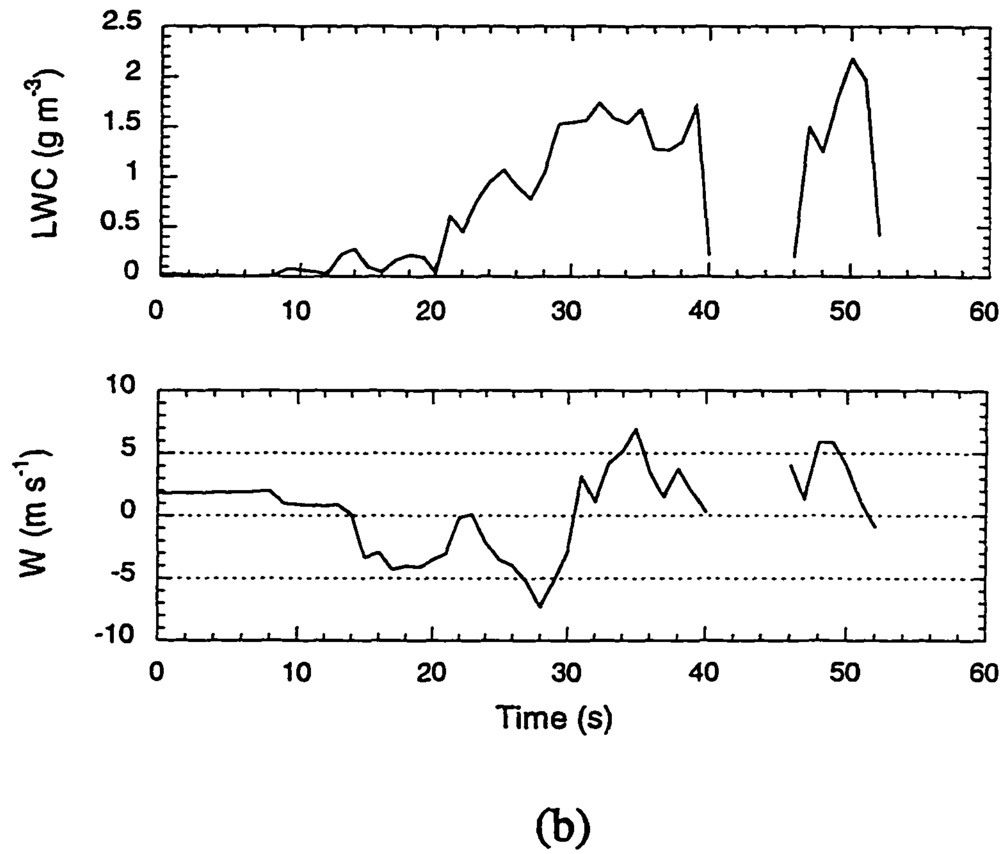

Figure 4-5 (continued).

defined (Fig. 4-5a). In the upper part of the cloud, downdrafts are more comparable to the updrafts in both occupied area and magnitude (Fig. 4-5b). The figure also shows good correlation between maximum vertical velocity and higher values of liquid water content.

While we cannot expect the model to mimic the nature exactly, it is important that the simulation reproduces closely the key bulk cloud properties. Since the development of the first steady-state one-dimensional models of convective clouds, researches have been looking for a meaningful way of comparison of simulation results with observations (Warner 1970, Cotton 1975). Although a large body of data has been collected and the quality of observations has significantly improved over last decades, aircraft measurements remain a random sampling of fields that are highly variable in time and space. Models, on the other hand, despite their ever increasing level of sophistication, still have limited resolution and are unable to fully reproduce natural variability, especially at smallest observable scales (currently, on the order of one meter). Thus, the comparison between models and observations is reduced mostly to the maximum values of some bulk properties and vertical profiles of horizontally averaged quantities. Several characteristic features of the simulated and observed clouds are compiled in Table 4-1.

The heights of cloud top and cloud base are the most readily observed features of cumulus clouds. Estimates of cloud-top altitude and temperature, shown in Table 4-1, are believed to be accurate to within 200 m and 2°C, respectively (Blyth and Latham 1993). In the model, the vertical extent of the cloud is controlled primarily by the environmental sounding, which determines the size of the initial boundary layer

Table 4-1. Simulated versus observed cloud properties.

	Observed	Simulated
Cloud-base altitude (km AGL)	1.7	1.8
Cloud-base temperature (°C)	7.4	7.3
Maximum cloud-top altitude (km AGL)	5.7*	5.6
Minimum cloud-top temperature (°C)	-15.0*	-13.8
Maximum cloud width (km)	4.5	4.1
Maximum vertical velocity (m s^{-1})	11.5	12.9
Minimum vertical velocity (m s^{-1})	-6.0	-5.5
Maximum LWC (g m^{-3})	2.5	4.2
Maximum cloud drop concentration (cm^{-3})	597	892
Maximum ice particle concentration (L^{-1})	38†	52

* estimate

† derived from the 2DC probe

disturbance among other parameters (see Section 3.4). The simulated cloud-top and cloud-base heights and temperatures match closely the observations, indicating that the sounding used in initializing the model is representative. The satisfactory agreement in the maximum cloud width also supports the chosen horizontal scale for the initial perturbation.

The somewhat large difference in maximum values of LWC might be expected taking into account limitations of cloud sampling by the aircraft. The aircraft was likely to miss regions of least diluted cloud-base air. In addition, there was no sampling of the upper portion of the cloud with the highest penetration at the level of about 4.3 km, or more than 1 km below cloud top.

For the same reason of scarcity of observations, it should be expected for the model data to have greater values of the vertical velocity, concentrations of cloud drops and ice particles, etc. In addition, as noted by Blyth and Latham (1993), actual ice particle concentrations are presumably higher than the reported values derived solely from the 2DC probe. Since this probe is unable to resolve particles smaller than 25 μm, a number of small ice crystals (splinters) may remain undetected.

At about 30 min, first precipitation is observed just below the base of the simulated cloud (Fig. 4-3d). Some of this precipitation reaches the ground several minutes later. Although most of the clouds observed during the field program also precipitated (Blyth and Latham 1993), no information is available on temporal and/or spatial distribution of precipitation on the ground. Therefore, a meaningful comparison between model output and observation is not possible in this aspect.

When comparing model results with observations one should keep in mind that the observed cloud system went through several cycles of growth and decay. There were times when more than one turret was rising from the same cloud, as well as when new turrets ascended through the remains of their predecessors. Altogether, the cloud system persisted for several hours. The active stage of the simulated cloud, on the other hand, lasted only for about 40 min. This agrees well with the lifetime of each individual turret. Furthermore, most observed turrets, including the one that produced the highest ice concentration, had only one well defined updraft region with downdrafts at cloud sides as we have seen in Figure 4-5. Thus, the present study can be viewed as a simulation of the most vigorous thermal-like turret. The effect of the debris of earlier clouds on microphysics of their successors may also be quite important and warrants further investigation in a separate study.

4.3. General Features of the Simulated Cloud

Time evolution of various model parameters is shown in Figure 4-6. As positively buoyant bubble accelerates upwards, the maximum vertical velocity in the domain increases from 0 to its maximum value of 13 m s^{-1} at 10 min. Maximum downdraft velocity lags updrafts by about 7 minutes. Throughout much of the cloud life cycle and especially in first 20 minutes, updrafts are much stronger than downdrafts. They are also narrower. This shows up in a vertical profile of skewness of vertical velocity (Fig. 4-7) which is positive throughout the cloud at the early stages of cloud development.

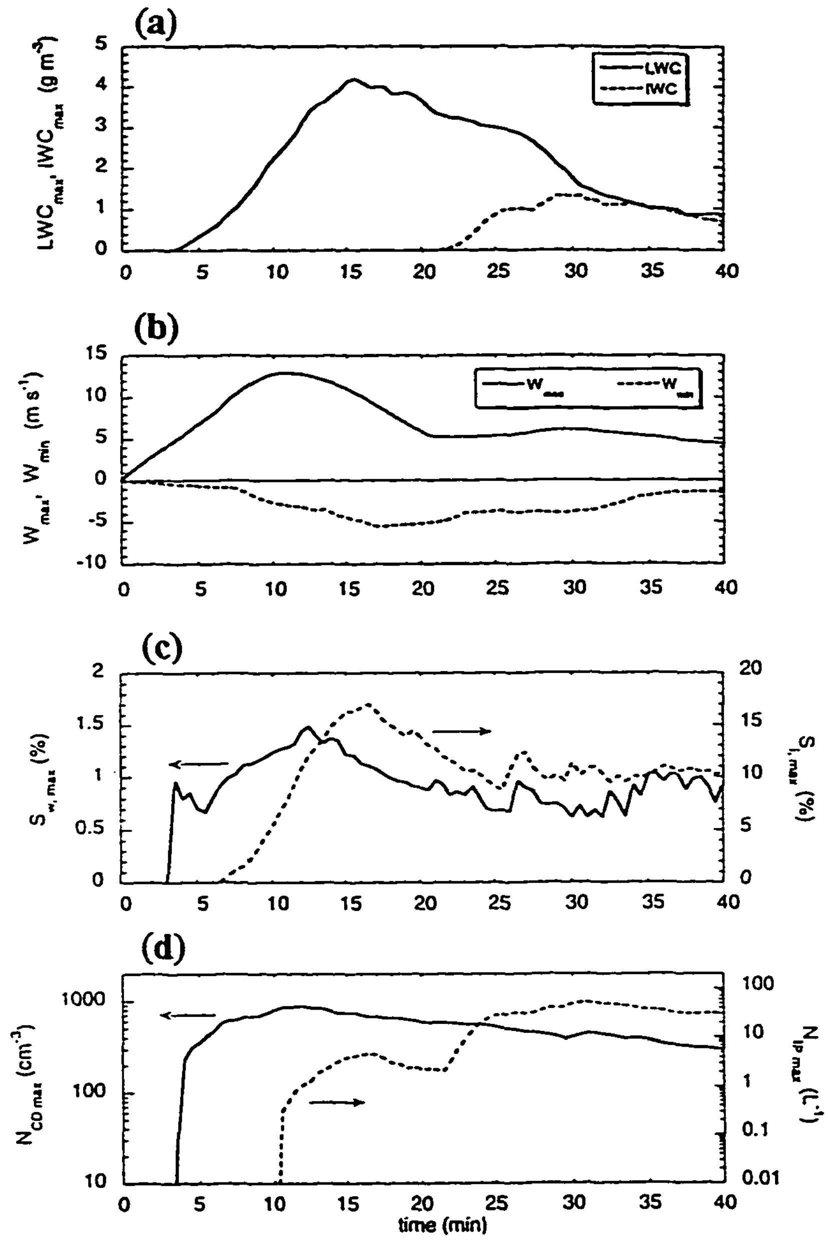

Figure 4-6. Time series of domain maxima of (a) liquid and ice water content (LWC_{max} and IWC_{max}, respectively); (b) updraft (W_{max}) and downdraft (W_{min}) speed; (c) supersaturation with respect to liquid water ($S_{w,max}$) and ice ($S_{i,max}$); and (d) concentration of liquid drops ($N_{CD,max}$) and ice particles ($N_{IP,max}$).

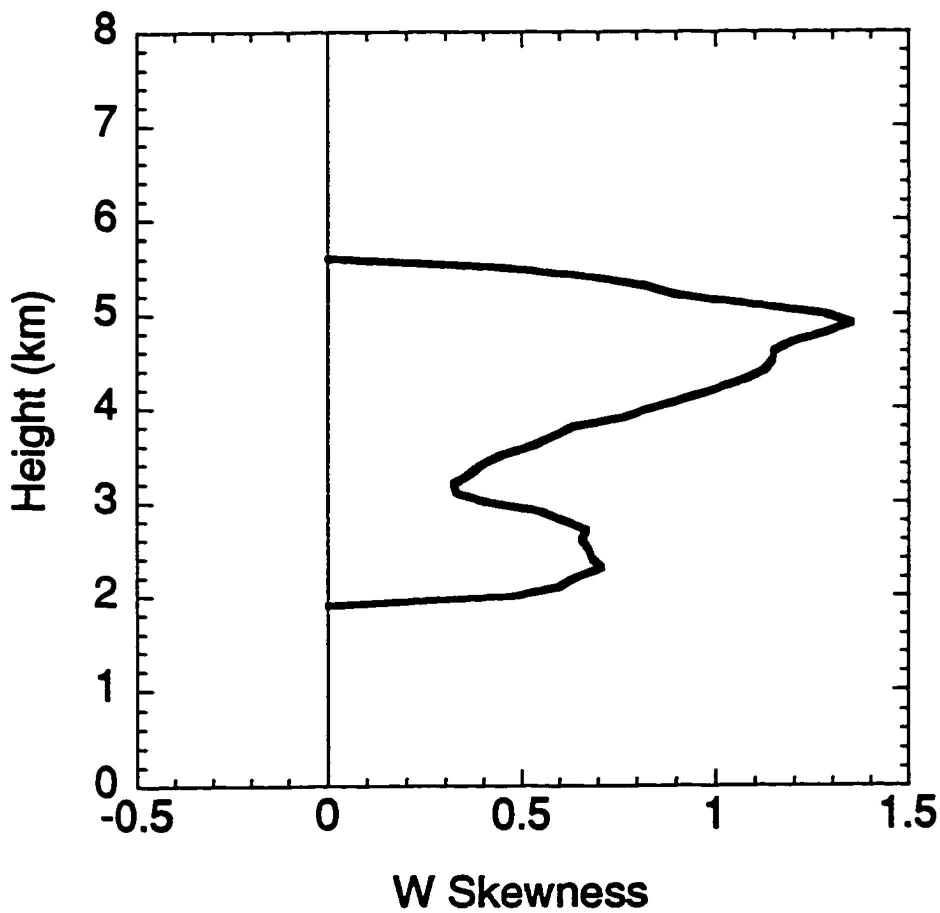

Figure 4-7. Vertical profile of the vertical velocity skewness at 20 min. Statistics is for cloudy points only.

Within four minutes into the simulation, the water vapor pressure reaches its saturation level for the first time, and condensation starts. From this point on, the maximum liquid water content (LWC) steadily increases to its maximum of 4.2 g m^{-3} at 15 min (Fig. 4-6). After that, the maximum LWC gradually decreases. The decrease becomes more rapid between 25 and 30 min, possibly due to intense liquid to ice conversion. During this period, maximum ice water content increases to about 1 g m^{-3}.

Evolution of supersaturation with respect to liquid water, $S_{w,max}$, correlates well with variation of maximum vertical velocity (Fig. 4-6). Predicted maximum of $S_{w,max}$ is 1.5% at 12 min. After that, time maximum supersaturation fluctuates between 0.5 and 1%. The model gives no indication of increase of $S_{w,max}$ in later times. Suggestions have been made that supersaturation may increase locally (in pockets tens of meters wide) to values of 5 to 10 and possibly up to 15 per cent with the beginning of intense coagulation between drops (Rangno and Hobbs 1991). Such an increase would have an important implication on ice nucleation (Baker 1992). Although current model resolution would not allow direct simulation of such small features, results suggest that the existence of pockets of highly enhanced supersaturation in isolated continental cumuli is rather unlikely. In relatively shallow thermal-like clouds, first precipitation particles form in the upper and outside portions of the cloud where updrafts, if any, are extremely weak. By the time large drops enter the main cloud core, either descending from above or through lateral entrainment, the main updraft is reduced substantially in both the magnitude and vertical extent. Therefore, at no point cloud elements containing large drops rise fast enough and long enough to produce unusually high values of supersaturation. Possibility still exists for the formation of region of increased supersaturation in maritime cumuli and in multithermal clouds or embedded convection. Maritime clouds with low concentration of cloud droplets may be able to produce precipitation particle earlier in their life span when updrafts are still strong. In case of embedded convection, rising cloud elements may encounter regions of preexisting large drops left by their predecessors. Whether any of these hypotheses works, must be determined in future studies.

Under condition of saturation with respect to liquid water, supersaturation with respect to ice increases as temperature decreases. Because $S_{w,max}$ deviates little from zero in the simulation, maximum supersaturation with respect to ice, $S_{i,max}$, is related more to the cloud-top temperature rather then to vertical velocity. $S_{i,max}$ has its maximum of 17% shortly after 15 min (Fig. 4-6) when cloud top reaches its highest position. The following subsidence of the cloud top reduces $S_{i,max}$ to about 10%. After that $S_{i,max}$ stays virtually unchanged until the end of the run.

The time evolutions of maximum concentrations of liquid drops and IPs are shown in the bottom panel of Figure 4-6. During the first twelve minutes, as the increasing updraft speed drives supersaturation with respect to liquid water to its highest value, the concentration of cloud droplets rises quickly from zero to nearly 900 cm^{-3}. After 15 min, fewer and fewer CCN are activated in response to weakening updrafts and reduced supersaturation. Consequently, the maximum drop concentration gradually decreases due to coalescence process, evaporation caused by either downdrafts or entrainment of dry air, and due to large drop fallout.

The time evolution of maximum IP concentration (Fig. 4-6) reveals two distinct stages of ice production; each dominated by a different process. The first increase in the number of IPs is due to primary ice nucleation. This process in a sense is similar to the activation of CCN; the number of newly activated ice crystals at this stage is determined primarily by the increasing supersaturation with respect to ice. The second much stronger rise in maximum IP concentration is a result of the H-M mechanism. Contribution of each of these mechanisms will be discussed in detail in the next chapter.

Between 30 and 40 min, the cloud enters the dissipation stage when all parameters change less rapidly.

4.4. Timing Tests

The improved physical formulation in the detailed microphysical model comes at the expense of increased computational cost. In the model employed in this study, for example, we use 12 categories to describe CCN, 28 for liquid drops, and 28 for ice particles - the total of 68 microphysical variables compared to just a few used in bulk parameterization. The CPU time that is required only for advection of all microphysical variables can easily exceed the computational expenses for the whole bulk microphysics model. Note that in order to eliminate the production of unrealistic negative values, positive-definite numerical schemes are preferred for advection of scalars, such number concentration of cloud particles in any particular size bin. However, such schemes, as for example, the algorithms of Smolarkiewicz (1984) or Smolarkiewicz and Grabowski (1990) used in this study are computationally demanding. Detailed microphysical calculations also take more time than calculations of bulk condensation and autoconversion. The question then arises as to the practicality of models with explicit microphysics.

Timing test for a model with liquid-phase microphysics was conducted by Kogan (1991). Since that time, the progress in computer technology has made possible to increase significantly the domain size and model resolution, as well as the number of microphysical variables. The results of the timing tests similar to that of Kogan (1991) for the current version of the model are presented in Table 4-2. Two tests have been conducted. In the first one, coordinate splitting one-dimensional positive definite advection transport algorithm (Smolarkiewicz 1984) is applied successively to calculate advection along the three spatial axes. In the second case, a three-dimensional nonoscilatory version of the scheme is used (Smolarkiewicz and Grabowski 1990).

The relative contributions of different processes obviously vary with the evolution of the cloud due to changes in cloud size and its composition (i.e., liquid, ice, or mixed-phase). The specific figures in Table 4-2 are for the simulation time of 1200 s when the cloud is already well developed and ice started to form.

Addition of the ice phase increases significantly the time of microphysical calculations. In contrast to ~58% in the simulation of liquid clouds (Kogan 1991), the simulation of the mixed-phase microphysics requires almost 93% of the CPU time. Note that the amount of the CPU time for some of the processes has increased by a factor greater than two. For instance, the coalescence process includes now ice-ice as well as ice-drop interactions in addition to the drop-drop collisions. In addition, a fairly expensive parameterization of aerosol scavenging has been added to the model. Most of these calculations have been combined into the "nucleation-condensation" category in Table 4-2, which is now the most time consuming segment of the model. In the liquid-phase model, coagulation was the CPU intensive microphysical process.

Table 4-2. Results of the timing test.

Process	% of the total		
	Present test with 1-D advection	Present test with 3-D advection	Kogan (1991) test
Advective and turbulent transport of the thermodynamic variables	*2.9*	*0.7*	*31.1*
Solving Poisson equation for pressure and calculation of pressure gradient force	*3.8*	*1.3*	*6.1*
Total for the dynamical part of the model	**6.7**	**2.0**	**37.2**
Advective and turbulent transport of the microphysical variables	*26.4*	*80.7*	*37.1*
Microphysical processes:			
Nucleation, condensation, and evaporation	30.2	8.2	5.3
Coagulation and breakup	25.1	6.5	15.2
Other	11.0	2.5	0
Total for the microphysical part of the model	**92.7**	**97.9**	**57.6**
Other (input/output, statistics, etc.)	**0.6**	**0.1**	**5.2**
Total per time step	**100.0**	**100.0**	**100.0**

The timing tests and numerical simulations were performed on a rather slow by today's standards DEC Alpha 150 MHz workstation. For the model with 75×75×75 grid points it takes about 100 hours of CPU time to run the model for one hour which is usually enough to study the evolution of an isolated convective cell. For coarser resolution (250m on 30×30×30 grid) the time is reduced to about 4 hours which makes such simulations suitable for numerous sensitivity tests. Much faster workstations are now available. In addition, the advection of many scalar fields, as well as microphysical calculations can be easily parallellized. Even with the current CPU expense, however, the simulations are still practical, given the fact that most of the modeler's time is spent on analysis of the huge volume of data generated by the model with the explicit microphysics.

Although detailed microphysics gradually finds its way into mesoscale modeling, the possibility of its use in forecast application is still very remote. Research oriented case studies, on the other hand, do not have many stiff restrictions of operational forecasting and have extremely wide possibilities for use of explicit microphysical formulation.

Chapter V

ICE FORMATION MECHANISMS

> "How this came about was a mystery. The theoretical villain, however, was what Dr. Breed called "a seed". He meant by that a tiny grain of the undesired crystal pattern. The seed, which had come from God-only-knows-where, taught the atoms the novel way in which to stack and lock, to crystallize, to freeze."
>
> *Kurt Vonnegut*, "Cat's cradle"

The model incorporates several ice production mechanisms. In this Chapter, we will look at how each of these contributes to ice formation in a simulated cloud. The time evolution of maximum ice crystal concentration (solid curve in Figure 5-1) clearly shows the two distinct stages of ice production. First increase in the number of IPs between 10 and 15 minutes is due to primary ice nucleation, while the second peak around 25 min is a result of the H-M mechanism. We will now look closely at each of these processes.

5.1. Ice Particle Nucleation

Among the three mechanisms of primary ice nucleation considered in the model the deposition and condensation-freezing mode is the most efficient in the present simulation. Figure 5-1 shows that until 20 min this type of nucleation dominates ice production. According to (3.7), the nucleation rate is greater when the supersaturation over the ice is large. Since the predicted water vapor pressure within the cloud deviates very little from its saturated value over liquid water, this means that the nucleation rate increases with decreasing temperature, or increasing height. The temperature

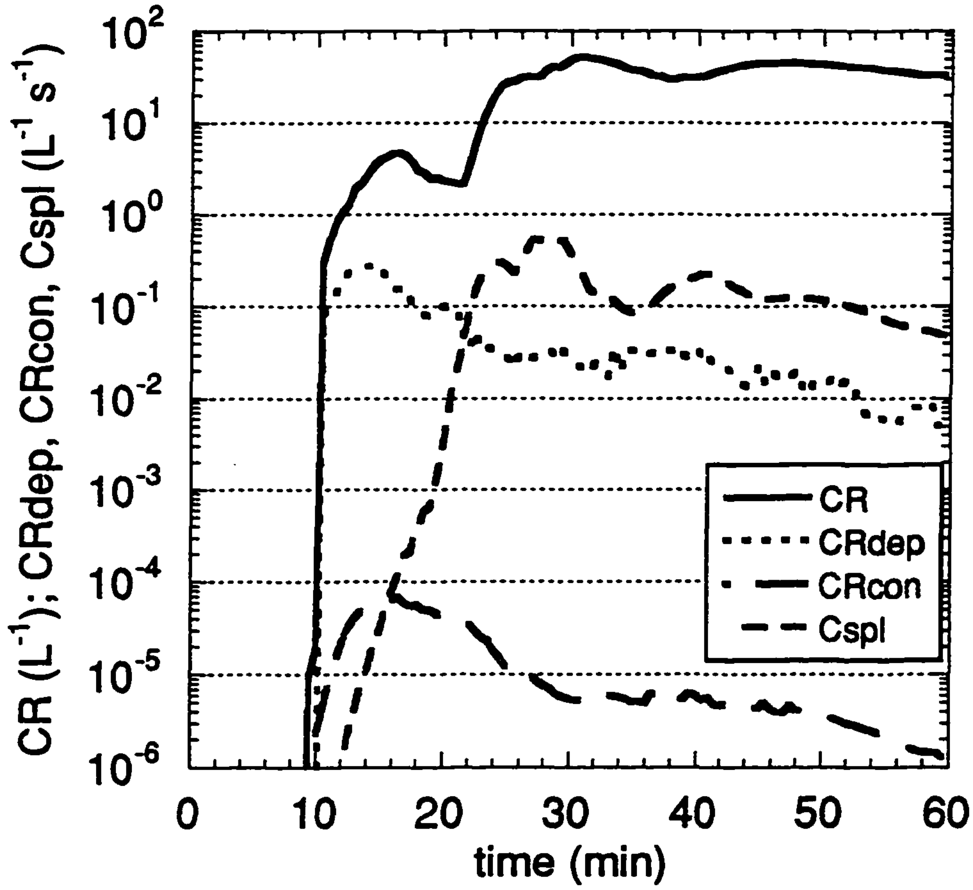

Figure 5-1. Time evolution of the maximum IP concentration (labeled CR), maximum IP production rates for deposition and condensation-freezing nucleation (CRdep), contact nucleation (CRcon), and maximum splinter production rate due to the Hallett-Mossop process (Cspl).

dependence in (3.7) (through S_i) is rather weak, however. This results in fairly uniform distribution of newly nucleated IPs throughout the upper portion of the cloud (Fig. 5-2b). At lower levels, there are few IPs along the side of the cloud while the middle portion of the cloud is virtually ice free (Fig 5-3b). The initial size of nucleated ice crystals is only 8 μm in the model, and probably even smaller in reality. This, together with relatively low concentrations (10^3 m^{-3} or less), suggests that these particles most likely would not be detected with existing instrumentation. It takes time for new ice crystals to grow to detectable sizes. At 15 min. into the simulation, as the cloud top ascends to its highest level, the maximum IP concentration reaches the value of about $4 \cdot 10^3$ m^{-3} (Fig. 5-1). After that, the nucleation of new ice crystals weakens due to the decreasing updraft and subsequent decrease in supersaturation.

The next stage of cloud evolution is very important in ice development, although the maximum IP concentration remains nearly constant, or even slightly decreases during this period. After small pristine ice crystals are formed, they begin to grow, mostly through deposition of water vapor. Because of the small sedimentation velocity, these particles are carried along with the flow from the region of their formation in the upper portion of the cloud (Fig. 5-2b) towards the cloud edges and downdraft regions (Fig. 5-4a) where they descend to lower levels (Fig. 5-2d). As the area occupied by downdrafts expands and updrafts in the upper portion of the cloud weaken (Fig. 5-4c), more IPs are transported to lower levels (Fig. 5-3d). Although downdrafts are not necessarily saturated with respect to liquid water, they are still likely to be supersaturated with respect to ice (Fig. 5-5). Thus, the diffusional growth of ice crystals

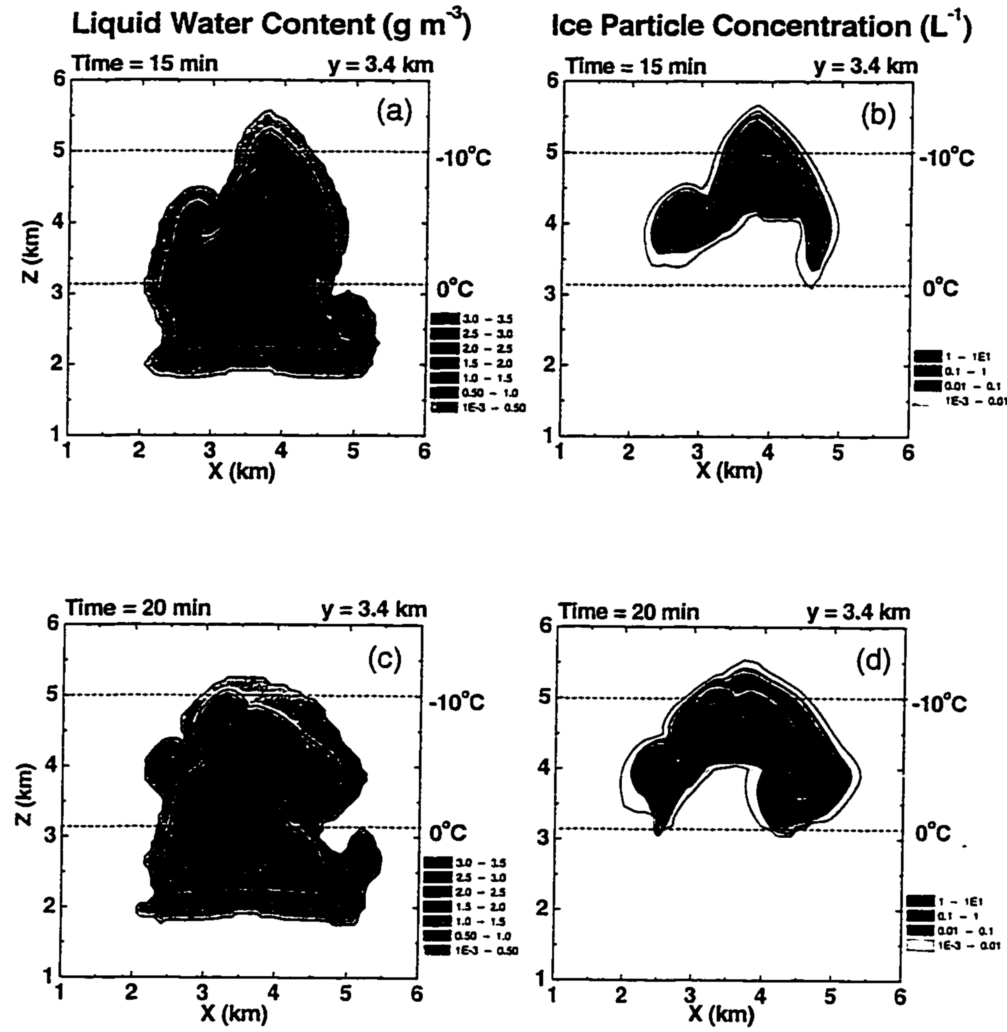

Figure 5-2. Vertical cross sections of liquid water content (a, c, e, and g) and ice particle concentration (b, d, f, and h) through the middle of the cloud (y = 3.4 km). Dashed lines represent isotherms labeled in °C. Only part of the domain is shown.

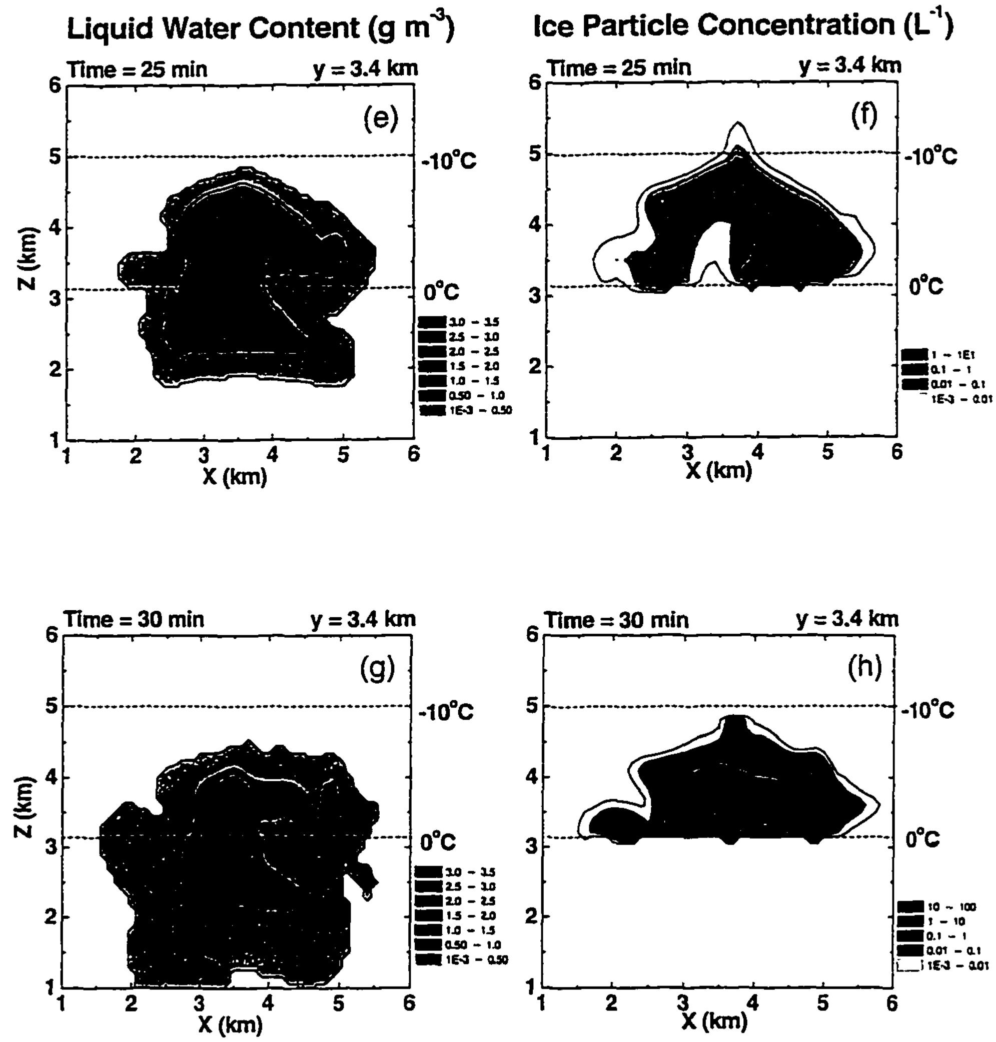

Figure 5-2 (continued).

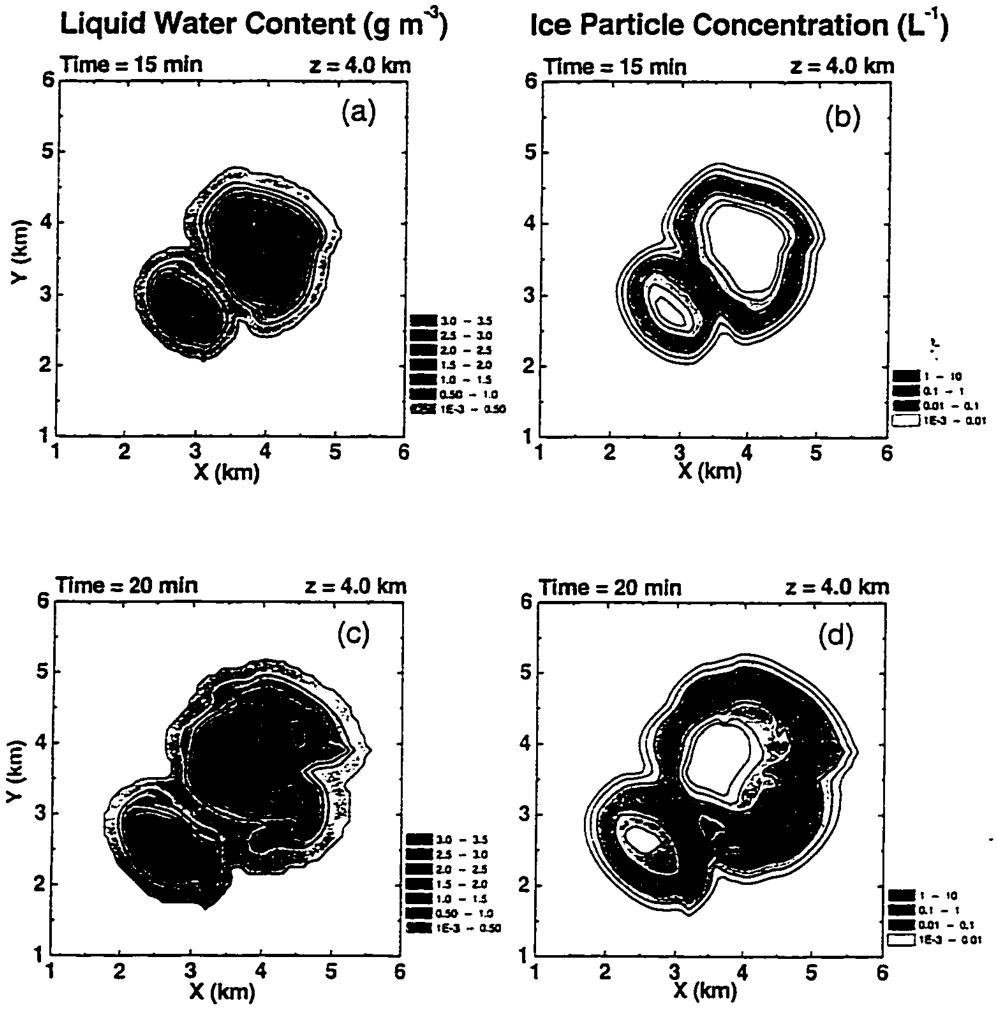

Figure 5-3. Horizontal cross sections of liquid water content (a, c, e,and g) and ice particle concentration (b, d, f, and h) at 4-km level. Only part of the domain is shown.

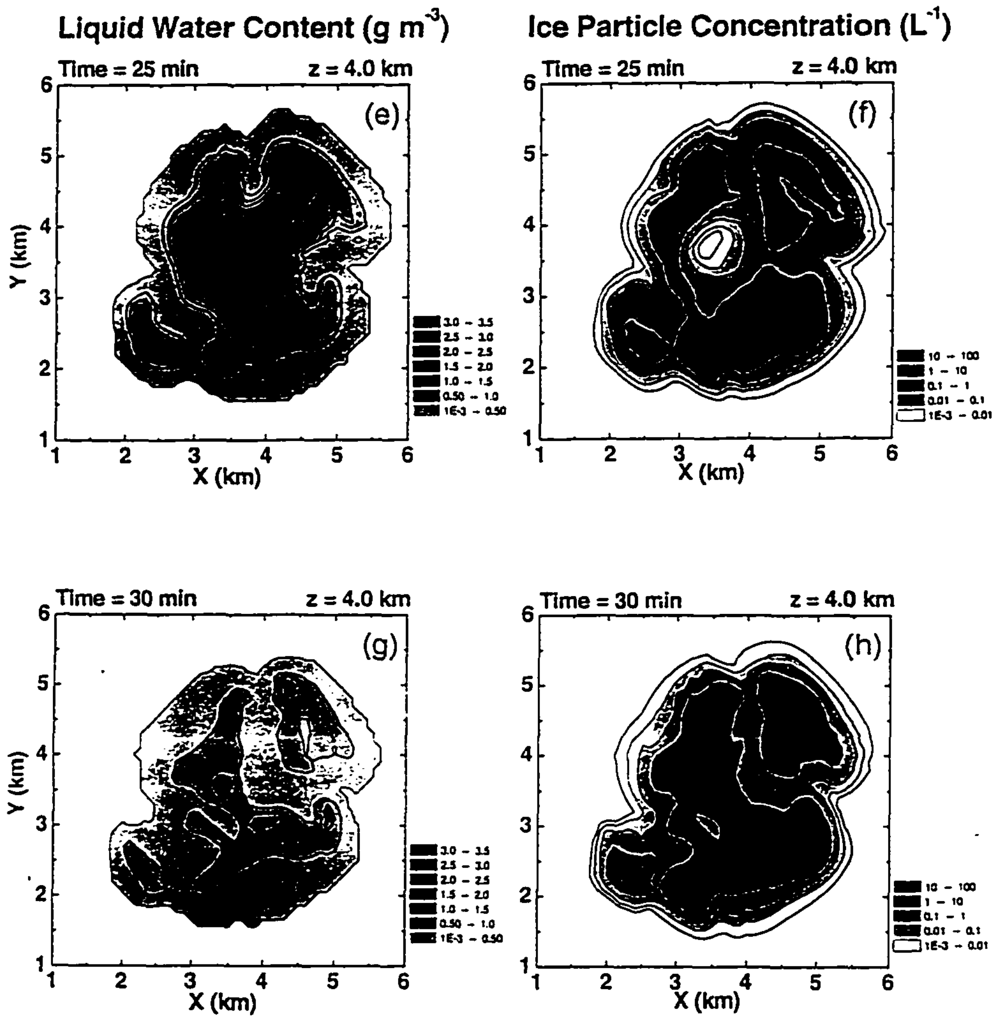

Figure 5-3 (continued).

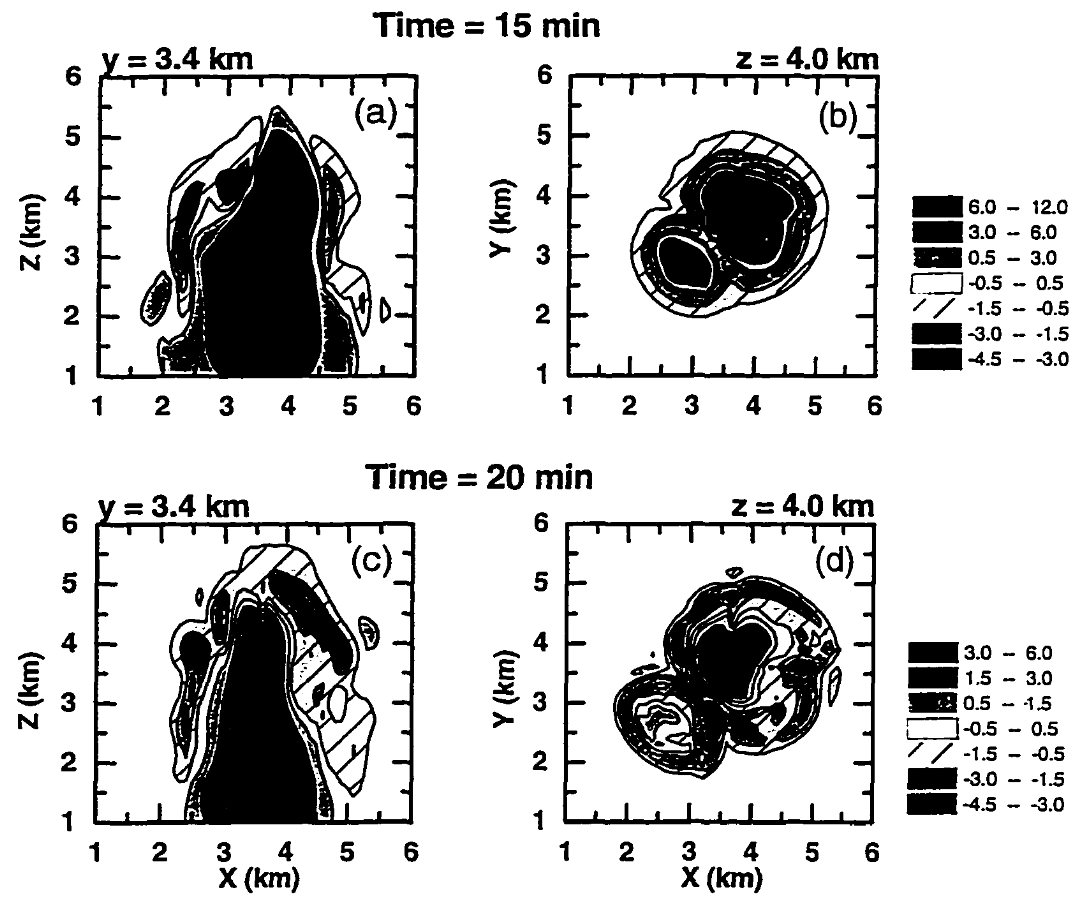

Figure 5-4. Vertical (a, c, e, and g) and horizontal (b, d, f, and h) cross sections of vertical velocity. Areas of downdrafts are hatched. Only part of the domain is shown.

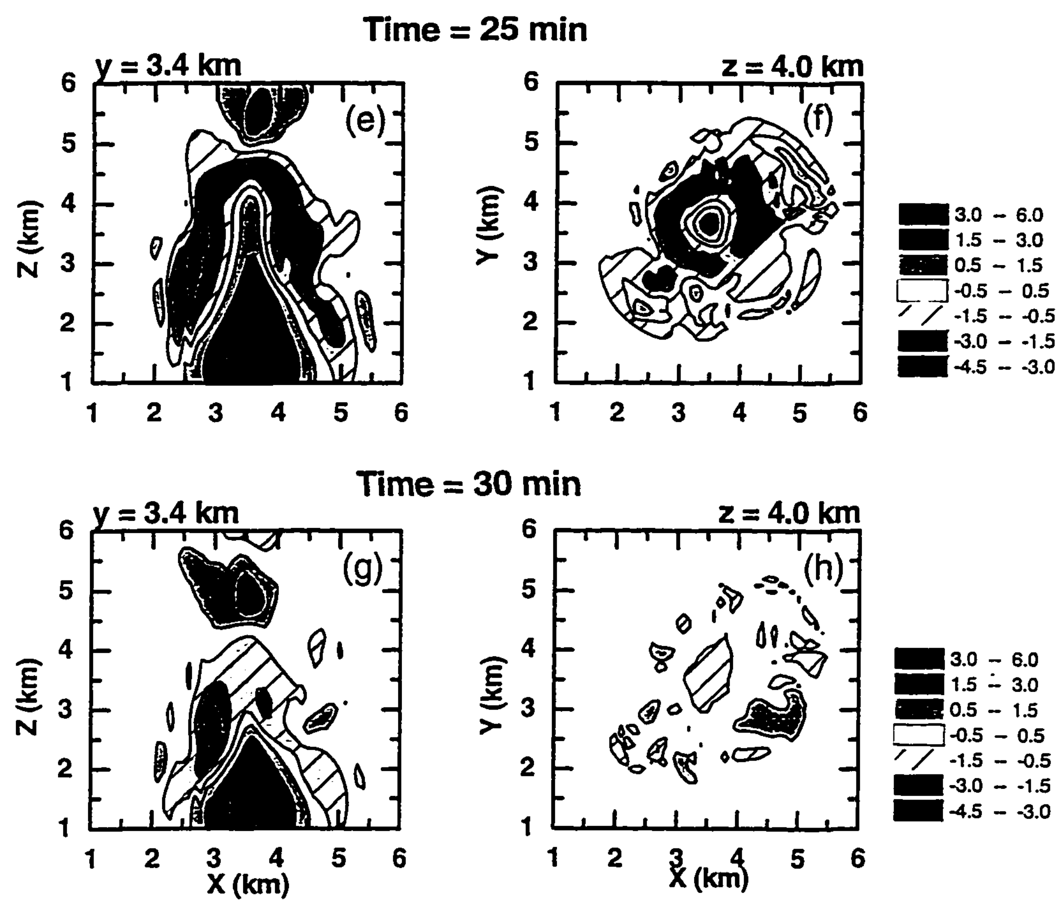

Figure 5-4 (continued).

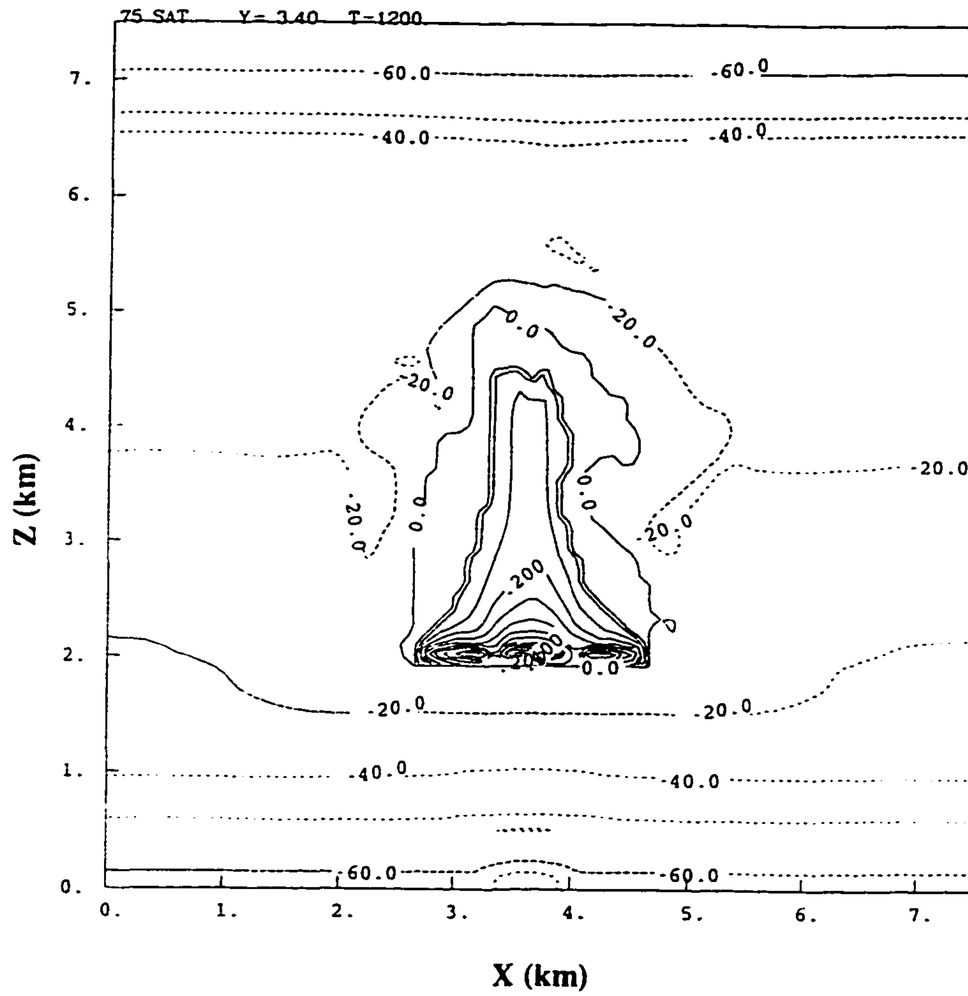

(a)

Figure 5-5. Vertical cross section of supersaturation with respect to liquid water (a) and with respect to ice (b). The cross sections are through the middle of the cloud (y = 3.4 km) and correspond to simulation time of 20 min.

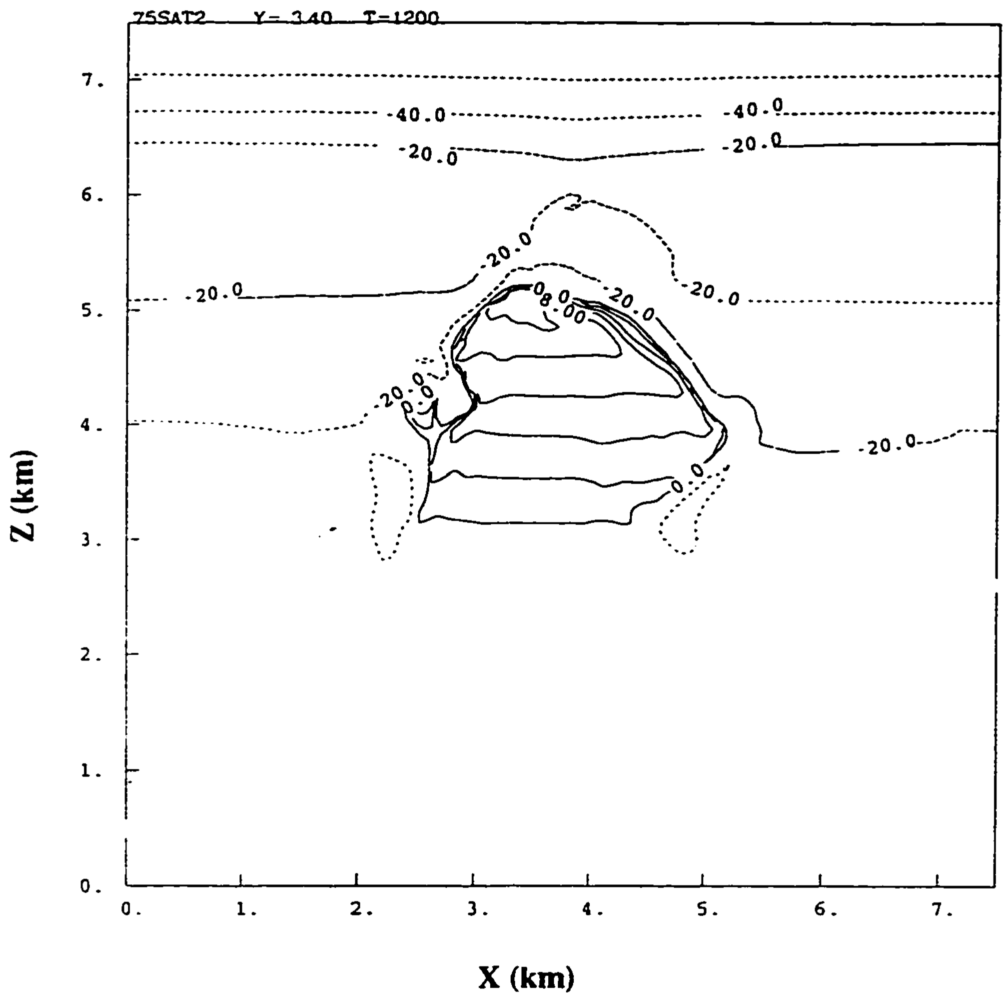

(b)

Figure 5-5 (continued).

continues and larger particles are formed. Figure 5-6 clearly shows that, although maximum values of the total concentration of ice crystals are very similar for grid points with positive and negative vertical velocities, at early stages of ice formation there are many more larger and, therefore, more easily detectable IPs in downdrafts than in updrafts. Note that concentrations smaller then 1 m^{-3} (10^{-3} L^{-1}) most likely would be missed when sampled by a 2DC probe. According to Blyth and Latham (1993), one of the repeatedly observed features in New Mexican cumulus clouds was the detection of first IPs in downdrafts while nucleation did not appear to occur preferentially in these regions. The model reproduces nicely this aspect of observations and confirms that this is an effect of cloud dynamics rather than nucleation mechanism.

The maximum rate of IP production through the contact nucleation is about 0.1% that of deposition and condensation-freezing mode (Fig. 5-1). Note that for the considered temperature range, -5° to -15°C, the number concentration of contact nuclei is of the same order of magnitude as the number concentration of deposition or condensation-freezing nuclei (Fig. 5-7). The huge difference in IP production rates results from the fact that less than one per cent of these contact nuclei is captured by drops. This is in quantitative agreement with calculations of Carstens and Martin (1982), Baker (1991), and Beard (1992). The model was able to reproduce this result because of the employed detailed parameterization of the scavenging process.

The fact that the maximum rate of contact nucleation is small does not necessarily mean that this process is unimportant, however. The reason contact nucleation is often considered in conjunction with enhanced IP concentrations is that

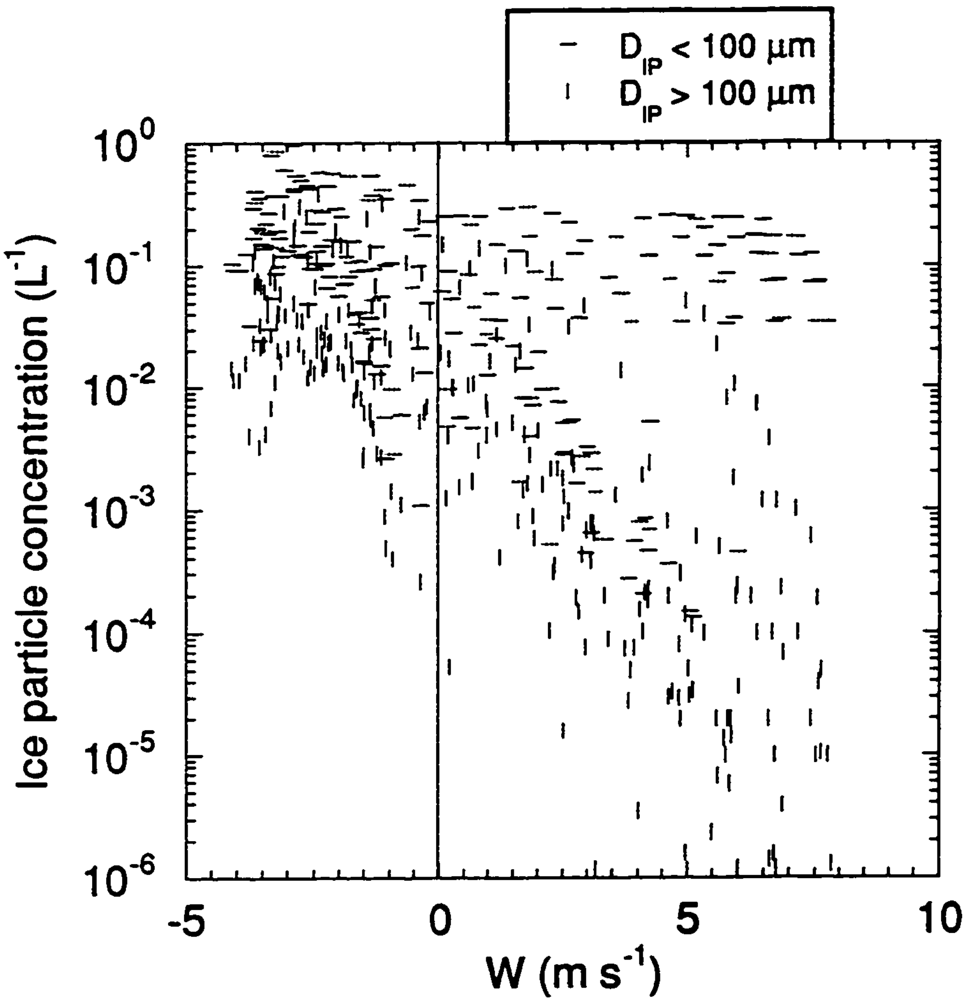

Figure 5-6. Concentration of IPs with equivalent drop diameter smaller (--) and larger (|) than 100 μm versus vertical velocity, W, at simulation time of 20 min.

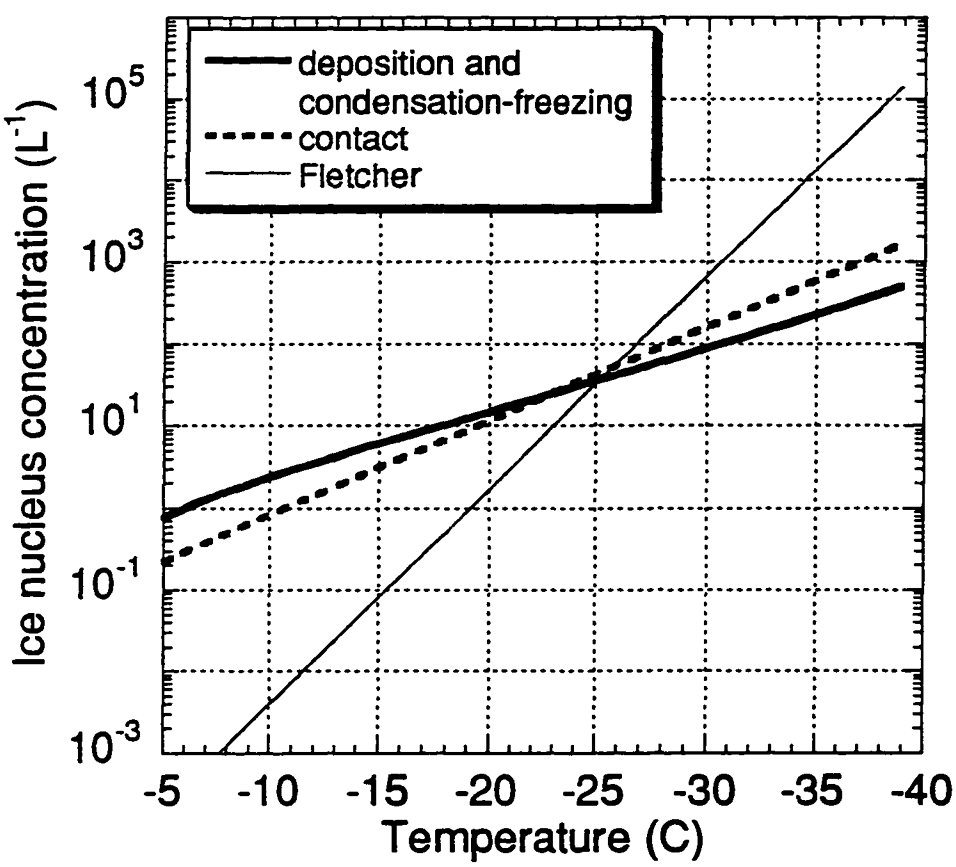

Figure 5-7. Number concentration of active deposition and condensation-freezing (thick solid line) and contact (thick dashed line) ice nuclei as a function of temperature. Fletcher parameterization is given by thin solid line for reference.

(1) - many nuclei increase their ice forming ability in contact mode and especially at relatively warm temperatures; and

(2) - for submicron nucleus size, thermophoresis contributes to fastest nucleation rate in dissipating parts of a cloud; the same regions where high IP concentrations occur.

Using an earlier version of the model, Ovtchinnikov et al. (1995) showed that for the nucleus size of 0.3 μm contact nucleation occurs primarily along the cloud edges and in the regions of downdrafts where evaporation of supercooled drops prevails. This and the present studies have also shown that for a realistic initial concentration of contact nuclei (for example, such as shown in Fig. 5-7) contact nucleation produces only on the order of 10 m^{-3} (10^{-2} L^{-1}) IP at most. This result is in agreement with other recent estimates (e.g., Baker 1991 and Beard 1992). Perhaps more important is the recognition that contact nucleation increases probability of larger drops to freeze. While this does not directly explain high IP concentrations, the presence of even a few large frozen drops may have important implications for ice multiplication and particularly for the Hallett-Mossop process.

5.2. The Hallett-Mossop Process

5.2.1. Cloud-scale consideration

As ice crystals are descending along the cloud edges some of them may be entrained back into the main cloud volume (Fig. 5-2c,d) where the liquid water content is higher and, therefore, chances for IPs to grow by riming are increased. This may be a mechanism responsible for the creation of first graupel. Graupel can also be created through freezing of large drops. If the conditions for the H-M process are met (wide cloud droplet spectrum and temperature between -3° and -8°C), some of these graupel particles may ignite an exponential growth in crystal concentration. Within 15 min after the start of primary nucleation (about 25 min of simulation time), the right conditions are developed outside the main updraft core. High IP concentrations (up to 10^5 m^{-3}) are found along the cloud edges (Fig. 5-3e,f). The regions of secondary ice production coincide with local LWC maxima. The central part of the cloud with the highest values of LWC, however, is practically free of ice at this time. The entrainment is too weak to bring graupel into this almost adiabatic core, while updrafts are too strong to allow ice crystals to fall through. As updrafts weaken and the core becomes more diluted, graupel and splinters appear there very rapidly (Fig. 5-2g,h and Fig.5-3g,h).

One notable model result is that H-M mechanism operates very locally. Initially, the size of the regions with largely enhanced IP concentrations does not exceed 300 to 500 m (Fig. 5-3d,f). The process can be triggered at several locations simultaneously or within a minor time difference; however, all these regions still occupy only few percent of the total cloud volume. In each of these places, the H-M mechanism operates for a few minutes. The entire multiplication process in the cloud takes no more than 10 to 15 minutes. This represents another interesting feature of the simulation, namely, that the predicted ice splinter production rate can be very high. The ice particle concentration may increase by an order of magnitude in less than three minutes (Fig. 5-1). This rate, however, may be overestimated in the model because we neglected the effect of the impact velocity on the splinter production rate. Possible effects of these and other approximations are evaluated in sensitivity tests described in the next chapter.

5.2.2. The H-M process at a specific location

To gain insight into how the H-M process starts we will now analyze the microphysical transformations at one particular point in space. In order to be able to use results of this analysis in model's sensitivity tests described in the next Chapter, in this section, we utilize microphysical data from a simulation with reduced spatial resolution. We have chosen a grid point (we will call it point A) within the cloud (x=4.75 km, y=4.00 km, z=3.75 km) at which the concentration of IP increases from 10 m^{-3} to 10^4 m^{-3} in about five minutes as a consequence of the rime splintering. The grid point is representative of an area where the H-M mechanism is very effective.

The time evolution of liquid and ice water content, vertical velocity, supersaturation with respect to liquid water and ice, and concentration of cloud drops and IPs is shown in Figure 5-7. It is interesting that at the time (t=13÷16 min) when LWC starts to increase, the point A is occupied by a downdraft. This means that first liquid water is brought to this location by advection rather than condensation. The point lies outside the main updraft and on the outer edge of the strongest and fast rising thermal. There are, however, weaker secondary thermals that lag the first one by about five minutes. One of them passes through the studied point at about 16 min, causing increase in the vertical velocity, LWC, and drop concentration. The complex cloud

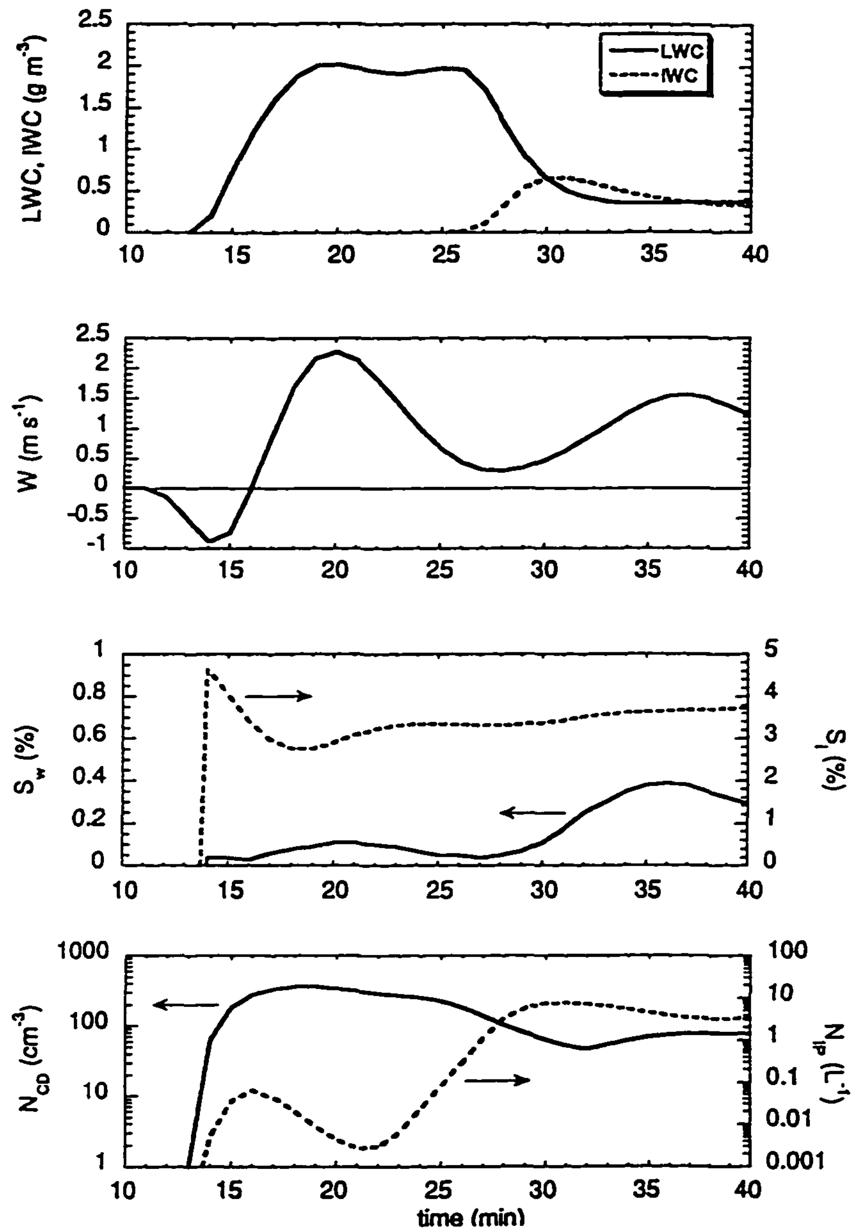

Figure 5-8. Time series (a) liquid and ice water content (LWC and IWC, respectively); (b) vertical velocity (W); (c) supersaturation with respect to liquid water (S_w) and ice (S_i); and (d) concentration of drops (N_{CD}) and ice particles (N_{IP}).

structure, though cumbersome to describe, can be more easily visualized with the help of Figure 4-3. By following a sequence of images in this figure, one can see that different parts of the cloud rise at different times, and some parts are still rising when the central portion of the cloud is already subsiding.

The curve corresponding to the concentration of IPs (bottom panel in Fig. 5-8) exhibits the same two-stage evolution as seen in Figure 5-1 for the maximum IP concentration in the whole domain. A closer look reveals, however, that not all of these particles are produced locally. In fact, the primary nucleation is extremely weak. IP production rates shown in Figure 5-9 indicate that the deposition nucleation does not occur at all in this location because the temperature is warmer than -5°C. When first drops are advected into the point and evaporate, some of them freeze via contact nucleation (Fig. 5-9). The majority of IPs, however, does not originate at this level but descend from above. Note that when vertical velocity increases between 15 and 20 min, concentration of IP decreases (Fig. 5-8). Since fall velocity of relatively small ice crystals can not counteract updrafts stronger than 1 m s^{-1}, these particles are transported upward.

The most prominent feature of the evolution of IP concentration is a sharp increase at around 25 min (Fig. 5-9). The splinter production rate, though smaller than the maximum rate from Figure 5-1, is high enough to increase IP concentration by about three orders of magnitude in about five-minute period. Not only the concentration of IP increases but the shape of IP spectrum changes drastically.

Figure 5-10 illustrates the transformation of cloud particle spectra at point A. At 20 min, there are very few (of order of 1 m^{-3}) ice crystals. Most of these are vapor

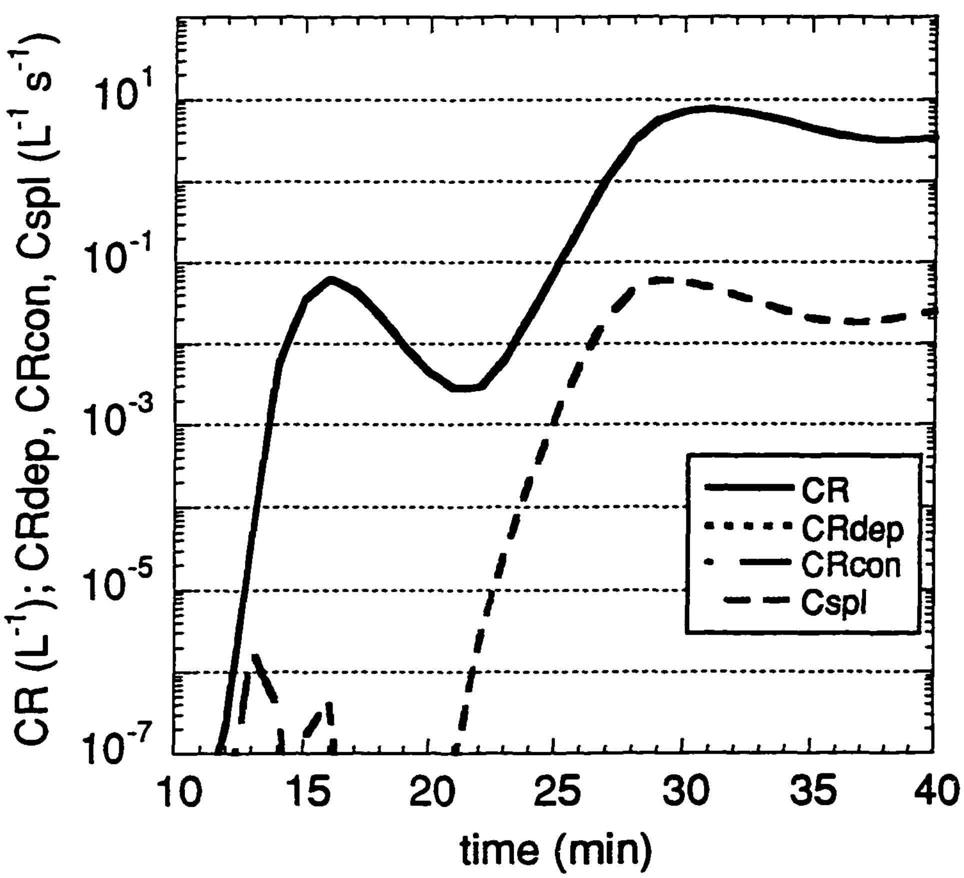

Figure 5-9. Time evolution of the IP concentration (labeled CR), IP production rates for deposition and condensation-freezing nucleation (CRdep), contact nucleation (CRcon), and splinter production rate due to the Hallett-Mossop process (Cspl).

grown from activated deposition and/or condensation-freezing ice nuclei although a small fraction may have originated from frozen droplets via contact nucleation. The concentration of drizzle-size drops does not exceed a few per liter at this time. The number of these drops, however, increases rapidly as the collection growth progresses. In only five minutes (from 20 to 25 min), the concentration of drops greater than 100 μm in diameter increases by almost an order of magnitude. An increase in concentration of larger drops is even greater and probably more important. Some of these drops collide with ice crystals and freeze forming riming centers necessary to initiate the H-M process. Since larger drops have greater probability to collect an ice crystal, they freeze faster. In fact, at 25 min a particle larger than about 1 mm (equivalent radius of 500 μm) has equal chances to be liquid or solid (Fig. 5-10). Of course, the concentration of such large particles is only around 1 m^{-3} or about the same as was the concentration of ice crystals five minutes earlier. The important difference, however, is that now these IPs are capable of collecting drops and, as long as there are drops larger than 24 μm, of producing ice splinters. Thus, the IP spectrum grows from both ends. Note the transformation from a single mode spectrum of IP at 20 min to nearly flat one at 25 min, and then into bimodal spectrum at 30 min. The number of graupel particles increases because of freezing large drops and riming of ice crystals. The number of small crystals increases because numerous ice splinters are produced by the H-M mechanisms.

It has to be understood that the spectra shown in Figure 5-10 are fixed to the particular location in space and are not from a closed parcel. The time evolution of these

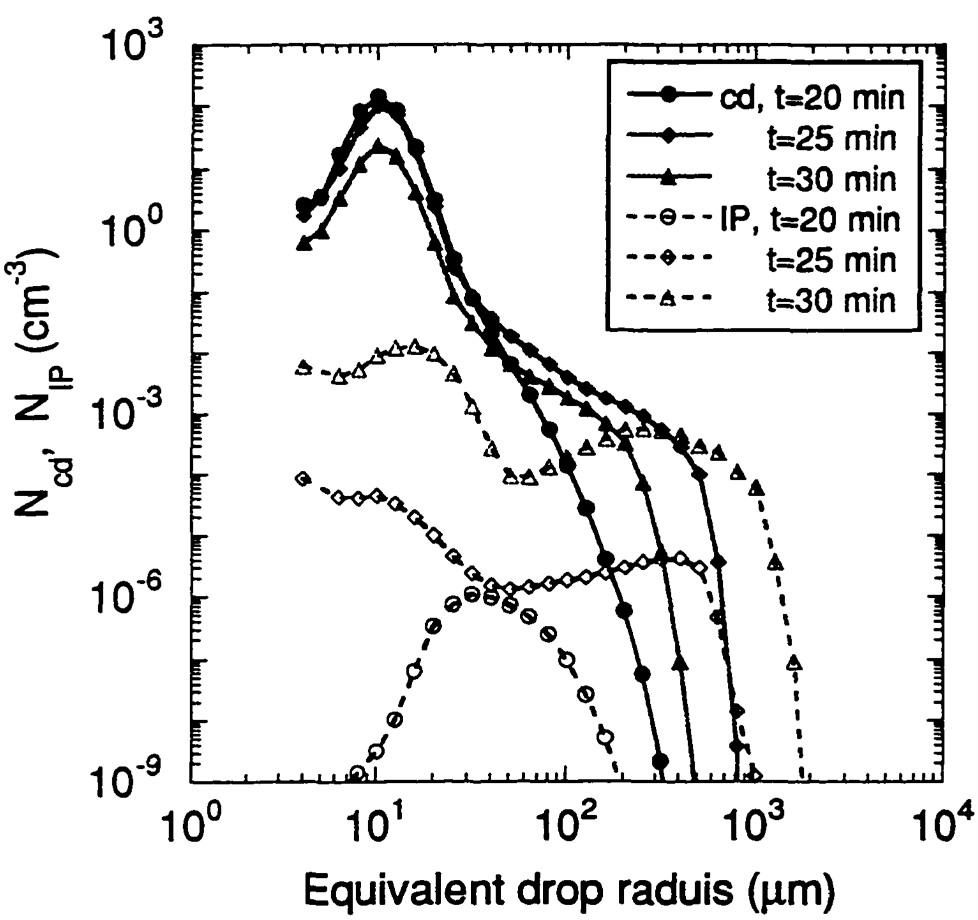

Figure 5-10. Time evolution of the cloud particle spectra (size distribution functions). Each symbol shows a number of particles in a particular bin category. Solid lines and filed symbols are for liquid drops; dashed lines and open symbols are for ice particles. The symbol shape indicates time.

spectra is thus a result of not only microphysical but also dynamical processes such as advection and turbulent mixing. This is in contrast to zero-dimensional or "parcel" models that implicitly assume uniform properties over a cloud column of significant vertical extent. (Note that the difference in terminal velocities between cloud droplets and raindrops will result in their vertical separation of hundreds of meters over a five-minute period.) One has to keep this in mind when interpreting results from parcel models as explained in the next section.

5.2.3. Comparison with earlier studies

Despite the fact that the H-M mechanism has been known for more than twenty years, only rather crude estimates of its efficiency in natural clouds have been made to date. This process strongly depends upon the spectra of ice and liquid cloud particles that are highly variable in space and time.

Aleksic et al. (1989) studied the H-M process in a two-dimensional cloud model with bulk microphysical parameterization. Aleksic et al. (1989) argued that it is not necessary for the cloud to be in its dissipating stage to initiate rime-splintering process. According to their results, ice multiplication occurs preferentially in the updraft part of the cloud where the cloud water content is high. This may be partly because the shape of the cloud drop spectrum was fixed in simulations by Aleksic et al. (1989). Under such formulation, the number concentration of large cloud droplets that contribute to splinter production is directly proportional to the liquid water content. This may not be the case in natural clouds and certainly is not true for our explicit microphysics model results. Cloud drop spectra change in space and time as we have seen in Figure 5-9, and the relation between drop concentration and LWC is much more complex.

Beheng (1987) studied the H-M process by simulating the time evolution of ice crystal and cloud drop spectra in a Lagrangian model. Neither nucleation nor diffusional growth were considered in the model and spectra evolved via collision-coalescence process only. The drop size distribution was initialized with a modified Gamma function with a liquid water content of 1 g m^{-3} and a mean radius of 12 µm. The initial spectrum of ice columns was represented by a Gaussian distribution function with a number concentration of 10 m^{-3} and a mean c-axis of 203 µm. In 30 minutes the IP concentration increased to 10^5 m^{-3} and the parcel glaciated almost completely with LWC depleted to 0.1 g m^{-3}. The results were compared to observations of Mossop (1985). A time scale for the observations was established by assuming IP concentration to be a predictor of the cloud age with younger clouds containing fewer ice particles. Simulated and observed data agreed quite nicely, although caution must be taken in quantitative comparison. It is highly unlikely that an isolated cloud element will persist for such a long time (more than 30 minutes) as implied in this Lagrangian model without being affected by dynamical and microphysical processes such as diffusional growth/evaporation of cloud aerosol, cloud particle size separation due to different fall velocities, etc.

Maximum splinter production rate in our simulation has a peak of just less than 1000 m^{-3} s^{-1} at about 30 min and stays at or above 100 m^{-3} s^{-1} for a substantial amount of time. In Beheng's (1987) calculations the maximum splinter production rate was also in the indicated range and peaked at approximately 300 m^{-3} s^{-1}.

Blyth and Latham (1996) attempted to quantify the role of H-M process by developing a multi-thermal model of cloud glaciation. Characteristics of the cloud are based on field studies. The cloud is composed of four regions: the main updraft, the quiescent (or debris) region, characterized by zero updraft velocity, the cloud top, and the downdraft region. In each of these regions, the values of updraft velocity and liquid water content are prescribed based on observation. At initial time, no ice crystals exist in the cloud, and graupel pellets of various sizes are introduced. The trajectories of these ice particles, together with those created as a consequence of the operation of H-M process, are followed as they grow by diffusion and riming and are transported around the cloud. The time evolution of the multiplication factor, defined as the ratio of the total number of ice particles at a given time to the number of initially introduced ice particles, is examined. Multiplication parameter is found to be most sensitive to the liquid water content.

Recently, Mason (1996) undertook a study in which he followed a life cycle of a sample graupel pellet in a slightly supercooled cloud with modest updrafts. It was shown that in passing between the -3° and -7°C levels the large graupel pellet shed more than 10^4 ice splinters by H-M process, 98% of these being produced within 750 s (12.5 min) and one-third of them in only 150 s (2.5 min). The cloud as a whole must have existed for more than an hour, however.

In contrast to the Beheng's parcel model, Mason (1996) and Blyth and Latham (1996) attempted to reproduce, though in crude, parameterized fashion, the growth of graupel in varying environment. Both latter models, however, neglected one aspect that seems to be important. Neither model accounted for freezing of large drizzle and raindrops due to collisions with ice splinters. The freezing of such large drops provides additional riming centers instantaneously, while evolution of an ice splinter into a riming crystal takes at least several minutes.

From our analysis, it appears that by the time the H-M starts, the precipitation-size drops already exist in the cloud. Observations also support this conclusion. For instance, in the 9 August 1987 cloud, Blyth et al. (1997) observed raindrops before the detection of the first ice. In their study, evidence for raindrops was found in both 1D and 2DC probes. Freezing of these drops and their conversion to graupel speeds up the multiplication process by producing new riming centers in shorter time than through diffusional growth of pristine ice crystals. This scenario, reproduced by the model, agrees with the concept of an *in situ* graupel production leading to ice multiplication chain reaction proposed by Hallett et al. (1978). Because of this process, the ice splinter production rate in the model is higher (and closer to the observed values) than in studies of Blyth and Latham (1996) and Mason (1996) where the freezing of large drops was not taken into account.

Chapter VI

MODEL SENSITIVITY STUDY

"Do not quench your inspiration and your imagination; do not become the slave of your model."

Vincent van Gogh

Any researcher who uses observational data must attempt to separate the fundamental physics of the studied process from the particulars of individual measurements. Similarly, in assessing results of numerical simulations, it is essential for any modeler to evaluate the model's sensitivity to various parameters and parameterizations used. This is especially important when the model includes parameterizations with a large degree of uncertainty such as the one for primary-ice nucleation.

6.1. Sensitivity to grid resolution

To study whether results depend on space resolution, the model was run with 250-m grid size. All other parameters were kept the same except for the amplitude of the initial temperature perturbation that was increased by 30%. Stronger initial impulse was necessary to produce a cloud of a depth similar to that in the simulation with finer resolution of 100 meters. Despite this adjustment, comparison of Figures 6-1 and 4-6 indicates that coarser resolution results in less vigorous simulated cloud where maximum values of vertical velocity and liquid water content decrease by about one

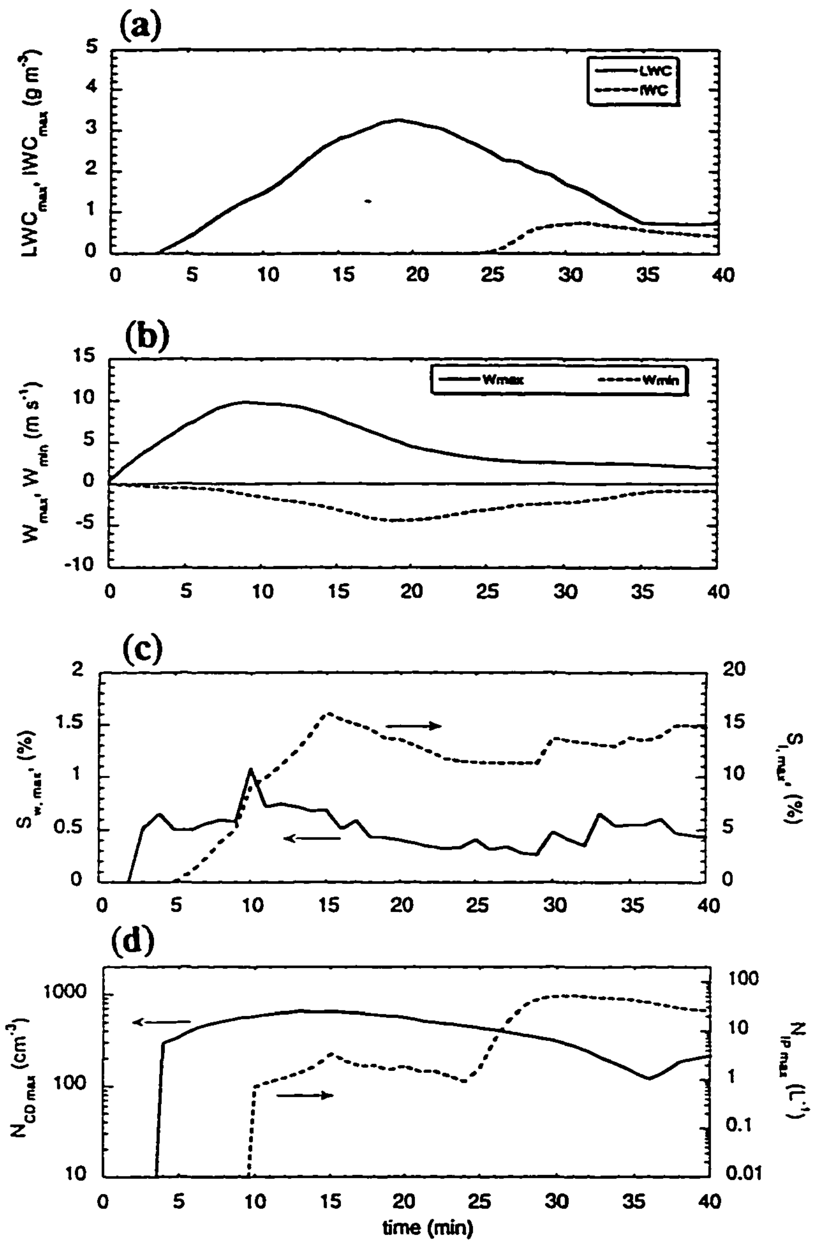

Figure 6-1. Statistics from the experiment with coarser (250 m) spatial resolution. Time series of domain maxima of (a) liquid and ice water content (LWC_{max} and IWC_{max}, respectively); (b) updraft (W_{max}) and downdraft (W_{min}) speed; (c) supersaturation with respect to liquid water ($S_{w,max}$) and ice ($S_{i,max}$); and (d) concentration of liquid drops ($N_{CD,max}$) and ice particles ($N_{IP,max}$).

third. Nevertheless, overall pictures are similar for the two simulations. It is encouraging to see (from comparison of Figures 6-2 and 5-1) similarities in the evolution of the maximum IP concentration as well as in ice production rates of various mechanisms. The general agreement between the two runs suggests that the essential physics is akin in both simulations.

One of the notable differences between the two runs is that the maximum supersaturation with respect to liquid water, $S_{w,max}$, is higher in the simulation with finer resolution. It is unclear at this point if $S_{w,max}$ will go even higher with further reduction of the grid size and how large it will get. Certainly, this question needs to be looked at in future studies. Until then, we can speculate based on the result of our comparison that although the maximum supersaturation is higher in the run with 100 m resolution, supersaturation in much of the cloud volume is nearly the same for either 100 or 250 m grid size.

Note that because of the three-dimensionality of the model an increase of a grid size by a factor of 2.5 reduces the CPU time by a factor of about 15. Because the lower resolution run was capable of capturing the essential physics of the phenomena quite well and in order to optimize computational resources, other sensitivity tests were conducted with 250-meter grid resolution.

6.2. Sensitivity to Primary Ice Nucleation

Current formulation of primary ice nucleation processes is known to have significant uncertainties in estimations of concentrations and sizes of ice nuclei. We, therefore, conducted tests that revealed the sensitivity of the model's dynamics and

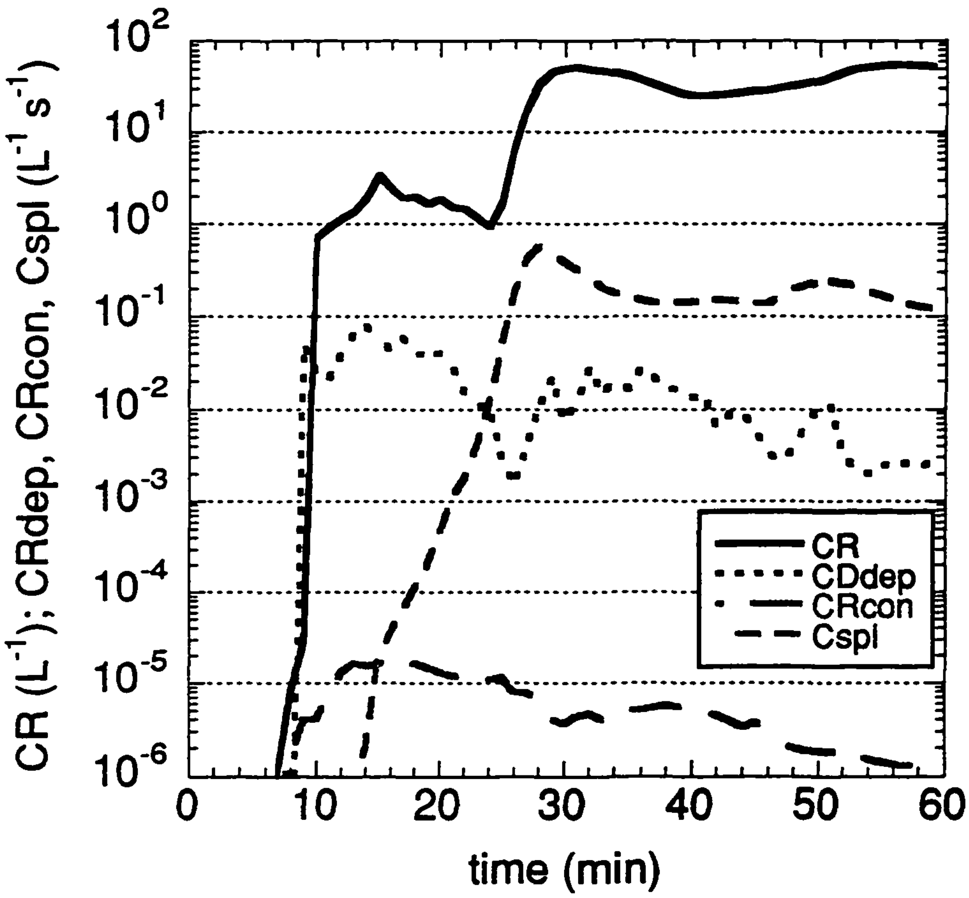

Figure 6-2. Statistics from the experiment with coarser (250 m) spatial resolution. Time evolution of the maximum IP concentration (labeled CR), maximum IP production rates for deposition and condensation-freezing nucleation (CRdep), contact nucleation (CRcon), and maximum splinter production rate due to the Hallett-Mossop process (Cspl).

microphysics to parameters of various ice nucleation modes.

To test the model sensitivity to the nucleation mechanism we rerun the model without the deposition nucleation. The concentration of contact nuclei is kept the same in both cases and given by (3-8). Figure 6-3 indicates that the concentration of primary ice crystals is reduced by a factor of 10^3 in a case when only contact nucleation was operating. Due to the H-M process, however, there is a sharp increase in the IP production rate at about 25 min. Consequently, the difference between the two simulations in the IP concentrations is small at the end of the runs. Therefore, when contact nucleation is the only significant source of primary ice (the effect of immersion freezing nucleation is negligible in both cases), much lower initial concentrations of IPs are still able to start the H-M process and produce significant IP concentrations after 40 min. Ice particles originated via contact nucleation are more likely to become centers for rime-splintering production. This is related to the difference in locations in the cloud where these mechanisms operate, as well as to the fact that contact nucleation may freeze drops already grown to larger sizes. Contact nuclei initiate drop freezing along the cloud edges and the temperature dependence for this type of nucleation is weak (Ovtchinnikov et al. 1995). In the previous chapter it was shown that condensation-freezing nucleation is capable of producing higher (by about three orders of magnitude) concentrations of pristine crystals. While these ice crystals spread throughout the cloud volume, their concentration decreases. The resultant difference in concentrations of IPs formed by these two mechanisms can be smaller in the lower than it is in the upper cloud levels. While this may be true for some rime-splintering zones, it was not the case for the specific location studied in Section 5.2.2.

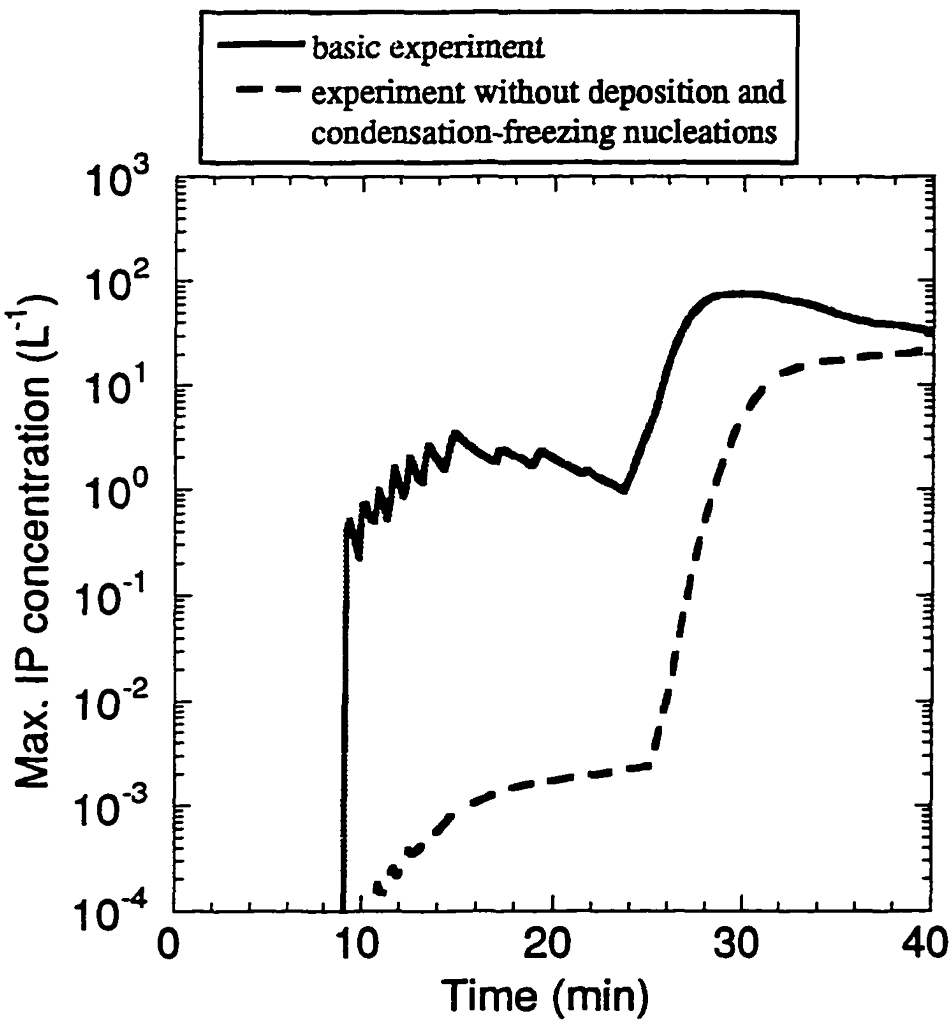

Figure 6-3. Time series of the maximum IP concentration for the model runs with (solid) and without (dashed) deposition and condensation-freezing nucleation.

In the previous chapter, it was shown that contact nucleation was active directly in the location where the H-M process starts, although most of pristine ice crystals are produced through deposition and condensation-freezing nucleation higher in the cloud and advected to this location by downdrafts. Comparison of Figures 6-4 and 5-9 indicates that when the deposition and condensation-freezing nucleation is not operational, the concentration of IP at point A at 20 min decreases by about three orders of magnitude, from 10^{-6} to 10^{-6} cm^{-3} (see Section 5.2.2 for the discussion of microphysical processes in this location). Despite much lower initial IP concentration, the H-M process still operates. At earlier times (between 20 and 25 min), it proceeds slower while at later times (between 25 and 30 min) faster than in the reference simulation.

The result of this sensitivity test suggests that in a cloud where the conditions for the H-M process are met, the source and even the initial concentration of IPs may not be very important, with liquid-phase microphysics being a more significant factor.

6.3. Sensitivity to the Ice Particle Properties

One of the challenges in simulating ice-containing clouds is that the variability of properties of IPs is much greater than that of liquid drops. Unlike liquid drops, the behavior of solid hydrometeors is determined not only by the mass but also by density, shape, and orientation of particles. Uncertainties in the above parameters lead to the uncertainties in particle fall velocity, riming and deposition growth rates, as well as other important properties. Variations of some parameters may be independent from each other, but they also could be correlated, either positively or negatively. For

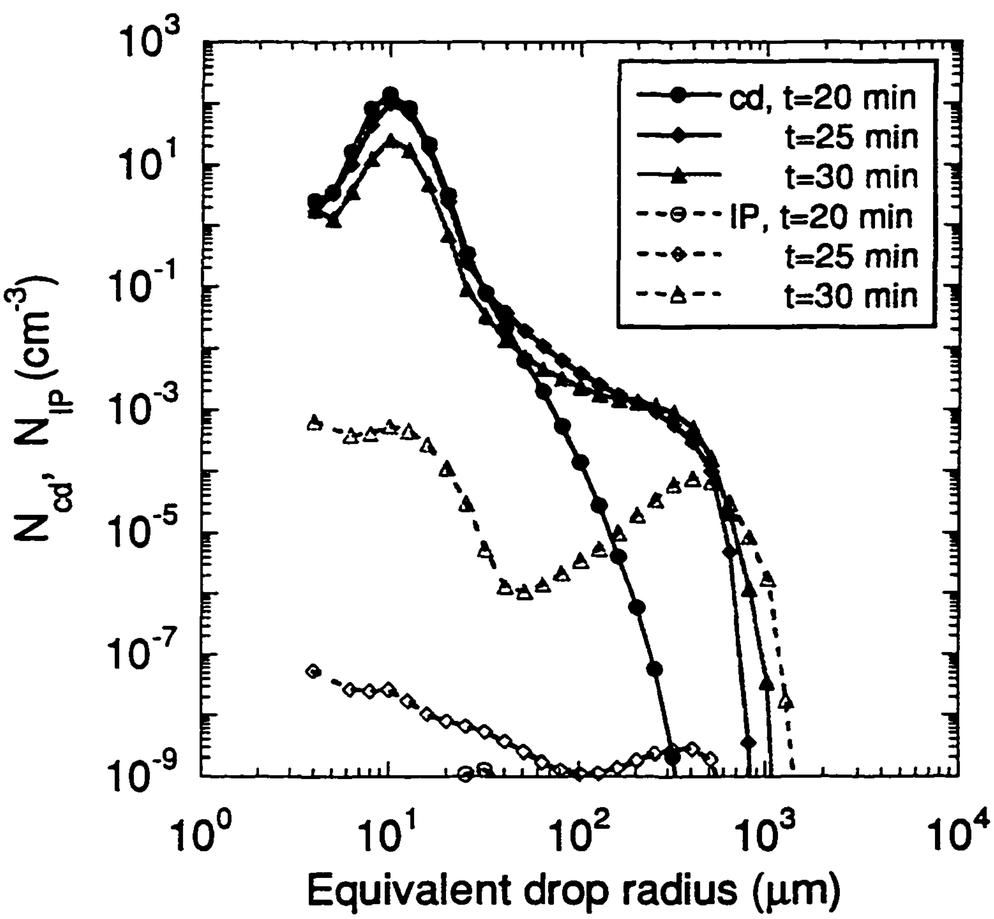

Figure 6-4. Time evolution of the cloud particle spectra (size distribution functions) at point A for the simulation without deposition and condensation-freezing nucleation. Each symbol shows a number of particles in a particular bin category. Solid lines and filed symbols are for liquid drops; dashed lines and open symbols are for ice particles. The symbol shape indicates time.

example, a less dense particle is likely to have larger horizontal cross section and, therefore, smaller fall velocity. The sweepout volume for such a particle, however, may not be much different from that for a smaller and denser particle that falls faster. Unfortunately, there are many possible feedbacks, for some of which even the sign is presently in doubt. Such complex, often nonlinear interactions between various processes make it difficult to quantify the net effect of numerous assumptions made in the model's formulation.

Even the most elaborated models do not reproduce the natural variability of IPs seen in real clouds. While the present model represents a significant step forward in terms of employing more parameterization that are based directly on physical processes, it still uses assumptions that have to be evaluated. In a few sensitivity tests, the description of which follows, we attempt to evaluate the range of changes in model's results due to variation in some important but not well known input parameters. Restricted by the number of tests we were able to run, we limit ourselves to varying only one parameter in each simulation. Where appropriate, a brief discussion is provided on how related changes in other parameters may affect the result.

6.3.1. Collection kernel for ice-drop and ice-ice interactions

As described in Chapter III, the collection kernel for ice-drop interaction is not well known and parameterized in the model using the collection kernel for interacting drops. The model sensitivity to the effectiveness of collision-coalescence process is tested by reducing the coefficient of proportionality between the two kernels from 0.8 first to 0.5 and then to 0.1. The time evolution of the maximum IP concentration is shown in Figure 6-5. The reduction of the collection kernel by nearly one third results in slowing down the H-M process (intermediate curve) but the maximum IP concentration is of the same order of magnitude as in the reference experiment. Cutting the collection kernel down by almost 90% leads to substantially lower IP concentrations (lowest curve in Fig. 6-5).

Although the reduction of the collection kernel by almost an order of magnitude may be too much, it is obvious that the ice-drop coalescence process is rather critical for studying ice multiplication. This is no surprise, since the splinter production rate is determined by the riming rate. Unfortunately, this is also an area where improvement of our understanding has been slow for the last decade. Further studies are much needed for better quantitative description of the collection process involving ice phase.

The collection kernel for ice-ice type interaction is also not well known and may experience large variations. A sensitivity test, however, has shown that this uncertainty does not impact the results in any significant way. In the simulated cloud, the contribution of the ice-ice interaction to the shaping of IP spectra is very small due to relatively low concentrations of IP compared to the drop concentrations.

6.3.2. Fall velocity of ice particles

In the basic simulation, we have assumed that ice crystals are of a plate-like shape. To evaluate the effect of fall velocity uncertainty we substitute the fall velocity of a drop of equivalent mass for the fall velocity of IP. Since ice plates are among the slowest falling particles and drops usually fall faster than any IP of the same mass, we expect the two runs to give us the range of possible variations in the model's predictions

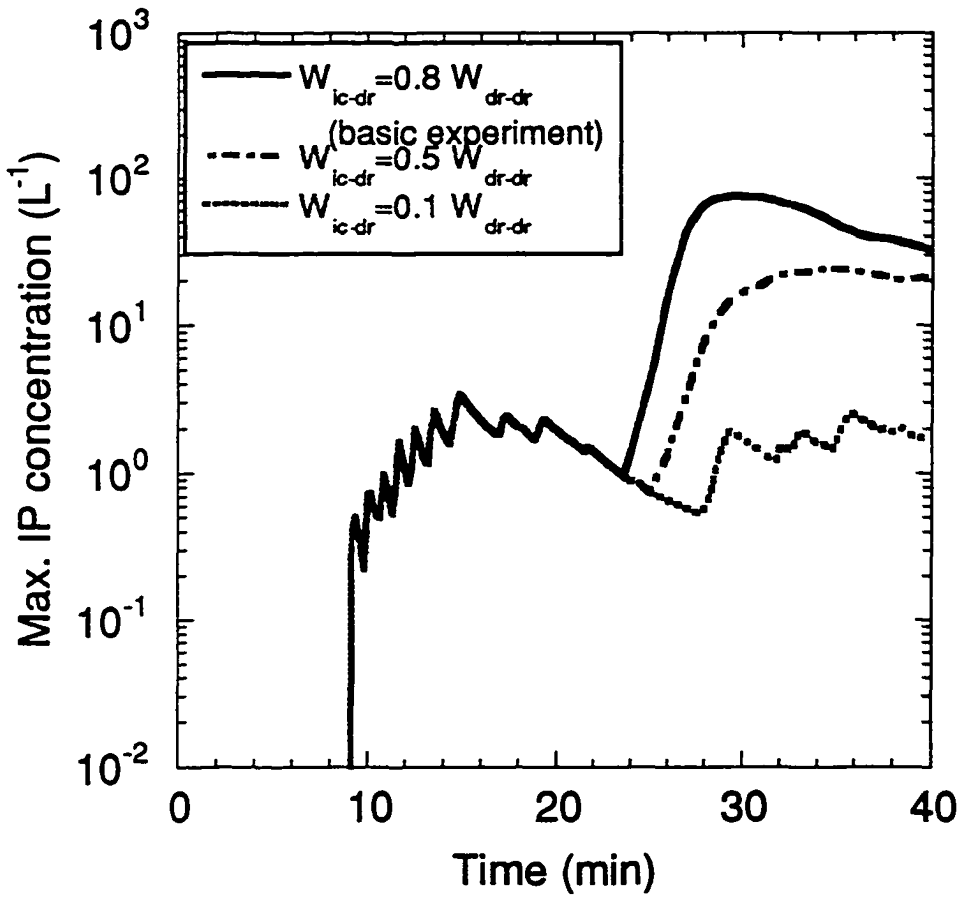

Figure 6-5.Time series of the maximum IP concentration for the model runs with different parameterizations of the ice-water collection kernel. See text for details.

due to uncertainty in IP fall velocity. The effect of fall velocity variation on the maximum concentration of IPs is presented in Figure 6-6. Surprisingly, the difference in the maximum concentration of IPs is negligible. This is another though indirect indication that in the studied cloud the production of secondary ice particles is governed primarily by liquid-phase microphysics, namely the abundance or lack of large drops.

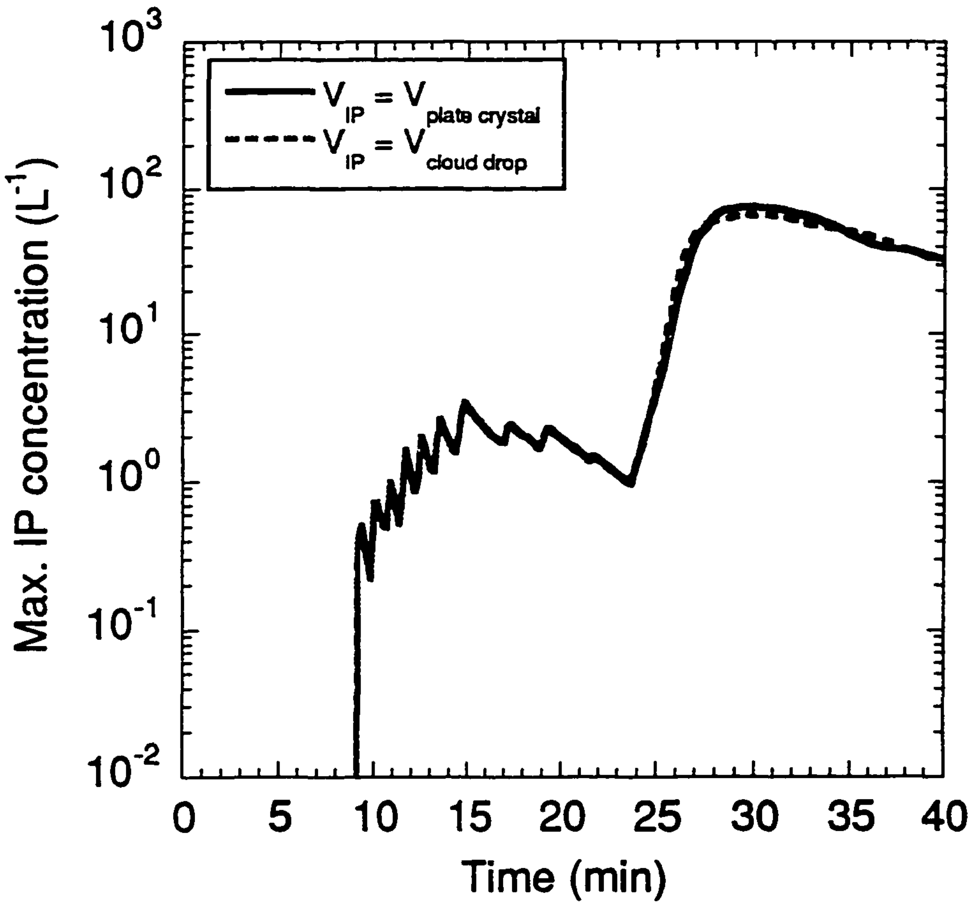

Figure 6-6. Time series of the maximum IP concentration for the model runs with different parameterizations of the IP fall velocity.

Chapter VII

SIMULATION OF A STRATIFORM CLOUD LAYER: CASE OF 7 APRIL 1997

"Nature is a mutable cloud which is always and never the same."

Ralph Waldo Emerson, "History"

The formulation of the Hallett-Mossop and other ice initiation processes in the model is quite general and based on our current understanding of the physics of these mechanisms. The parameterization has not been specifically tuned up for the New Mexican case that we have presented. The same ice-phase module that has been tested in a simulation of a convective cloud can be applied to stratiform clouds as well. In this chapter, we present results from a simulation of midlevel stratiform clouds over the Southern Great Plains of the USA.

During the day of April 7, 1997 a mixed-phase stratiform layer formed over the northern Oklahoma. The cloudiness persisted for several hours. During this period, the cloud layer was sampled by the Citation research aircraft of the University of North Dakota as well as by surface cloud observation instrumentation. The flight was part of the Cloud Radar Intensive Observational Period (IOP) conducted under the Atmospheric Radiation Measurement (ARM) Program. The obtained data sets provide a wealth of information for testing and developing cloud retrieval algorithms for various combinations of remote sensing devices used by ARM program. The model simulation complements the in situ measurements in providing detailed 3-D microphysical characteristics of clouds, needed to improve the retrieval algorithms. In this study, however, we limit ourselves to the comparison of model results with direct microphysical observations. Our purpose is to find out how the role of ice formation mechanisms changes in a different environment.

7.1. Model Initialization

The initialization of a stratiform cloud layer necessarily differs from that of an isolated cumulus cloud. This is because a persistent stratiform cloud deck is often in a quasi-steady state, and some spin-up time is required for the model to reach a quasi-stationary state.

The environmental soundings for the day are available from balloons that were launched from the Central Facility approximately every 3 hours. The sounding that was used to initialize the model corresponds to 1730 UTC and is shown in Figure 7-1. There is a prominent moist layer between 700 mb (~2.75 km) and 550 mb (~4.5 km) with a nearly moist adiabatic lapse rate and water vapor pressure close to saturation. The layer is capped by drier and more stable layer above 4.5 km. The lower troposphere is also dry with relative humidity around 40%. The boundary layer is separated from the free atmosphere by an inversion at 1.5 km.

At the beginning of the integration, a saturated layer is specified between 3 and 4 km. Random temperature perturbations of small amplitude (a few tenths of a degree) are used to send the layer in motion.

Aerosol properties were measured between 1900 and 2030 UTC by instrumentation onboard the Gulfstream-1 research aircraft. By that time clouds practically disappeared and most of the flight was under clear-sky conditions.

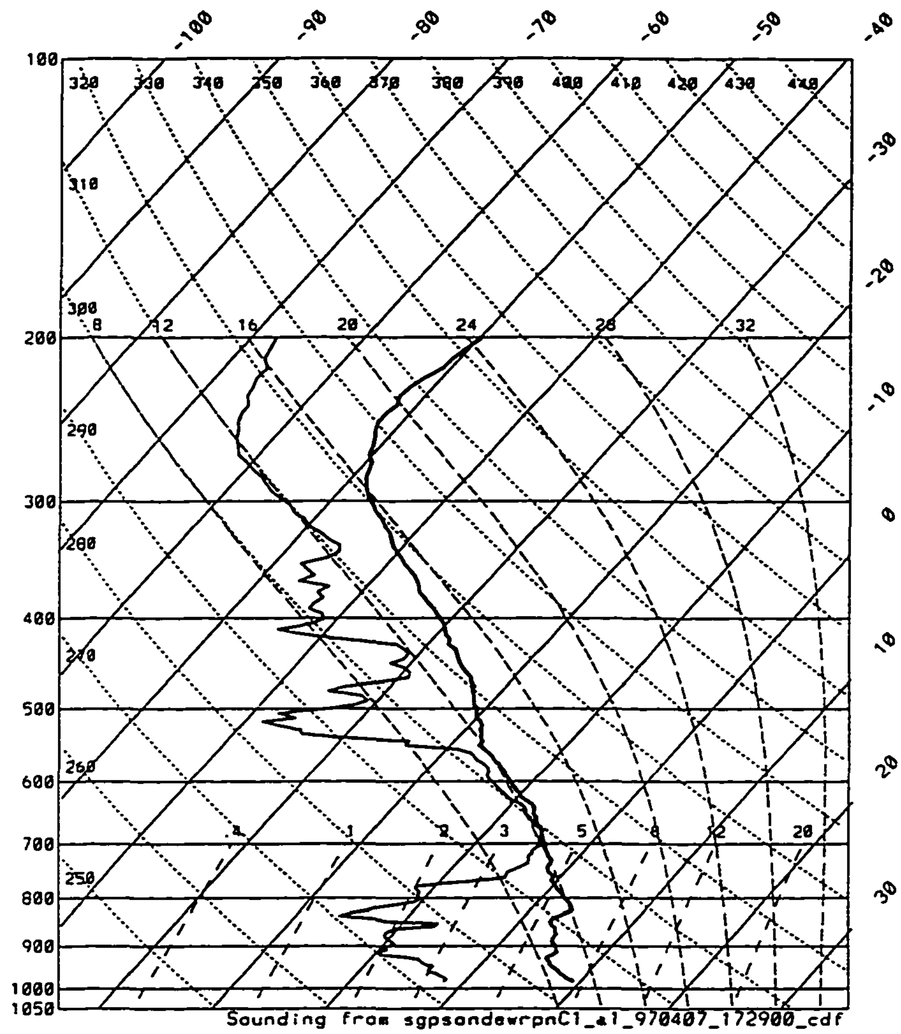

Figure 7-1. Skew T - log P diagram of environmental conditions for the case study. Temperature and dew point temperature profiles are represented by thick and thin lines, respectively. The skewed abscissa is temperature (°C) and the ordinate is pressure (mb). Short-dashed lines labeled in Kelvins represent dry adiabats, while curved long-dashed lines labeled in ºC are pseudoadiabats. Straight dashed lines are the lines of constant saturation water vapor mixing ratio, with values labeled in g kg^{-1}.

The vertical profile of the total aerosol concentration in 0.11 to 2.75 μm size range is shown in Figure 7-2. Note that the inversion layer, though slightly lifted since 1730 UTC, prevents high aerosol concentrations in the boundary layer from penetrating into the middle troposphere. The microstructure of the cloud, which was above 2.5 km, was not affected by the polluted boundary layer. In order to obtain the aerosol size spectrum representative of the cloud layer, we averaged data over all flight legs flown at or near 2.6 km. The resultant spectrum is shown in Figure 7-3. To a good approximation, all aerosol particles in the shown size range act as CCN. Thus, the same spectrum was used to describe the initial CCN size distribution in the model.

The three-dimensional domain used in the simulation covers $8\times8\times8$ km^3 with 250-meter resolution.

7.2. Cloud Structure

Figure 7-4 outlines the simulated cloud boundary as seen from below. The cloud base is rather flat except for the regions where drizzle or small raindrops are falling out. The upper part of the cloud layer is much more variable. The vertical structure is shown in more detail in Figure 7-5. Although the simulation corresponds to overcast conditions, both the LWC and drop concentration fields are highly variable. The simulated structure is supported by the aircraft observations (Fig. 7-6). Lower-level penetrations show nearly solid cloud deck, while at higher altitudes the cloud field is broken.

Compared to the case of the New Mexico cumuli, the stratiform cloud in the present simulation is characterized by much smaller vertical velocities and lower values

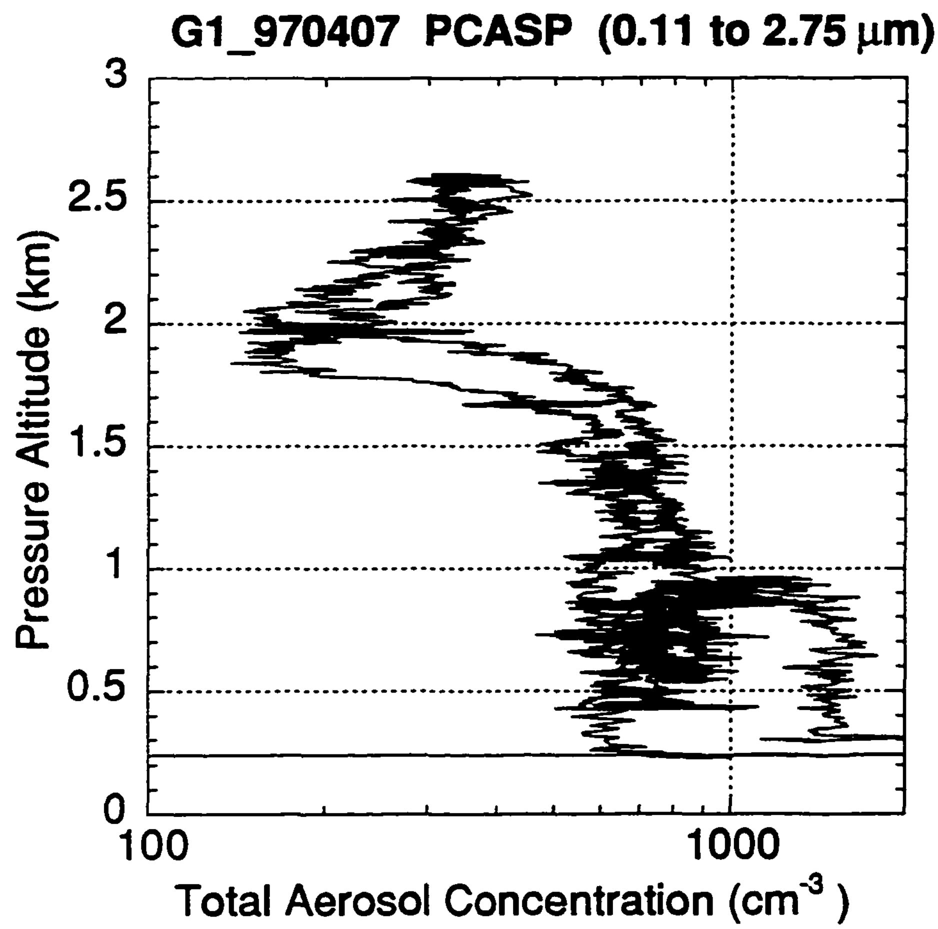

Figure 7-2.Total concentration of aerosol particles in a 0.11 to 2.75 μm size range measured by the PCASP as a function of height. The data are from the 1900 to 2030 UTC flight of the Gulfstream-1 research aircraft on 7 April 1997.

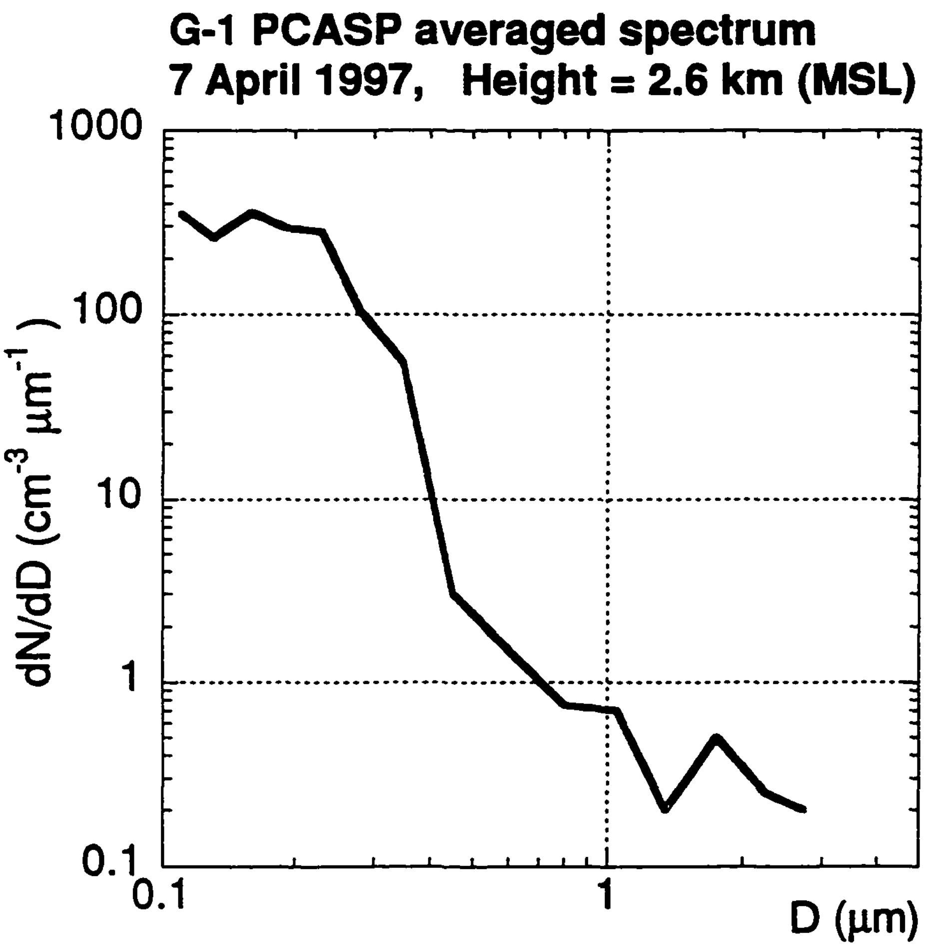

Figure 7-3. Size distribution of aerosol particles for the 7 April 1997. The spectrum is an average for all lags at or near the height of 2.6 km.

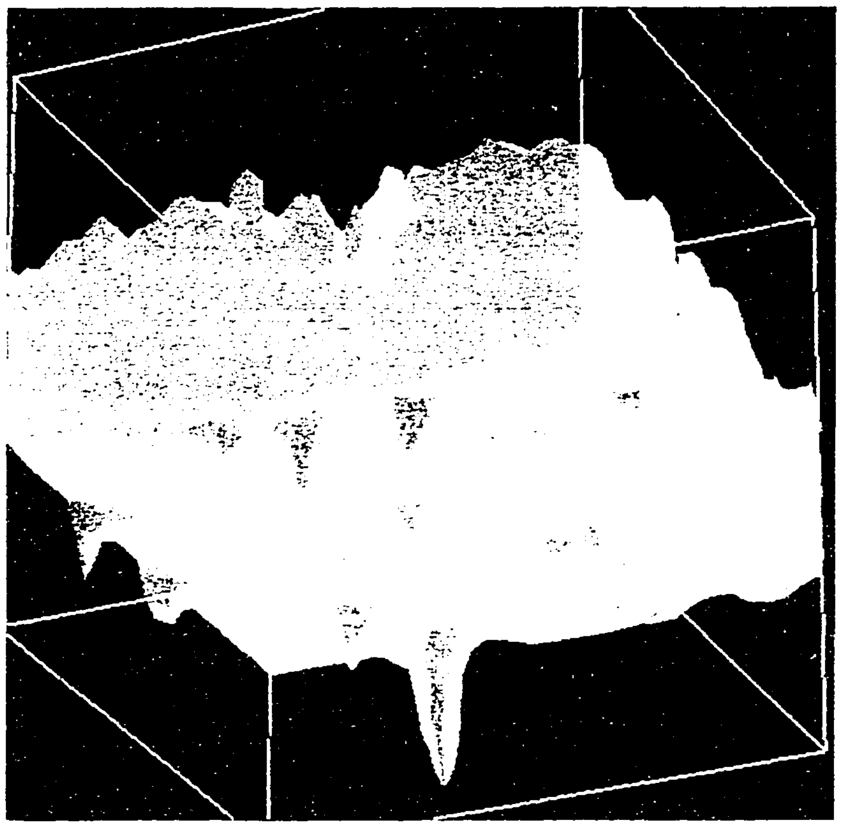

Figure 7-4. General view of the simulated stratiform cloud deck. Cloud boundary is defined as 0.01 g m^{-3} isosurface of the liquid water content.

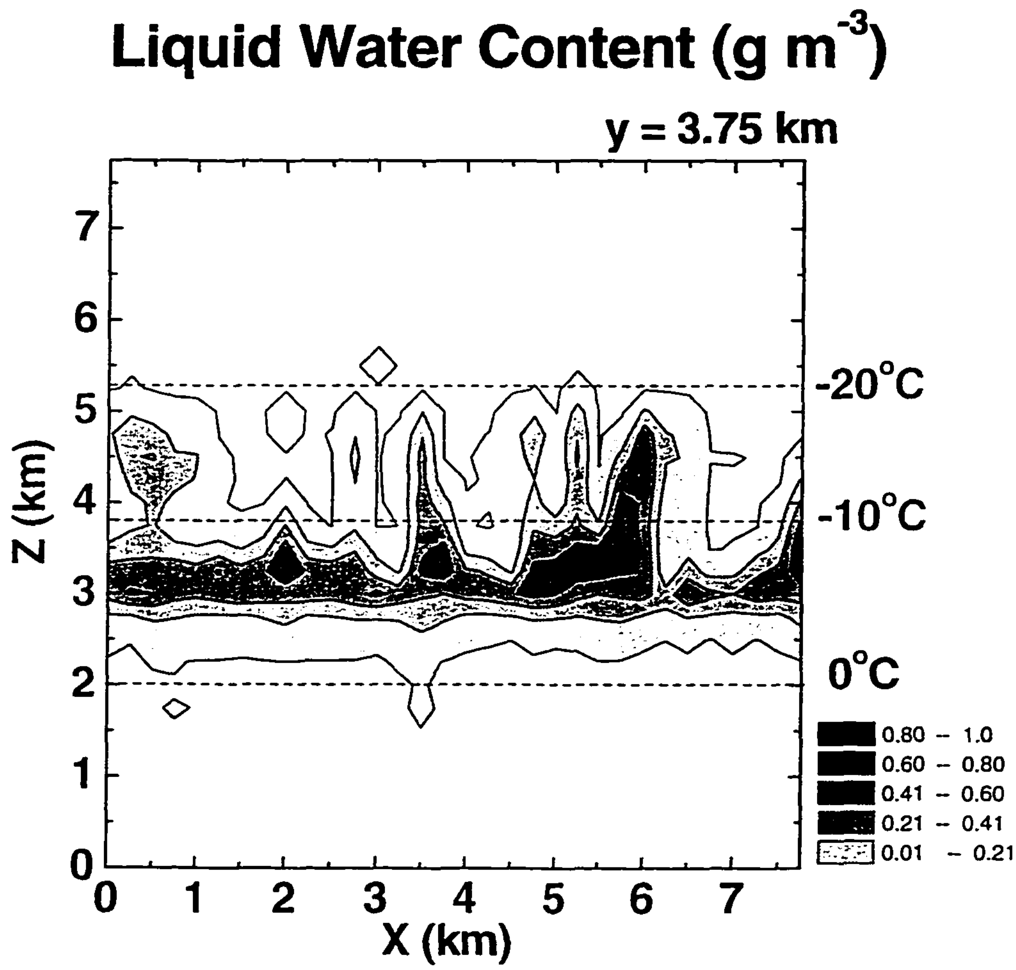

(a)

Figure 7-5. Vertical cross section of the LWC (a) and cloud drop concentration (b) fields.

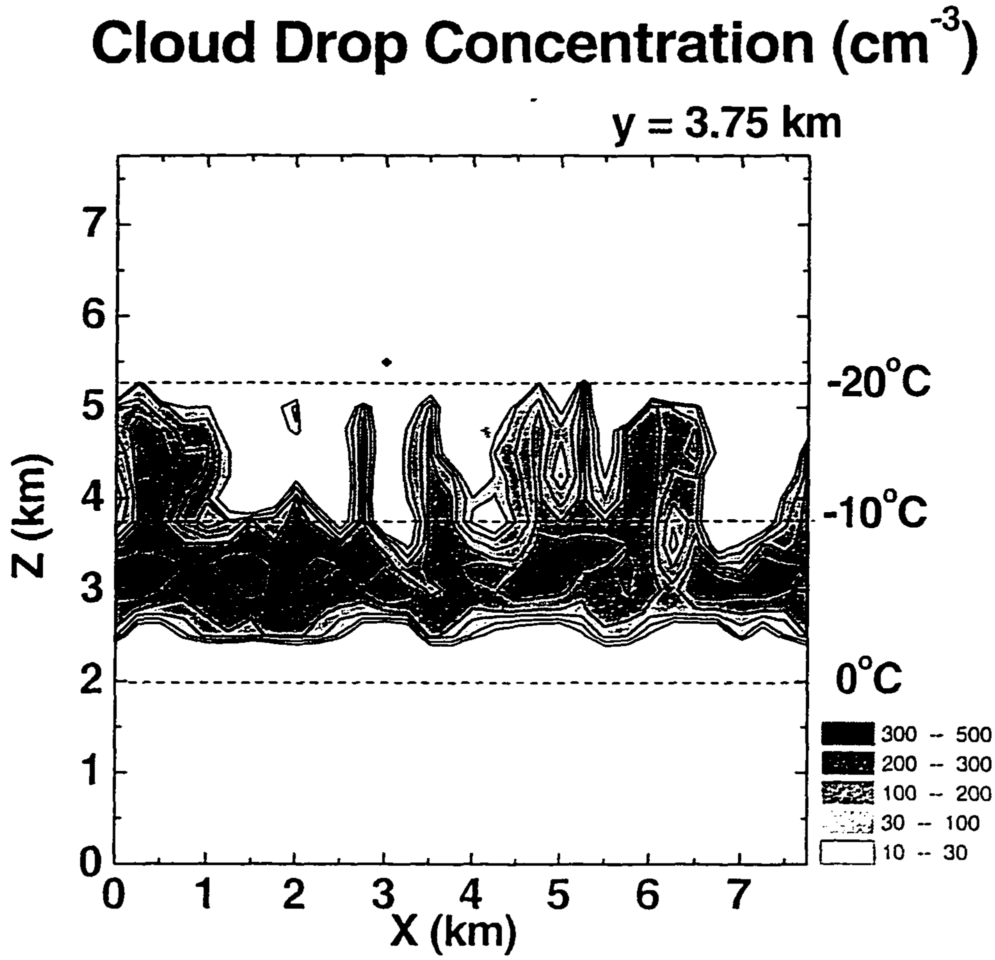

(b)

Figure 7-5 (continued).

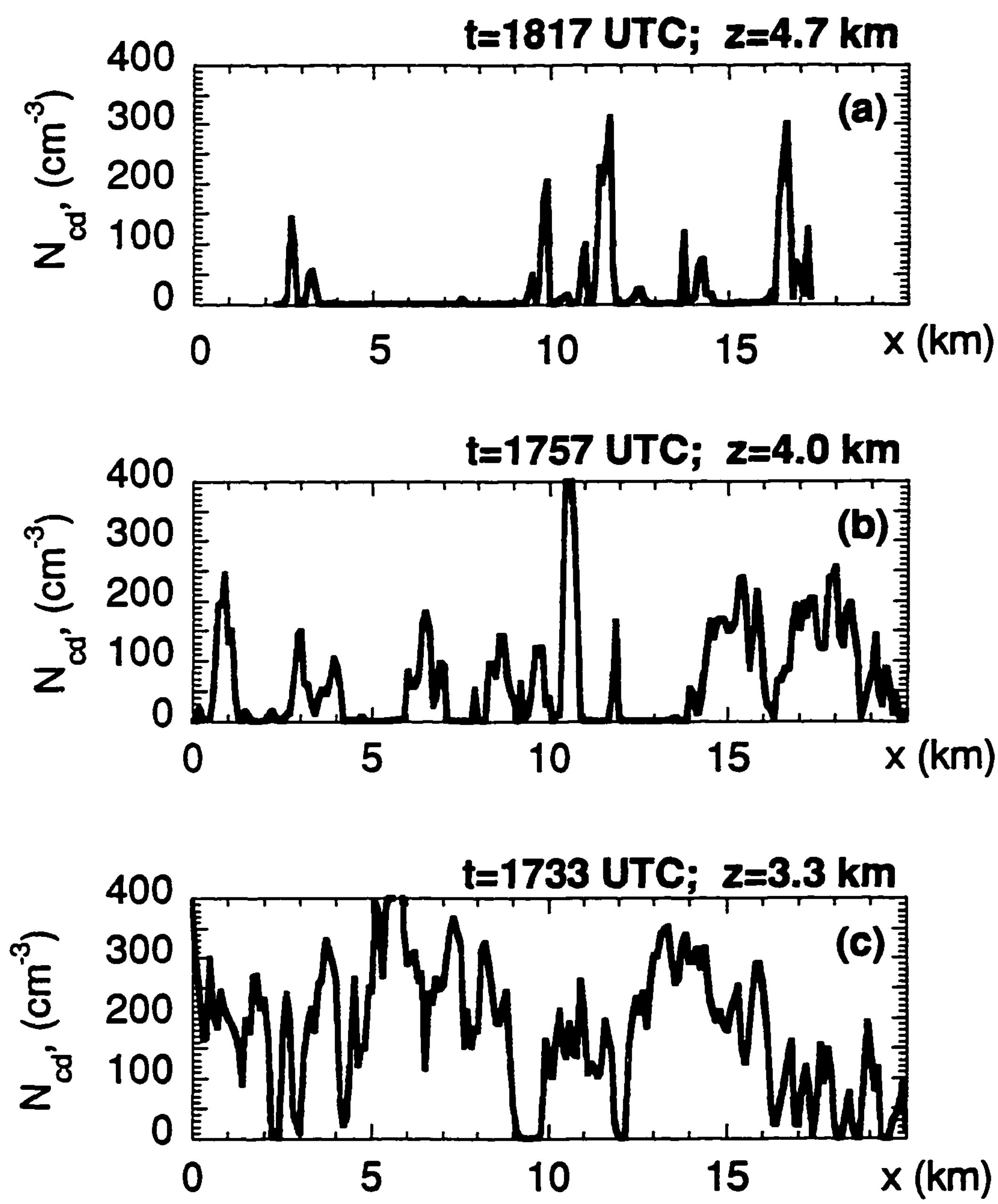

Figure 7-6. Total concentration of cloud drops as measured by FSSP during three flight legs at various heights. The height and time of the beginning of each leg is indicated.

of LWC. The maximum liquid water content in the model is only slightly above 1 g m^{-3}. This is in general agreement with observations, although the comparison is complicated by partial contamination of the measurements with ice (M. Poellot, personal communication 1997).

7.3. Ice Formation Mechanisms

The maximum concentration of IP changes little during the simulation, fluctuating between 8 and 10 L^{-1}. The cloud simulated in this experiment has a colder cloud top than the cloud in the convective case. At the same time, it has the maximum IP concentration that is lower by about an order of magnitude. Since the same ice formation mechanisms are employed in both simulations, the difference must be in the production rates of these mechanisms.

It turns out, that the nucleation rates in the stratiform case are nearly constant during the simulation. The maximum rate of deposition and condensation-freezing nucleation is around 10^{-1} L^{-1} s^{-1}, and the maximum rate of contact nucleation 10^{-4} L^{-1} s^{-1}. Comparison of these to the nucleation rates in Figure 5-1, shows that in fact they are a little higher than in the cumulus case. The enhanced primary ice formation compared to the New Mexico case is due to the colder cloud-top temperature in the present case. Primary nucleation is now able to produce IPs in concentrations of up to 10 L^{-1}.

Vertical cross section of IP concentration, shown in Figure 7-7, indicates that local maxima occur not only near the cloud top but in the lower part of the cloud as well. The latter are attributed to the H-M process. The productivity of the H-M process in this case, however, is very limited. The splinter production rate in the stratiform

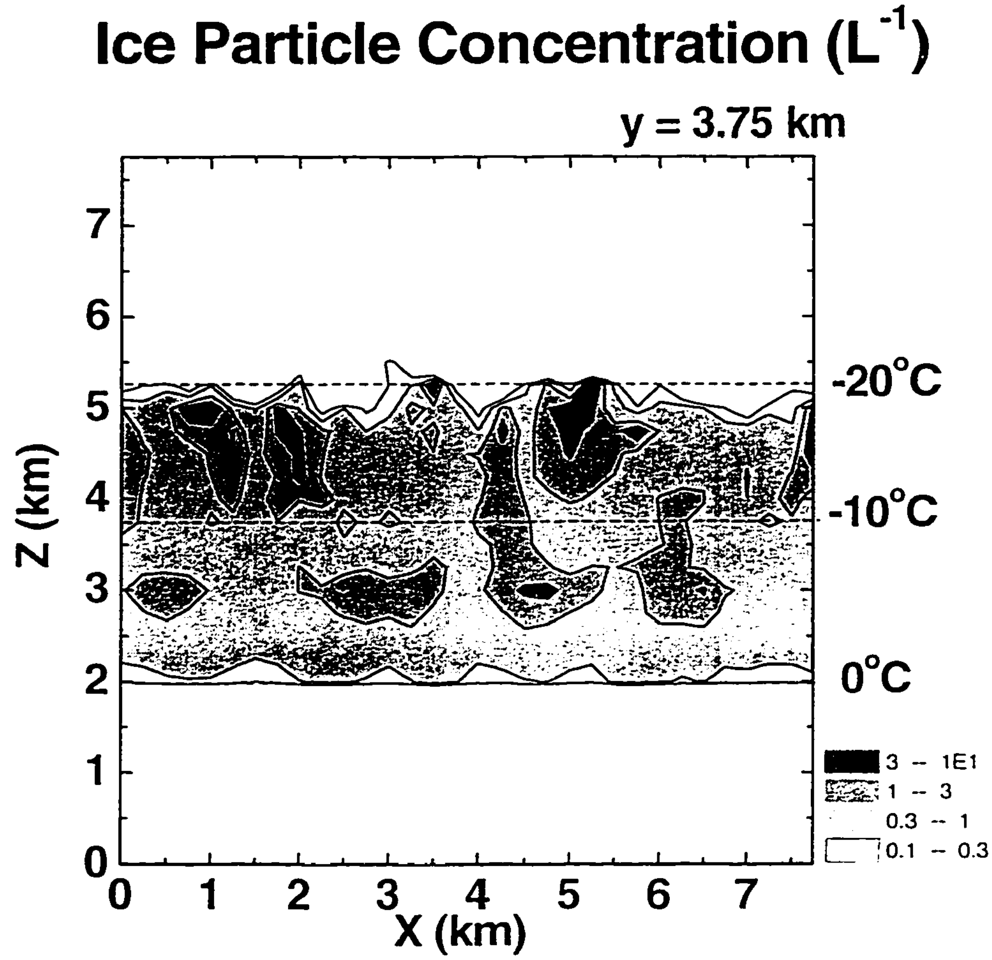

Figure 7-7. Vertical cross section of the IP concentration.

cloud never exceeds the rate of deposition and condensation-freezing nucleation while in the convective case it dominates IP production after 20 min (Fig. 5-1). In order to determine why the H-M process is inhibited in the stratiform case, we have to look at the differences in liquid phase microphysics.

One of the most pronounced differences is in the LWC. Remember that the maximum LWC in the present simulation is only slightly above 1 g m^{-3}, compared to more than 4 g m^{-3} in the case of cumulus convection. The difference is largely because the cloud base is now colder by about ten degrees. For clouds of comparable vertical extent, colder cloud-base temperatures result in lower values of LWC. Since cloud drop concentrations are similar in both cases, convective cloud with larger values of LWC has broader cloud drop spectra.

Although some drops larger than 24 μm are available to support rime splintering in stratiform case, their concentration is very limited. In addition, warm-rain process is weak and raindrops are virtually absent. That eliminates the important mechanism of in situ graupel production that was so efficient in the simulation of New Mexico cumulus. The analysis of images from the 2DC probe for the case of 7 April also confirms that there were no raindrops above the freezing level. The number concentration of drops in the 25 to 100 μm size range are not easy to obtain from the available measurements since it is not always possible to discriminate between liquid and frozen particles.

The data from the 2DC probe, which registers particles in the 25 μm to 1 mm size range, indicate the presence of IPs at all heights between 2.5 and 5 km. A scatter plot of IP concentration versus height shows rather uniform vertical distribution of IPs (Fig. 7-8). Similar distribution is produced by the model (Fig. 7-7). The observed concentrations of IPs, however, are higher than predicted by the model, by about a factor of two or three on average. The reason for this is not known. An explanation could involve some unknown ice multiplication process, not considered in the model. More likely, however, that the difference is due to natural fluctuations in IN concentration.

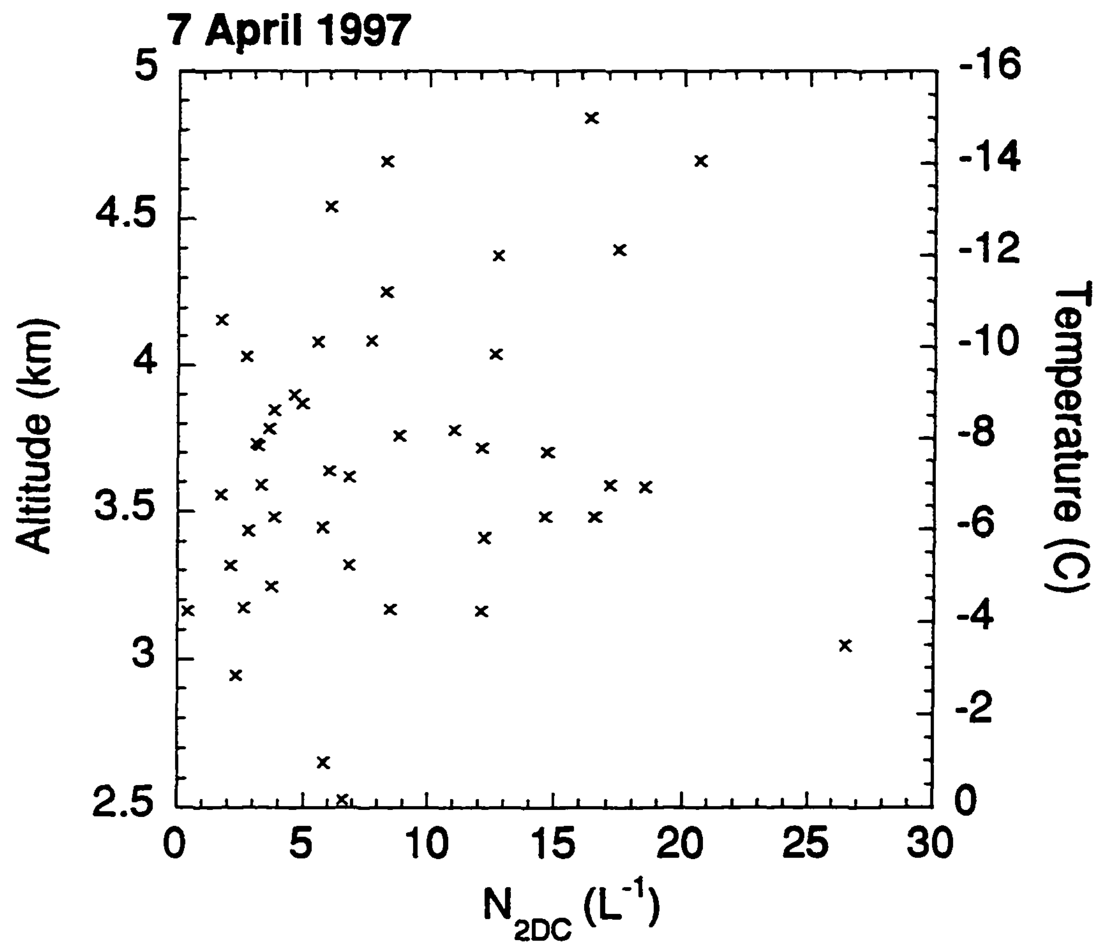

Figure 7-8.Ice particle concentration derived from the 2DC probe versus height. Approximate temperatures at specific levels are shown on the right.

Chapter VIII

CONCLUSIONS

"The clouds may drop down titles
and estates, wealth may seek us; but
wisdom must be sought."

Young (1683-1765)

A new cloud-scale model that combines a three-dimensional dynamics with an explicit ice and liquid-phase microphysics and a detailed treatment of ice origination processes has been developed. One of its the most important novel features is that the effect of the Hallett-Mossop ice multiplication process is explicitly calculated in the model with coupled dynamics and microphysics. It has been demonstrated that high-resolution simulations with a 100-m grid size can be run in a large integration domain (~ 75^3 grid points) even on moderate-power workstations. Based on our experience we can expect that the present high-end workstations can easily handle an increase in the number of grid points by an order of magnitude. Thus, detailed microphysical simulations of larger-scale clouds are also practical.

The formulation of the Hallett-Mossop and other ice initiation processes in the model is quite general and based on our current understanding of the physics of these mechanisms. Therefore, it can be applied to both stratiform and cumuliform clouds.

Two cases have been simulated: (1) the cloud formed over the Magdalena Mountains, New Mexico, on 9 August 1987; and (2) midlevel stratiform cloud layer over the northern Oklahoma on 7 April 1997. The model reproduces well the observed clouds in terms of cloud geometry, liquid water content, and concentrations of cloud drops and ice particles.

Although the same detailed microphysical parameterization is used in both cases, the ice mechanisms operate differently in the two environments. The difference has been attributed to the changes in the liquid-phase microstructure. The following specific conclusions can be drawn from the two case studies.

In the case of the New Mexico cumulus cloud, it is difficult to define a specific location for primary ice nucleation. The model indicates, however, that particles of detectable sizes (100 μm and larger) are more likely to be found in downdrafts. This correlates well with observations. Under simulated conditions of a moderate convective continental cloud, the Hallett-Mossop process is shown to be able to produce ice crystals in concentrations of order 100 L^{-1} in about 10 minutes. Comparison with the observations suggests that the secondary ice crystal production is the most likely explanation for the large ice particle concentrations found in New Mexican summertime cumulus. The revealed extreme inhomogeneity in concentration of secondary ice crystals within the simulated cloud suggests that the current sampling techniques may be inadequate to determine the production rate of this mechanism, especially at its early stage.

Several sensitivity tests have been conducted in order to evaluate the effect of uncertainties in the employed parameterizations. One test was aimed specifically to determine relative importance of various modes of ice nucleation. The results of the test indicate that, in a cloud where conditions for the Hallett-Mossop process are met, high concentrations of ice splinters can be produced even when the concentration of primary

IPs is very low. Instead, the efficacy of the rime-splintering mechanism depends strongly on the liquid-phase microphysics. Whether first graupel particles originate from riming ice crystals or frozen raindrops, presence of drizzle-size drops and their freezing by capture of ice splinters are essential to accelerate the Hallett-Mossop process.

The presented conclusions are necessarily limited to the case of moderate convection considered here. While these clouds are quite common, less vigorous clouds are also reported to produce high concentrations of IPs (Hobbs and Rangno 1985). The multithermal structure of such clouds may contribute to the more rapid formation of large drops. There is evidence that the preconditioning of air by successive convective cloud elements modify the environment in such a way that each successive parcel have broader drop spectrum and form precipitation more readily (Roesner et al. 1990).

In the case of the stratiform cloud deck on 7 April 1997, ice particle concentration is lower than in the convective case, despite the fact that the cloud-top temperature is colder. Due to lower liquid water content, the production of large drops is inhibited in the stratiform cloud. Consequently, the Hallett-Mossop process is relatively inefficient in this case. Thus, when there are few or no raindrops, as in the case of the simulated stratiform layer, the primary nucleation dominates ice production in the cloud.

We did not find, in either case, the support for the existence of localized cloud regions where supersaturation with respect to liquid water is extremely high. Suggestions have been made (Hobbs and Rangno 1990) that such regions could contribute to high concentration of IP. However, if the clusters are as small as suggested by Hobbs and Rangno (on the order of tens of meters), they could not be explicitly resolved by the present version of the model.

Successful simulations of clouds in two different environments suggest the model is suitable for several practical applications. The case studies, such as the ones described in this work, provide detailed 3-D microphysical information much needed for validation and improvement of existing retrieval algorithms for surface and spaceborne cloud observation systems. Another possible development is quantifying the relations linking ice production to liquid cloud microstructure for refining bulk parameterization of ice-phase processes.

REFERENCES

Aleksic, N. M., R. D. Farley and H. D. Orville, 1989: The numerical cloud model study of the Hallett-Mossop ice multiplication process. *Atmos. Res.*, **23**, 1-30.

Baker, B. A., 1991a: On the role of phoresis in cloud ice initiation. *J. Atmos. Sci.*, **48**, 1545-1548.

Baker, B. A., 1991b: On the nucleation of ice in highly supersaturated regions of clouds. *J. Atmos. Sci.*, **48**, 1904-1907.

Beard, K. V., 1992: Ice initiation in warm-base convective clouds: An assessment of microphysical mechanisms. *Atmos. Res.*, **28**, 125-152.

Beard, K. V., and S. N. Grover, 1974: Numerical collision efficiencies for small raindrops colliding with micron size particles. *J. Atmos. Sci.*, **31**, 543-550.

Beheng, K. D., 1987: Microphysical properties of glaciating cumulus clouds: Comparison of measurements with a numerical simulation. *Quart. J. Roy. Meteorol. Soc.*, **113**, 1377-1382.

Bennetts D. A., and F. Rawlins, 1981: Parameterization of the ice-phase in a model of mid-latitude cumulonimbus convection and its influence on the simulation of cloud development. *Quart. J. Roy. Meteor. Soc.*, **107**, 477-502.

Bergeron, T., 1933: On the physics of clouds and precipitation. *Proc. 5th Assembly U.G.G.I.*, Lisbon, 156-178.

Berry, E. X, and R. J. Reinhardt, 1974: An analysis of cloud drop growth by collection: Part I. Double distributions. *J. Atmos. Sci.*, **31**, 1814-1824.

Blanchard, D. C., 1957: The supercooling, freezing, and melting of giant waterdrops at terminal velocity in air. In: Artificial Stimulation of Rain. Pergamon, New York, pp. 233-249.

Blyth, A. M. and J. Latham, 1990: Airborne studies of the altitudinal variability of the microphysical structure of small, ice-free, Montanan cumulus clouds. *Quart. J. Roy. Meteorol. Soc.*, **116**, 1405-1423.

Blyth, A. M. and J. Latham, 1993: Development of ice and precipitation in New Mexican summertime cumulus clouds. *Quart. J. Roy. Meteorol. Soc.*, **119**, 91-120.

Blyth, A. M. and J. Latham, 1996: The Hallett-Mossop process in New Mexican summertime cumuli. *Proc. 12th Int. Conf. on Cloud and Precip.*, Zurich, 154-157.

Blyth, A. M., R. E. Benestad, and P. R. Krehbiel, 1997: Observations of supercooled raindrops in New Mexico summertime cumuli. *J. Atmos. Sci.*, **54**, 569-575.

Braham, R. R. Jr., 1963: Some measurements of snow pellet bulk-densities. *J. Appl. Meteor.*, **2**, 498-500.

Braham, R. R. Jr., 1964: What is the role of ice in summer rain-showers? *J. Atmos. Sci.*, **21**, 640-645.

Carpenter, R. L., 1994: Entrainment and detrainment in numerically simulated cumulus congestus clouds. Ph. D. dissertation, School of Meteorology, University of Oklahoma.

Carpenter, R. L., K. K. Droegemeier, and A. M. Blyth, 1997: Entrainment and detrainment in numerically simulated cumulus congestus clouds. Part I: Model initialization, general results, and comparison with observations. *J. Atmos. Sci.*, submitted.

Carstens, J. C. and J. J. Martin, 1982: In-cloud scavenging by thermophoresis, diffusiophoresis and Brownian scavenging. *J. Atmos. Sci.*, **39**, 1124-1129.

Clark, T. L., 1973: Numerical modeling of the dynamics and microphysics of warm cumulus convection. *J. Atmos. Sci.*, **30**, 857-878.

Clark, T. L., 1979: Numerical simulations with a three-dimensional cloud model: lateral boundary condition experiments and multicellular severe storm simulations. *J. Atmos. Sci.*, **36**, 2191-2215.

Cooper, W. A., 1980: A method of detecting contact ice nuclei using filter samples. Preprints, *Eighth International Conf. on Cloud Physics*, Clermont-Ferrand, France, 665-668.

Cotton, W. R., 1972: Numerical simulation of precipitation development in supercooled cumuli, I & II. *Mon. Wea. Rev.*, **100**, 757-784.

Cotton, W. R., 1975: On parameterization of turbulent transport in cumulus clouds. *J. Atmos. Sci.*, **32**, 548-564.

Cotton, W. R., G. J. Tripoli, R. M. Rauber and E. A. Mulvihill, 1986: Numerical simulation of the effect of varying ice crystal nucleation rates and aggregation processes on orographic snow-fall, *J. Climate Appl. Meteor.*, **11**, 1658-1680.

Deshler, T., 1982: Contact ice nucleation by submicron atmospheric aerosol. Ph.D. dissertation. Dept. of Physics and Astronomy, University of Wyoming, 107 pp.

Deshler, T., and G. Vali, 1992: Atmospheric concentrations of submicron contact-freezing nuclei. *J. Atmos. Sci.*, **49**, 773-784.

Dong, Y., and J. Hallett, 1989: Droplet accretion during rime growth and the formation of secondary ice crystals. *Quart. J. Roy. Meteorol. Soc.*, **115**, 127-142.

Farley, R. D., and H. D. Orville, 1986: Numerical modeling of hail-storms and hailstone growth. Part I: Preliminary model verification and sensitivity tests. *J. Climate Appl. Meteor.*, **25**, 2014-2035.

Ferrier, B. S., 1994: A double-moment multiple-phase four-class bulk ice scheme. Part I: Description. *J. Atmos. Sci.*, **51**, 249-280.

Fletcher, N. H., 1962: *Physics of Rain Clouds*, Cambridge University Press, 386 pp.

Gokhale, N. R., and J. Goold, Jr., 1968: Droplet freezing by surface nucleation. *J. Appl. Meteor.*, **7**, 870-874.

Greenfield, S. M., 1957: Rain scavenging of radioactive particulate matter from the atmosphere. *J. Meteor.*, **14**, 115-125.

Griggs, D. J., and T. W. Choularton, 1983: Freezing modes of riming droplets with application to ice splinter production. *Quart. J. Roy. Meteorol. Soc.*, **109**, 243-253.

Hall, W. D., 1980: A detailed microphysical model within a two-dimensional dynamic framework: model description and preliminary results. *J. Atmos. Sci.*, **37**, 2486-2507.

Hallett, J., and S. C. Mossop, 1974: Production of secondary ice crystals during the riming process. *Nature*, **249**, 26-28.

Hallett, J., R. I. Sax, D. Lamb, and A. S. R. Murty, 1978: Aircraft measurements of ice in Florida cumuli. *Quart. J. Roy. Meteor. Soc.*, **104**, 631-651.

Heymsfield, A. J., 1972: Ice crystal terminal velocities. *J. Atmos. Sci.*, **29**, 1348-1357.

Hill, G. E., 1974: Factors controlling the size and spacing of cumulus clouds as revealed by numerical experiments. *J. Atmos. Sci.*, **31**, 646-673.

Hobbs, P. V., and A. L. Rangno, 1985: Ice particle concentrations in clouds. *J. Atmos. Sci.*, **42**, 2523-2549.

Hobbs, P. V., and A. L. Rangno, 1990: Rapid development of high ice particle concentrations in small polar maritime cumuliform clouds. *J. Atmos. Sci.*, **47**, 2710-2722.

Hoffer, T. E. and R. R. Braham, Jr., 1962: A laboratory study of atmospheric ice particles. *J. Atmos. Sci.*, **19**, 232-235.

Huffman, P. J., and G. Vali, 1973: The effect of vapor depletion on ice nucleus measurements with membrane filters. *J. Appl. Meteor.*, **12**, 1018-1024.

Khain, A.P., and I.L. Sednev, 1996: Simulation of tropical mixed-phase cumulonimbus convection using a one-dimensional spectral-microphysics model. *Atmos. Res.*, submitted.

Klemp, J. B., and R. B. Wilhelmson, 1978: The simulation of three-dimensional convective storm dynamics. *J. Atmos. Sci.*, **35**, 1070-1096.

Klemp, J. B., et al., 1981: Observed and numerically simulated structure of a mature supercell thunderstorm. *J. Atmos. Sci.*, **38**, 1558-1580.

Koenig, L. R., 1963: The glaciation behavior of small cumulonimbus clouds. *J. Atmos. Sci.*, **20**, 29-47.

Kogan, Y. L., 1991: The simulation of a convective cloud in a 3-D model with explicit microphysics. Part I: Model description and sensitivity experiments. *J. Atmos. Sci.*, **48**, 1160-1189.

Lew, J. K., and H. R. Pruppacher, 1983: A theoretical determination of the capture efficiency of small columnar ice crystals by large cloud drops. *J. Atmos. Sci.*, **40**, 139-145.

Lipps, F. B., and R. S. Hemler, 1982: A scale analysis of deep moist convection and some related numerical calculations. *J. Atmos. Sci.*, **39**, 2192-2210.

Mason, B. J., 1996: The rapid glaciation of slightly supercooled cumulus clouds. *Quart. J. Roy. Meteor. Soc.*, **122**, 357-365.

McCumber, M., W.-K. Tao, J. Simpson, R. Penc, and S.-T. Soong, 1991: Comparison of ice-phase microphysical parameterization schemes using numerical simulations of tropical convection. *J. Appl. Meteor.*, **30**, 985-1004.

McNider, R. T., and F. J. Kopp, 1990: Specification of the scale and magnitude of thermals used to initiate convection in cloud models. *J. Appl. Meteor.*, **29**, 99-104.

Meyers, M. P., P. J. DeMott, and W. R. Cotton, 1992: New primary ice-nucleation parameterizations in an explicit cloud model. *J. Appl. Meteor.*, **31**, 708-721.

Mossop, S. C., 1976: Production of secondary ice particles during the growth of graupel by riming. *Quart. J. Roy. Meteor. Soc.*, **102**, 25-44.

Mossop, S. C., 1985: The microphysical properties of supercooled cumulus clouds in which an ice particle multiplication process operate. *Quart. J. Roy. Meteorol. Soc.*, **111**, 183-198.

Mossop, S. C., and J. Hallett, 1974: Ice crystal concentration in cumulus clouds: influence of the drop spectrum. *Science*, **186**, 632-634.

Murakami, M., 1990: Numerical modeling of dynamical and microphysical evolution of an isolated convective cloud. The 19 July 1981 CCOPE Cloud. *J. Meteor. Soc. Japan*, **68**, 107-128.

Murakami, M., T. L. Clark, and W. D. Hall, 1994: Numerical simulation of convective snow clouds over the Sea of Japan; two-dimensional simulation of mixed layer development and convective snow cloud formation. *J. Meteor. Soc. Japan*, **72**, 43-62.

Ochs, H. T., 1978: Moment-conserving techniques for warm cloud microphysical computations. Part II: Model testing and results. *J. Atmos. Sci.*, **35**,1959-1973.

Ogura, Y., and N. A. Phillips, 1962: Scale analysis of deep and shallow convection in the atmosphere. *J. Atmos. Sci.*, **19**, 173-179.

Ovtchinnikov, M. V., Y. L. Kogan, and B. N. Sergueev, 1995: Study of the ice nucleation mechanisms in a 3D cloud model with explicit formulation of ice-phase and warm rain microphysics. Proceedings of AMS Conference on Cloud Physics. Dallas, USA, 199-202.

Pflaum, J. C., and H. R. Pruppacher, 1979: A wind tunnel investigation of the growth of graupel initiated from frozen drops. *J. Atmos. Sci.*, **36**, 680-689.

Pruppacher, H. R., and J. D. Klett, 1997: *Microphysics of Clouds and Precipitation, 2nd ed.*, Reidel, 954 pp.

Randall, D. A., and G. J. Huffman, 1982: Entrainment and detrainment in a simple cumulus cloud model. *J. Atmos. Sci.*, **39**, 2793-2806.

Rangno, A. L., and P. V. Hobbs, 1991: Ice particle concentrations and precipitation development in small polar maritime cumuliform clouds. *Quart. J. Roy. Meteor. Soc.*, **117**, 207-241.

Rangno, A. L., and P. V. Hobbs, 1994: Ice particle concentrations and precipitation development in small continental cumuliform clouds. *Quart. J. Roy. Meteor. Soc.*, **120**, 573-601.

Reisin, T., Z. Levin, and S. Tzivion, 1996: Rain production in convective clouds as simulated in an axisymmetric model with detailed microphysics. Part I: Description of the model. *J. Atmos. Sci.*, **53**, 497-519.

Rösner, S., A. I. Flossmann, and H. R. Pruppacher, 1990: . *Quart. J. Roy. Meteor. Soc.*, **116**, 1389-1400.

Schlesinger, R. E., 1975: A three-dimensional numerical model of an isolated deep convective cloud. Preliminary results. *J. Atmos. Sci.*, **32**, 934-957.

Scott, B. C., and P. V. Hobbs, 1977: A theoretical study of the evolution of mixed-phase cumulus clouds. *J. Atmos. Sci.*, **34**, 812-826.

Slinn, W. G. N., and J. M. Hales, 1971: A reevaluation of the role of thermophoresis as a mechanism of in- and below-cloud scavenging. *J. Atmos. Sci.*, **28**, 1465-1471.

Smolarkiewicz, P. K., 1984: A fully multidimensional positive definite advection transport algorithm with small implicit diffusion. *J. Comput. Phys.*, **54**, 325-362.

Smolarkiewicz, P. K., and W.W. Grabowski, 1990: The multi-dimensional positive definite advection transport algorithm: Nonoscillatory option. *J. Comput. Phys.*, **86**, 355-375.

Steiner, J. T., 1973: A three-dimensional model of cumulus cloud development. *J. Atmos. Sci.*, **30**, 414-435.

Straka, J. M., 1989: Hail growth in a highly glaciated central High Plains multi-cellular hailstorm. Ph. D. dissertation, Department of Meteorology, University of Wisconsin-Madison.

Takahashi, T., 1976: Hail in an axisymmetric cloud model. *J. Atmos. Sci.*, **33**, 1579-1601.

Telford, J. W., S. K. Chai, and S. Ionescu-Niscov, 1987: Comments on "Ice particle concentration in clouds". *J. Atmos. Sci.*, **44**, 902-909.

Twomey, S., and T. A. Wojciechowski, 1969: Observations of the geographical variation of cloud. *J. Atmos. Sci.*, **26**, 684-688.

Vali, G., 1974: Contact ice nucleation by natural and artificial aerosols. Preprints, *Conf. Cloud Physics*, Tucson, Amer. Meteor. Soc., 34-37.

Vali, G., 1975: Remarks on the mechanism of atmospheric ice nucleation. *Proc. 8th Int. Conf. on Nucleation*, Leningrad, 23-29 Sept., I. I. Gaivoronsky, ed., Gidrometeorizdat, 265-269.

Vali, G., 1976: Contact-freezing nucleation measured by the DFC instrument. Preprints, *Third International workshop on Ice Nucleus Measurements*, Laramie, Univ. of Wyoming, 159-178.

Wang C., and J. S. Chang, 1993: A three-dimensional numerical model of cloud dynamics, microphysics, and chemistry. I. Concepts and formulation. *J. Geophys. Res.*, **98**, D8, 14,827-14,844.

Warner, J., 1970a: The microstructure of cumulus clouds. Part III. The nature of the updraft. *J. Atmos. Sci.*, **27**, 682-688.

Warner, J., 1970b: On steady-state one-dimensional models of cumulus convection. *J. Atmos. Sci.*, **27**, 1035-1040.

Young, K. C., 1974: The role of contact nucleation in ice phase initiation in clouds. *J. Atmos Sci.*, **31**, 768-776.

Young, K. C., 1974b: A numerical simulation of wintertime, orographic precipitation. I: Description of model microphysics and numerical techniques. *J. Atmos. Sci.*, **31**, 1735-1748.